Control of Wind Turbines during Symmetrical and Asymmetrical Grid Faults

Göksu, Ömer

Publication date:
2012

Document Version
Publisher's PDF, also known as Version of record

Control of Wind Turbines during Symmetrical and Asymmetrical Grid Faults

by

Ömer Göksu

Dissertation submitted to the Faculty of Engineering, Science & Medicine at Aalborg University
in partial fulfillment of the requirements for the degree of
Doctor of Philosophy in Electrical Engineering

Aalborg University
Department of Energy Technology
Aalborg, Denmark
December 2012

Aalborg University
Department of Energy Technology
Pontoppidanstraede 101
9220 Aalborg East
Denmark
Phone: +45 9940 9240
Fax: +45 9815 1411
Web: http://www.et.aau.dk

Printed in Denmark by UniPrint
ISBN 978-87-92846-18-1

Abstract

As installed capacity of the wind power plants (WPPs) in power system of certain countries increases, stability of the power system becomes more critical. In order to sustain stable power system operation with high share of wind power, system operators of some countries are enforcing more stringent grid code requirements, which are targeting to make the WPPs operate in a closer manner to the conventional power plants. Common to most of the grid codes, WPPs are required to stay connected during short-circuit grid faults, and also inject reactive current in order to support the grid voltage regulation. The uninterrupted operation of WPPs is required even when the grid voltage drops down to zero; and the current injection requirement is defined as positive sequence reactive current irrespective of the fault type; symmetrical or asymmetrical.

In this project, the response of full-scale converter type wind turbines (WTs), in an AC connected WPP, is investigated and control algorithms are designed for minimum disrupted operation and improved grid support, for both symmetrical and asymmetrical grid faults. WTs' response with conventional control algorithms is studied regarding the impact on the WTs and the grid. Alternative control methods are proposed, which are basically active and reactive current reference generation algorithms in positive sequence and also in negative sequence.

It is observed that when WTs inject pure positive sequence reactive current in case of asymmetrical faults in accordance with the grid code requirement, positive sequence grid voltage is boosted, but negative sequence grid voltage is also boosted due to the coupling. As a result higher overvoltages at the non-faulty phases occur. In this thesis

an alternative injection method, where WTs are injecting both positive and negative sequence currents, is given and compared with the conventional method in the sense of grid support performance. Additionally, effect of the coupling between positive, negative and zero sequences during asymmetrical faults, is investigated, which was not considered in the wind power studies before.

It is shown that when reactive current injection is performed during severe symmetrical faults, where the grid voltage is dropping down close to zero, the wind turbines can lose the synchronism with the grid fundamental frequency, which potentially creates risk of instability for the control. This Loss of Synchronism (LOS) situation is investigated based on active and reactive current transfer limits which are derived first time in this thesis, together with stability analysis of the grid synchronization of WTs. Novel control algorithms are developed to generate necessary active and reactive current references, which provide stable operation of the WTs and result in improved grid support.

In summary, the response of the WTs to symmetrical and asymmetrical faults is improved by means of the proposed control solutions, which provide compliance with stringent grid codes, improved grid support with minimum disrupted operation, and a WPP behavior in a closer manner to conventional power plants.

Resumé på dansk

Som installeret kapacitet på vindkraftværkerne (WPPs) i et elsystem stiger, bliver stabiliteten af elsystemet med høj andel af WPPs mere kritisk. For at opretholde en stabil elsystem drift med høj andel af vindkraft, er operatørerne i lande håndhæve strengere grid kodens krav, der er rettet mod at gøre WPPs fungerer på en lignende måde som de konventionelle kraftværker. Fælles for de fleste af de netkrav er WPPs forpligtet til at holde forbindelsen ved kortslutning netfejl, og også tilføre reaktiv strøm for at støtte nettet spændingsregulering. Den uafbrudte drift af WPPs er nødvendig, selv når netspændingen falder til nul, og den aktuelle injektion krav er defineret som positiv sekvens reaktiv strøm uanset fejltype, symmetrisk eller asymmetrisk.

I dette projekt er respons i fuld Convertertype vindmøller (WTs), som står i et AC tilsluttet WPP, undersøgt og reguleringsalgoritmer er designet til minimum forstyrret drift og forbedret grid støtte, for både symmetriske og asymmetriske netfejl. WTs svar med konventionelle reguleringsalgoritmer studeres for virkningerne på WTs'en og gitteret. Alternative metoder er foreslået, som er dybest set aktive og reaktive nuværende referencesatser algoritmer til generering i positiv rækkefølge og også i negativ rækkefølge.

Det bemærkes, at når WTs indsprøjte rene positiv sekvens reaktiv strøm i tilfælde af asymmetriske fejl i overensstemmelse med forsyningsnetkodeks krav, er positiv sekvens netspændingen boostet, men negative sekvens af netspændingen stiger også på grund af koblingen. Som følge højere overspændinger ved den ikke-defekte faser forekommer. I denne afhandling en alternativ injektionsmetode, hvor WTs er injektion

både positive og negative sekvens strømme, er angivet og sammenlignet med den konventionelle fremgangsmåde i betydningen bæringer ydeevne. Desuden effekt af koblingen mellem positive, negative og nul sekvenser under asymmetriske fejl, undersøges, som ikke blev behandlet i de vindenergiproducerende studier før.

Det vises, at når reaktiv strøm injektion udføres under kraftige symmetriske fejl, hvor netspændingen falder ned tæt på nul, er vindmøller mister deres synkront med nettet grundfrekvens, hvilket potentielt giver risiko for ustabilitet for kontrollen. Dette tab af synkronisme (LOS) situation undersøges baseret på aktive og reaktive løbende overførsler grænser, som er afledt første gang i denne afhandling, sammen med stabilitet analyse af nettet synkronisering af WTs. Hidtil ukendte styrealgoritmer er udviklet til at generere de nødvendige aktive og reaktive aktuelle referencer, som giver stabil drift af WTs'en og resultere i forbedret bæringer.

Sammenfattende er respons WTs'en til symmetriske og asymmetriske fejl forbedret ved hjælp af de foreslåede kontrolopløsninger, der giver overholdelse af strenge netkrav, forbedret gitter støtte med mindst forstyrret driften og en WPP adfærd på en måde svarende til konventionelle kraftværker .

Acknowledgements

I acknowledge that this doctorate study was supported by the Aalborg University-Vestas Wind Systems A/S partnership under Vestas Power Program.

I express my sincerest thanks to my main supervisor Remus Teodorescu, co-supervisor Claus Leth Bak from Aalborg University (March 2012 – December 2012), co-supervisor Pedro Rodriguez from Technical University of Catalonia (October 2009 – December 2011), and to Vestas Reference Group members; Florin Iov, Philip Carne Kjær, and Lars Helle from Vestas Wind Systems A/S for their guidance, support, encouragement, and valuable contributions throughout my doctorate study.

I would like to thank Tamas Kerekes for his help involved in experimental work in the department laboratory. I wish to thank all employees in Vestas Technology R&D Singapore, where I spent my four-month study abroad period with their kind hospitability and where I was familiarized with wind turbine and wind power plant control development in a professional R&D environment.

I would like to thank all my colleagues in Vestas Power Program and Department of Energy Technology for their friendship throughout my doctorate study. I wish to thank to the staff of Department of Energy Technology and Doctoral School of Engineering, Science, and Medicine for their help throughout my doctorate study.

I want to dedicate this thesis to Kirse to express my gratefulness for her love making life meaningful and to all my family and friends in Turkey for their generous and continuous moral support.

Table of Contents

List of Abbreviations

AC	Alternating current
CM	Conventional method
CPP	Conventional power plant
DC	Direct current
DFIG	Doubly fed induction generator
DLG	Double line-to-ground
DS	Dual-Sequence
ENTSO-E	European Network for Transmission System Operators for Electricity
FSCWT	Full-scale converter wind turbine
FRT	Fault ride-through
HVDC	High voltage direct current
LL	Line-to-line
LVRT	Low-voltage ride-through
NS	No-support
PCC	Point of common coupling
PI	Proportional and integral
PLL	Phase-locked loop
PR	Proportional resonant
PWM	Pulse-width modulation
RCI	Reactive current injection
RMS	Root-mean-square
SCC	Short-circuit capacity
SCR	Short-circuit ratio
SLG	Single line-to-ground

STATCOM	Static reactive power compensator
TSO	Transmission system operator
VSC	Voltage source converter
WPP	Wind power plant
WT	Wind turbine

Chapter 1

Introduction

In this chapter, background of the thesis is given, as brief review of classical power system stability, changes and challenges in the power system with installation of renewable energy sources. The weak grid issue, which is gaining increasing importance with high penetration of wind power plants in recent years, is discussed up to an extent, together with severe grid faults. Progress of power system needs and correspondingly developed grid codes are discussed. Details of the grid codes, specifically fault requirements, including the dynamic response requirements, for wind power plants are given, which will construct the basis for the problems identified and solved in the following chapters of this thesis. The conventional and state-of-the-art current injection methods by wind power installations are reviewed. The objectives, scope and outline of the thesis are provided at the end.

1.1 Background

The electric power system, being continent wise interconnected, is considered to be the largest controlled system in the world. Stability of the power system has been provided successfully by means of implementation of hardware and software schemes on the power system elements, such as generator controls, protection units, load management, and also regulatory schemes applied by the responsible power system operators of countries worldwide. Power system stability is classified as angle (frequency) and voltage stability [1], where both are classified as large disturbance and small disturbance and also as mid-term and long-term. Short-circuit grid faults, which are the main focus of this thesis, are considered as large disturbances for both angle and voltage stability of the power system.

1.1.1 Power System Response to Grid Faults

Reasons for grid faults are known to be environmental, such as lightning over a tower, fall of a tree on an overhead line, or internal, such as short-circuits due to physical wearing in power system units [2]. Grid faults can be classified as symmetrical (three-phase) and asymmetrical (one, two-phase), where short-circuit to ground can also occur for both types. Positive sequence grid voltage decreases for both symmetrical and asymmetrical faults, whereas negative sequence (and zero sequence) voltage arises in case of asymmetrical faults. As a general practice the "faulted period" ends when the fault is cleared by disconnection of faulted part (line) of the network by means of protection units (relays, circuit breakers) within few hundred milliseconds, and the power system undergoes the "recovery period" taking few seconds back to normal operation unless it is an unstable system [1].

It is known from power system theory that due to the low magnitude of (positive sequence) grid voltage during a fault, rotational machines (generators and motors) can exhibit angle instability, also depending on many factors such as prefault power level, strength of the grid connections, fault clearing time [1]. Not only the rotational machines but also other power system units (e.g. constant power loads) experience problems due to the low grid voltage. The effect of low grid voltage is mitigated when the grid voltage during fault is boosted, which inherently occurs with high fault currents flowing from nearby synchronous generators of conventional power plants (CPP). Hence, in general the grid voltage during a fault is observed to be higher if there exists CPPs nearby the fault and/or the impedance of the network connections is low, which together implies a high Short-Circuit Capacity (SCC) and strong grid. Hence, as a general conclusion, stability of the grid is improved when the grid voltage is boosted towards rated value during fault.

As stated above, during asymmetrical faults negative (and zero) sequence voltages arise in the grid, whereas the drop of positive sequence voltage is not as severe as the symmetrical faults [1]. Therefore, risk of instability during asymmetrical faults is quite low compared to symmetrical faults. However, high zero sequence and negative sequence voltages cause overvoltages in the non-faulted phases; and also the negative sequence voltage causes problems like power (and torque) oscillations in the power

system elements like generators, motors, and grid-connected converters (e.g. distributed generation units, adjustable speed drives). The synchronous generators of CPPs have the capacity for flow of negative sequence currents, which in turn helps to mitigate the negative sequence voltage, whereas the magnitude of zero sequence voltage is mainly dependent on the neutral grounding of the system, mainly through transformers [3]. Effect of asymmetrical faults is assessed in detail in the related parts of the thesis. As a general conclusion, the impact of asymmetrical faults is mitigated when the grid positive sequence voltage is boosted towards rated; and negative (and zero) sequence voltages are attenuated towards zero during fault.

Following the clearance of the fault via disconnection of the faulted part (line) of the network by protection units, power system undergoes the recovery period (post-fault), where the power system recovers back to normal operation [1]. The synchronous generators of CPPs can stay connected during faults and can recover to normal operation after fault unless they are disconnected from the grid due to disconnection of the faulted part. Compared to the prefault conditions, after the fault the system continues with a new equilibrium point with some part of the grid disconnected. The balance for generation and consumption of active and reactive power after fault is crucially important considering the frequency and voltage stability. Additionally, during the recovery period, where the grid voltage is rising back to rated, all the power system elements experience transients, such as re-magnetization of the asynchronous motor loads, restoration of active power consumption. Hence, it is crucial that the power plants stay connected (do not disconnect) during a fault and properly restore back to stable operation. In summary, in case of a fault (which is assumed to be cleared securely by protection units), power system stability requires that;

- power plants stay connected to guarantee power balance after the fault,
- positive sequence grid voltage is boosted towards rated value to mitigate impact of low voltage during fault,
- negative sequence voltage is attenuated towards zero (phase voltages are balanced) to mitigate unbalance effects during fault,
- active and reactive power generation is ramped-up properly during the recovery period to provide restoration of the power system to a new stable point.

1.1.2 Renewable Energy Sources in Power Systems

As the price of the fossil fuels is rising and risk for their availability is appearing worldwide; and above all as the environmental problems and climate change due to excessive use of fossil fuels are being considered seriously by countries, renewable energy, especially the wind energy is becoming more and more important. Hence, more renewable energy sources, especially the wind power plants are being installed in power systems [4], both as new additional units and as replacement of CPPs. As discussed above, CPPs, which are based on synchronous generators directly connected to the grid, have inherent capabilities to provide stable power system operation and participate in the balancing act. The replacement of CPPs with WPPs has influence on the security of the supply since the WPPs do not exactly replace the functional behavior of the CPPs, due to the specific characteristics of the WPPs [5] – [7]. In conjunction with progress of available technology and parallel to the requirements of market and grid, newly installed WPPs are based on the modern wind turbine type of variable speed wind turbines, which can be considered as two types as Full-Scale Converter Wind Turbines (FSCWT) and Doubly-Fed Induction Generator (DFIG) wind turbines [8] – [10]. The variable speed wind turbines have the common characteristics that the active and reactive power (current) are controlled as to be within rated limits and the generation is non-synchronous as machines are connected to the grid through power electronics. Most importantly, disconnection of WPPs in case of grid faults is found to be a huge risk for the power system considering the active and reactive power balance during recovery period of the fault and the balance after the fault [11], [12]. A generic WPP structure is given in figure 1.1, which is the basis within this thesis. As seen in figure 1.1, in a generic WPP, wind turbines have voltage and current feedback at the low-voltage side of their transformers, where they perform controlled active and reactive current (and power) injection; the WPP employs voltage and current measurements, which can be utilized for WPP control actions, at the Point of Common Coupling (PCC), where it is connected to the AC grid; and communication between WPP controller and WTs exist [9], [13].

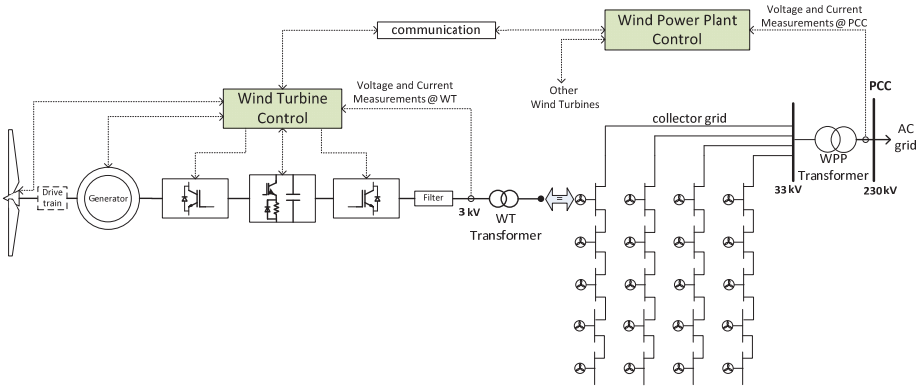

Figure 1.1 Generic WPP system based on FSCWTs.

In order to provide stable power system operation with increasing capacity of WPPs, the countries, especially the ones with high wind penetration, have been applying regulations for WPPs as grid codes for wind power integration, with extent being increased continuously [14] – [21]. In recent grid codes, WPPs are required even to contribute to frequency and voltage stability of the power system, via responding with synthetic inertias, primary frequency control, voltage regulation and power oscillation damping functions [21]. Regarding the faults, common to most of the grid codes as a fundamental requirement, WPPs are required to stay connected (not to be disconnected) in case of grid faults, in order to sustain active and reactive power balance after the fault. This action of staying connected, which is called as Fault Ride-Through (FRT), is required even when the grid voltage drops down to zero in certain grid codes [17], [21]. In addition to FRT requirement, WPPs are required to support the grid voltage via injecting reactive currents during the fault, including both the faulted and recovery period, in order to regulate the grid voltage towards rated value. This action of injecting reactive current during fault, which is called as Reactive Current Injection (RCI), has magnitude limited to rated current of wind turbines in accordance with their technology. The WPPs are required to inject reactive current during faults, which can be considered as a voltage control action, in order to regulate the grid voltage during fault to improve angle stability of the power system [22], and to support the grid during recovery period of the fault to avoid any voltage collapse event [23]. Details of the grid

code fault response requirements are given in the following sections. In summary, with the grid codes, WPPs are aimed to behave in a similar manner to CPPs.

As stated above, WPPs are not having the same functional capabilities and capacities as CPPs considering active and reactive power generation and control. Regarding the faults, current injection from WPPs is limited by their rated values (e.g. 1pu) or can be slightly higher for short-term (e.g. 1.25pu), which is quite low compared to high (2-5pu) fault currents from CPPs. Additionally, when the wind resources are far from generation and consumption centers, the WPPs are connected with long lines and the power system is expanded with long connections. As a result of these and replacement of CPPs with WPPs, the grid with high penetration of WPPs becomes weak grid. In conclusion, installation of WPPs to power system is a challenge for providing the power system stability.

1.1.3 Weak Grid and Severe Fault Considerations

With the increasing share of renewable energy sources and also due to other reasons discussed below, power systems are becoming less strong, i.e. weak grid. Strength of a grid, or specifically of a bus in the grid, can be represented by its Short-Circuit Capacity (SCC), which is related to the amount of current flowing to a solid fault at this bus [24]. When grid seen from a bus is represented by its Thevenin equivalent as seen in figure 1.2-(b), the SCC is calculated as below;

$$SCC = \frac{V_{grid}}{Z_{grid}} \tag{1.1}$$

Hence, lower the Thevenin equivalent impedance, stronger the grid is. The Short-Circuit Ratio (SCR) of a bus, where a WPP is connected, is ratio of the SCC at the related bus to the rating of the WPP(s) connected at this bus;

$$SCR = \frac{SCC}{S_{WPP(s)}} \tag{1.2}$$

The following is a definition of the strength of an ac system in [25]:

- strong system, if the SCR of the ac system is greater than 3.0.
- weak system, if the SCR of the ac system is between 2.0 and 3.0.
- very weak system, if the SCR of the ac system is lower than 2.0.

In German VDN grid code [17], it is stated that the initial SCC present at the grid connection point and also after fault clearance shall be greater than 6 times the total amount of nominal active powers of all wind energy plants connected at the related connection point; implies that a strong network with minimum SCR of 6 (Z_{grid} smaller than 0.17pu) is guaranteed by the related Transmission System Operators (TSO) for the connection of the WPP. In Danish grid code [20], SCR is suggested to be used as 10 within system studies, implying a very strong system, which is possible in Denmark. However, in certain countries and in certain cases and with the increasing installation of renewables, SCR can go lower [26] – [32], even below 2. A grid becomes weak grid;

- if network has high impedance lines, and/or not connected to strong neighboring networks, expanded to a large area with long lines, then the related network has low SCC overall (weak grid);
- if the power system becomes highly renewables based generation replacing the CPPs as seen in figure 1.2-(a), then the SCC at all buses gets lower (weak grid),
- if network has poor lines and/or the bus, where WPP is connected, is located far away, then the related bus has low SCC (weak bus),
- if rich wind resources are further away from centers, then there is need for a connection line which would result lower SCC at PCC of WPP (weak bus),
- additionally, if the WPP has high internal impedance (transformers and collector grid), SCC becomes even lower at WT terminals (for a grid fault external WPP).

Severity of a fault is highly related with the duration of the fault and the voltage drop during fault [1]. Voltage drop during a fault is mainly related to fault impedance and strength of the grid. In this thesis, a “severe fault” for a WPP means a fault, where the voltage at the PCC of the WPP is measured lower than a certain value (e.g. 20%); and a “non-severe fault” is a fault with voltage higher than that certain value. A severe fault for a WPP occurs due to some or all of the below cases;

- if fault location is near to WPP (e.g. at PCC or at buses 1 to 4 in figure 1.2-(a))
- if the fault impedance is very low (i.e. solid fault)
- if the bus, where the WPP is connected, is a weak bus (low SCC); which means that the WPP is located far from the central generation and/or it is a weak grid.

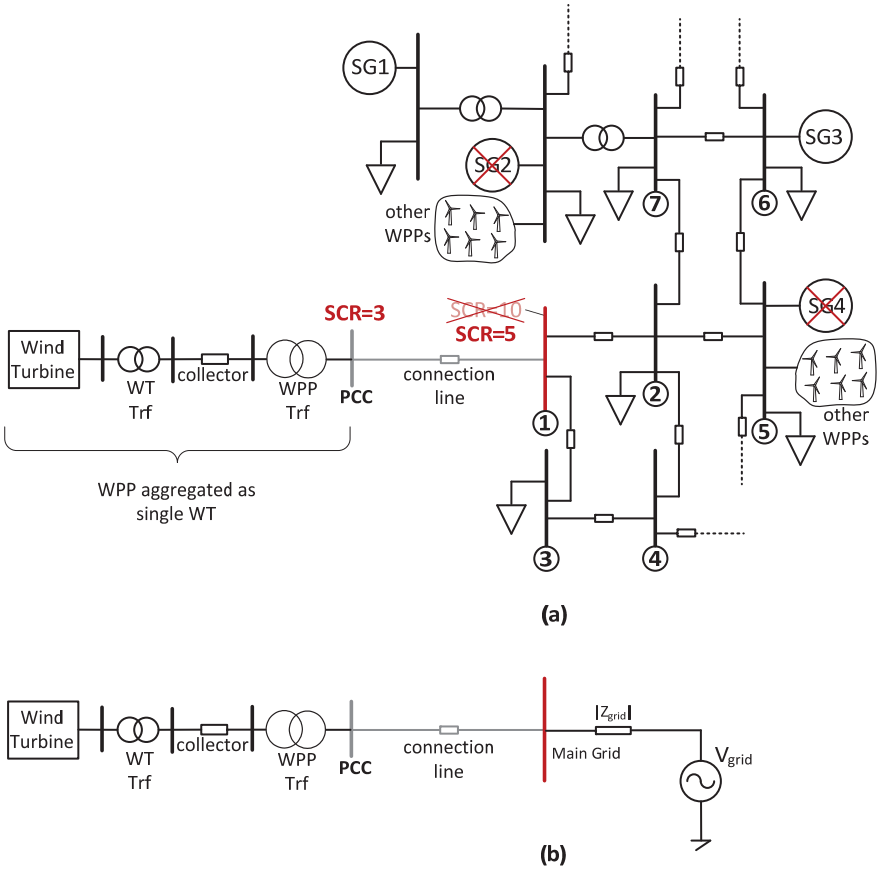

Fig. 1.2 (a) Low SCR connection with representative SCR values, (b) Thevenin equivalent of main grid.

Fault impedance magnitude and characteristics has not been paid sufficient attention in previous wind power studies, though it is a very important factor affecting the severity of a fault. In previous wind power fault studies, which are reviewed in the following sections, the fault impedance magnitude is adjusted to obtain a remaining voltage convenient for the scope of the related study. In practical, a symmetrical solid fault at PCC or nearby can result in a very low (e.g. 2%) voltage at the faulted point, even for a strong system with low grid impedance. Such low voltage occurrences are also covered within grid code requirements, which are detailed below.

1.2 Overview of Grid Code Requirements

In this section, in relation to the main scope of this thesis, grid codes are reviewed focusing on the fault response requirements for WPPs and wind turbines. Requirements from two exemplary grid codes are reviewed with details; namely the German VDN grid code [17], which is one of the most established grid codes in the world inspiring the followers, and the recently published European Network for Transmission System Operators for Electricity (ENTSO-E) grid code, which is prepared by a consortium to be the common grid code frame for all European countries [21].

The German VDN grid code [17], covering WPPs connected to transmission and sub-transmission voltage levels, is introducing the FRT and RCI requirements for the WPPS. Regarding the FRT requirements, the WPPs are expected to stay connected even when the grid voltage drops down to zero, as seen in figure 1.3-(a). The RCI requirement is requested as a proportional voltage control scheme, where the gain can be adjustable between 0 and 10 and with a deadband applied to the voltage deviation, as seen in figure 1.3-(b). The reactive current during fault is requested as additional to the prefault reactive current, where the total reactive current magnitude is limited to the rated (1pu) value. As a result, with a moderately selected gain of 2, which is the default value [17], 1pu reactive current is injected when the voltage drops below 50%. Active current is allowed to be decreased in order to keep the total current within capability of the wind turbine. Additionally, dynamics of step response for the reactive current is defined as seen in figure 1.3-(c). It is requested that the reactive current rise time is 30msec and settles within a tolerance of -10%/+20% within 60msec, following the occurrence of the fault. In [17], the FRT requirement is defined for the PCC of the WPP; whereas the RCI requirement is stated to be realized at the wind turbine level at low-voltage side of the wind turbine transformer, but also verification at PCC level is encouraged in order to allow innovative WPP solutions.

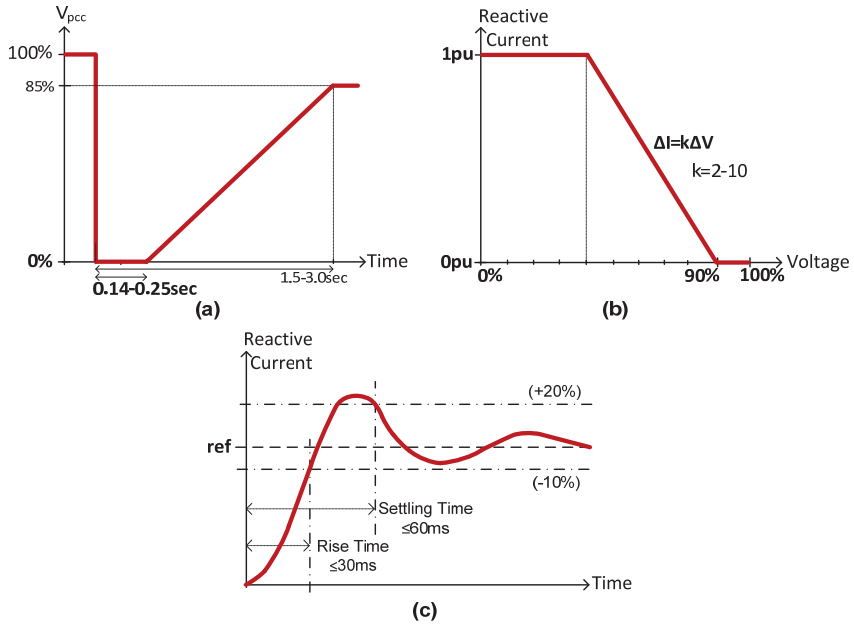

Fig. 1.3 German VDN grid code fault response requirements; (a) FRT, (b) RCI, (c) RCI step response requirements [17].

Regarding the recovery period of the fault, the RCI injection based on voltage drop is required to be continued for 500 milliseconds following the clearance of the fault, and active power ramp-up requirement is set as increase of active power between 10% and 20% of the nominal value per second.

In summary, German VDN grid code is requesting the WPPs to realize a proportional voltage control scheme at the PCC point and behave in a similar manner to CPPs during faults. There are similar requirements in many of the grid codes from other countries and TSOs [14] - [15].

Regarding the fault response requirements, ENTSO-E code is similar to the German VDN grid code, with few differences. As seen in figure 1.4, the FRT requirement of ENTSO-E is almost the same as VDN's, requiring the transmission level connected WPPs to stay connected even when the grid voltage drops down to zero. The dynamic step response requirement for the RCI is more stringent in ENTSO-E than in VDN. It is stated that the WPP or the individual WTs "shall be capable of providing at least 2/3 of

the additional reactive current within a time period specified by the relevant TSO, which shall not be less than 10 milliseconds and the target value of this additional reactive current shall be reached with an accuracy of 10% within 60 milliseconds from the moment the voltage deviation has occurred" [21].

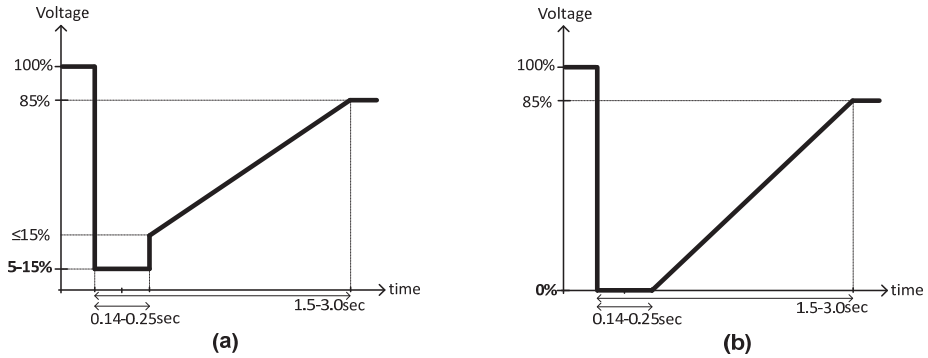

Fig. 1.4 ENTSO-E grid code FRT requirements (a) <110kV, (b) ≥110kV [21].

Regarding the asymmetrical faults, the maximum reactive current requirement in VDN grid code [17] is set to be 40% of the rated, much lower than the 100% for symmetrical faults; however any explanation is not provided. Additionally in Spanish grid code [18], [19] only informative statement is given about the flow of negative sequence currents. In ENTSO-E grid code, FRT response during asymmetrical faults and current injection is stated to be defined by agreements between system and plant operators. It can be commented that asymmetrical faults are not targeted exclusively within grid codes, likely due to the reason that asymmetrical faults are not severe faults and do not carry high risk for power system stability [33]. However, in the transmission system of power systems, asymmetrical faults are observed more frequently with occurrences as single line-to-ground (SLG) faults with 70%, line-to-line (LL) faults with 15%, double line-to-ground (DLG) faults with 10%, than symmetrical faults with only 5% occurrence [34]. Considering that asymmetrical faults are occurring more frequently than symmetrical faults, specific requirements for asymmetrical faults can be more beneficial.

In summary, the existing grid codes are requiring the WPPs to stay connected and inject positive sequence reactive currents proportional to the voltage deviation, irrespective of the fault type is symmetrical or asymmetrical; and even for severe faults with grid voltage close to zero. In this thesis, two specific problems, which are explored in case of reactive current injection during severe symmetrical faults, and pure positive sequence reactive current injection during asymmetrical faults, are investigated and solved by proposed methods in the following chapters.

1.3 Review of Grid Support by Wind Turbines during Faults

In accordance with the grid code requirements, modern wind turbines are equipped with the capability to stay connected and to support the grid during faults [13]. The conventional method for current injection during faults, complying with the RCI requirement, is given in figure 1.5 below. In the figure, I_{gcm} is the grid code maximum reactive current value, which is required as the rated current (1pu) value in general.

As seen in figure 1.5, which is employed as the conventional control method during faults, active and reactive current references are generated based on the voltage at the feedback terminals, and DC link voltage regulation, respectively. During a low voltage fault, the active power that can be injected to the grid decreases due to low grid voltage. Additionally, since priority is given to reactive current injection in order to fulfill the grid code requirement, low or zero capacity remains for the active current, depending on the current capability of the wind turbine. Due to these reasons, the excess active power flowing from the machine side converter, which cannot be injected to the grid, is dissipated on the chopper resistance. In figure 1.5, block-1 generates the reactive current reference based on the grid code profile and the voltage measured at the terminals. The consideration for prefault reactive current value is omitted for simplicity in figure 1.5. In block-3, the remaining current capacity ($I_{active\text{-}limit}$) is calculated based on the current capability of the wind turbine grid side converter ($I_{capable}$) and the reactive current reference. Then, the active current reference is limited to be less than limit ($I_{active\text{-}limit}$) value.

Two representative cases for active and reactive currents are shown on the grid code reactive current profile in figure 1.6. It is important to note that, the grid code

maximum reactive current requirement value (I_{gcm}) can be either equal to or smaller than the wind turbine current capability ($I_{capable}$). Wind turbine grid-side converter can have higher capacity (e.g. 1.25pu) or can be overloaded for a short-term during fault; hence as in figure 1.6-(b) there can be remaining capacity for active current even when the reactive current reference reaches grid code maximum reactive current value. The active current can be injected as any value in the scanned areas, depending on the active power flow from machine-side converter.

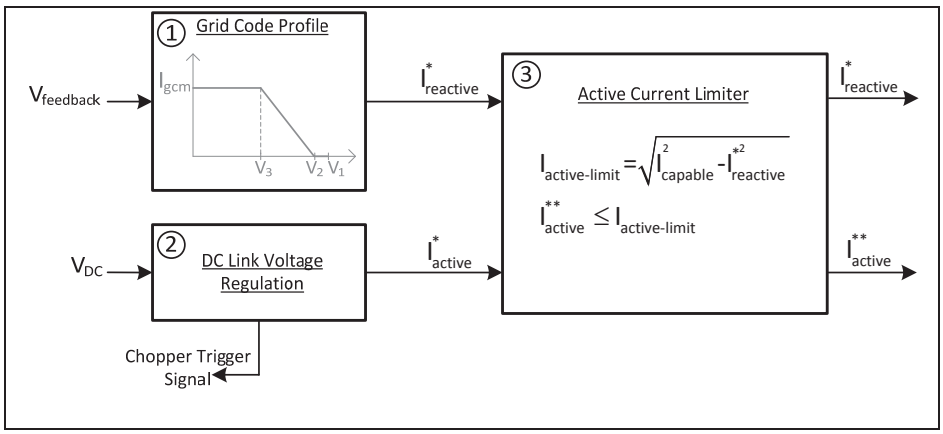

Fig. 1.5. Conventional method for current reference generation during fault.

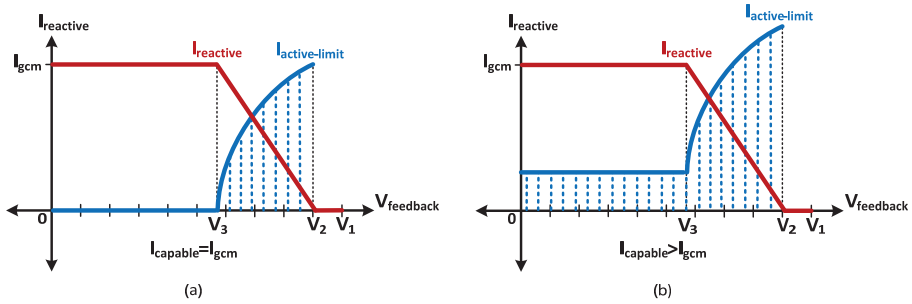

Fig. 1.6. Current references with conventional method (a) $I_{capable} = I_{gcm}$ (b) $I_{capable} > I_{gcm}$.

In accordance with the grid code requirements and operational requirements, modern wind turbines are designed to have the capability of injecting active and reactive

current (power) independently, i.e. as vector current control with the required dynamic bandwidth. In order to realize active and reactive current control at the wind turbine terminals, well-established current control and grid synchronization methods are utilized [35] – [43]. In general, current control can be performed in two ways; as a double synchronous frame regulator based on PI compensator and as a stationary frame regulator based on a PR compensator. Both control structures employ grid synchronization schemes as Phase Locked-Loop (PLL) or Frequency Locked-Loop (FLL).

The current regulator and grid synchronization algorithms are designed and tuned to provide the necessary dynamic response requirements. As a general approach, current regulation bandwidth, which is also highly dependent on sampling and switching frequency of the wind turbine converter, is designed to reach a time constant of 0.5ms – 5ms [44], which even complies with the stringent 10msec rise time requirement of ENTSO-E grid code. The grid synchronization is tuned to have a time constant larger than fundamental period (e.g. 20msec) to track the grid angle with necessary dynamic response and to realize high performance vector current control. Details of the current regulator and grid synchronization functions and parameter settings in this thesis are given throughout the related parts of the thesis and also in appendix.

As the fundamental requirement common to most of the grid codes [14] – [21], FRT and RCI requirements has drawn great attention both by academia and wind power industry. Several research studies on requirement, impact, implementation of FRT and RCI have been accomplished [45]-[73].

Regarding FRT of wind turbines during symmetrical faults [45] – [56], research has been concentrated on two main topics; impact of faults on wind turbine stability (e.g. dc link voltage control, generator speed, current control) and impact of wind turbines' fault response on the grid (stability of the power system and nearby units). In [45], transient oscillations occurring in the dc link voltage and generator speed of a full-converter type wind turbine is proposed to be solved. In [46] – [48], rise of dc link voltage during symmetrical faults due to incoming active power from generator side is suggested to be solved by use of chopper, additionally blocking due to high dc link voltage and restart of converters is studied in [47]. Impact of wind turbines' fault

behavior on power system stability is thoroughly studied in [49] – [53]. Response of an induction motor load nearby PCC is compared for cases with and without RCI support from wind turbines, and improvement obtained is given in [49]. Transient stability of part of the network nearby a WPP is investigated and RCI schemes to improve angle stability of nearby synchronous generators are proposed in [50]. In [53], advanced control methods to control current of a converter during grid faults to avoid over current events are proposed. In [54], interaction between wind turbine fault response and structural behavior of tower and blade oscillations is investigated. In [55], wind turbines connected as a WPP are investigated for their stability against resonance within the collector network, considering the shunt capacitances of the cables; and a method is proposed to be implemented for each wind turbine to avoid resonance due to interaction of the closed loop current control of wind turbine grid side converter. Hence, the previous symmetrical fault studies are either focusing on wind turbine stability in the sense of dc link and generator side; or impact of wind turbine response on the grid side. Additionally, within these fault studies, the grid voltage is analyzed to drop down to 10% of rated but not lower; despite the grid codes [14], [17], [21] have requirements for zero grid voltage. In practical, during a symmetrical solid fault near PCC of a WPP, voltage can drop down close to zero for the WPP, which is a case not comprehensively covered in the previous studies. In this thesis, a previously underestimated and omitted phenomenon of converter (angle) instability problem as Loss of Synchronism (LOS) is explored, investigated and solved, which is specifically encountered during RCI to very low voltage (for example less than 10% of rated) fault cases. The mentioned problem with very low voltage faults is handled only in [56], which targets only highly active current injection during fault, as will be assessed in detail in the related chapter five. In [57], simulation and test results are given for a full-converter wind turbine, for a zero voltage fault, however fault is created at the turbine terminals, not at PCC of the WPP, and detailed information about active and reactive current (power) injection scheme is not provided.

Regarding the asymmetrical faults, considerable amount of research is conducted for analysis and control development for wind turbines' response during asymmetrical faults. Main focus topics have been mitigation of the impact of asymmetrical faults on

the wind turbines. For instance in [58] – [65], control schemes are developed to mitigate twice the grid frequency oscillations occurring during asymmetrical faults. In [66], oscillations are damped also considering the power loss on the filter impedance. Classifications for unbalanced voltage profiles observed at the wind turbines terminals is provided in [67], whereas proposals for asymmetrical test procedures are given in [68]. From the grid point of view, the approach of reducing the negative sequence voltage (balancing the grid voltages) via injecting underexcited (inductive) reactive currents by wind turbines is studied in [69] – [72], and as a Statcom capability in [72]. However, most of the previous asymmetrical fault studies are focusing on control via wind turbine point of view, not many are considering the impact of wind turbines' response on the power system. Only in [73], overvoltage problem at the non-faulty phases is handled. However, with increasing share of wind power, a need for assessment of wind turbines impact on the power system during asymmetrical faults arises. In this thesis, impact of wind turbines' reactive current injection on the power system is investigated comparing conventional method of positive sequence reactive current injection with alternative methods of injecting both positive and negative sequence reactive currents. The physical phenomenon of coupling between positive, negative and zero sequence networks during asymmetrical faults, which has not been considered in the previous studies, is explored and taken into account in wind turbine control.

In summary, this thesis is contributing to the fault literature with the two focus areas below;

- Stability of full-converter wind turbines during current injection to severe symmetrical grid faults (e.g. 5% voltage at PCC); exploring the Loss of Synchronism (LOS) problem and proposing novel solutions to provide wind turbine stability.
- Impact of reactive current injection of full-converter wind turbines on the power system voltages during asymmetrical grid faults, which are occurring at or near to PCC of a WPP.

1.4 Motivation and Objectives

Main motivation of this project is to develop new control strategies for wind turbines' fault response that can enable increased wind power penetration in existing power systems without degrading the stability. As discussed above and in literature, risks for security of a stable power system arise with high penetration of wind power, mainly due to distinct characteristics of wind power installations. In this project the purpose of making the WPPs behave similar to CPPs is targeted, focusing on the response of WPPs during symmetrical and asymmetrical grid faults. In the FRT and RCI requirements of certain grid codes [14], WPPs are expected to stay connected and inject reactive current during symmetrical faults even when the grid voltage drops down to zero. WPPs are also required to stay connected and inject positive sequence reactive current during asymmetrical grid faults, which in turn helps to boost the positive sequence grid voltage.

First, it is shown that when reactive current is injected during severe symmetrical faults with grid voltage close to zero (e.g. 5% of rated), wind turbines lose their synchronism with the fundamental frequency (e.g. 50Hz) of the main grid, named as Loss of Synchronism (LOS) problem. In this thesis the LOS problem is explored in detail and novel methods are developed to provide wind turbine stability and in turn helping the power system stability during severe symmetrical faults.
Secondly, it is shown that when pure positive sequence reactive current is injected during asymmetrical grid faults, positive sequence grid voltage is boosted, but negative and zero sequence voltages are also boosted due to coupling between sequences. As a result, higher phase overvoltages at the non-faulty phases and higher negative sequence voltages in the grid are observed. In this thesis detailed analysis of asymmetrical faults and improved grid support is obtained by means of an alternative injection method.

Focusing on two specific cases, which have not been studied thoroughly before, the main objectives are set as below;

- Provision of reactive current injection during severe symmetrical grid faults even when the grid voltage drops down close to zero, such that the wind

turbines are not disconnected and continues stable operation during fault, the grid voltage is supported; and the wind turbines can continue their operation without interruption.

- Provision of positive and also negative sequence current injection during asymmetrical grid faults, the positive sequence grid voltage is boosted, negative sequence grid voltage is attenuated; and the grid voltage support is improved compared to the conventional method.

1.5 Scope of the thesis

As stated in the objectives, the response of WPPs during symmetrical and asymmetrical grid faults is investigated and control solutions are developed within this thesis. Two specific cases are investigated and control solutions are developed for problems occurring during these cases. For both of the cases only the faulted period (from the instant of the fault occurrence till the clearance) of the fault is considered, excluding the recovery period. Any disturbance caused by disconnection of any (faulted) line in conjunction with the fault clearance is kept out of scope.

The WPP under investigation is an AC connected WPP, which can be onshore and offshore as well, and composed of several FSCWTs, with several MW (e.g. 5MW) ratings. Being not limited; the WPP rating is chosen to be around few hundred megawatts (100MW) and connected to sub-transmission (e.g. 100kV) or transmission (e.g. 230kV) levels. However, the analysis and developed solutions can be applied to wind turbines singly connected to medium voltage (e.g. 30kV) level. The WPP under scope is not considered to have any units connected to its PCC point, such as Statcom or cap banks.

The studied asymmetrical faults are shunt (parallel) type asymmetrical faults, which are commonly observed in the transmission system [34], as; single line-to-ground (SLG), double line-to-ground (DLG), line-to-line (LL). Rarely observed series (open circuit) asymmetrical faults are not considered within scope.

Mathematical analysis is accomplished based on the Thevenin equivalent of the grid at the connection point, whereas a connection line (e.g. overhead line or underground cable) is included with its PI models. The WPP in mathematical analysis is an aggregated WPP structure, as a single wind turbine with rating equal to the rating of the WPP, and with equivalent collector network impedance [74] – [76].

Within the mathematical analysis, simulation models, and analysis of the response of the wind turbine during faults, the rotor aerodynamics of the FSCWT, the generator side converter, the generator itself and the dc link are represented as a constant dc voltage source since these parts have low bandwidth compared to the short duration of the faults [77], and additionally since the focus is given to grid impact and control of wind turbine current injection during faults. Additionally, since the scope is not having power electronics aspect, the switches in the grid-side converter of the wind turbine are neglected and the converter is modeled using ideal controlled voltage sources [78].

The outline of the thesis is as follows;

Chapter 1: Introduction, presents background of the project, including impact of wind power plants on power system stability during faults, and correspondingly developed grid code requirements for wind power plants; also provides an overview of wind turbine control during faults and the conventional method for current reference generation during faults. The chapter is concluded with motivation, objectives and scope of the project.

Chapter 2: Identified Problems during Grid Faults*,* provides detailed representation of the problems encountered when the conventional method of current reference generation is utilized during grid faults, with simulation results of several cases. The phase overvoltage and coupling problems observed during asymmetrical faults and Loss of Synchronism (LOS) problem during severe symmetrical faults are introduced.

Chapter 3: Active and Reactive Current Transfer Limits*,* is derivation of current transfer limits between two buses, which is a basic but fundamental theoretical reference for active and reactive current injection from wind turbines.

Chapter 4: Analysis of Loss of Synchronism (LOS) during Symmetrical Faults, explores the source of the LOS problem observed during severe symmetrical faults,

showing the relation with the active and reactive current transfer limits. Results and stability limits derived from large-signal stability analysis of the grid synchronization scheme (PLL) are also given, which shows consistency with the current transfer limits derived in chapter 3. In this chapter, simulation results of observed LOS problem are verified with experimental investigation on a grid-connected converter. Small-signal stability analysis of the PLL is also accomplished, which serves for development of control algorithms in the next chapter.

Chapter 5: Proposed Solutions for Loss of Synchronism during Symmetrical Faults, starts with review and assessment of state-of-the-art solutions for LOS problem, and continues with detailed presentation of solutions proposed in this thesis. The proposed novel PLL frequency based current reference generation algorithm is verified with simulation and experimental investigations. At the end, comparison of current reference generation schemes from point of view of wind turbines' fault ride-through and reactive current injection requirements is done.

Chapter 6: Analysis of Asymmetrical Faults, explains the cause of identified problems during asymmetrical faults, which were shown in first part of chapter 2. Additionally, effects of unbalance both for short-term and long-term are summarized as a reference for negative sequence current injection.

Chapter 7: Control Solutions for Asymmetrical Faults**,** reviews control methods during asymmetrical faults, and presents the alternative dual-sequence current injection method, which is shown to yield improved grid support with simulation results.

Chapter 8: Multi-Turbine Case with Proposed Method, involves application of proposed control solution as implementation for multi-turbines.

Chapter 9: Conclusion, summarizes the thesis and lists the main contributions and future work.

Appendix includes analysis for impact of WPPs' support on the grid voltage, emphasizing the importance of fault impedance characteristics and parameters used within wind turbine control algorithms.

1.6 List of publications

Publication 1 reviews the grid code requirements, which are given in chapter 1. Publication 2 is incorporated in chapter 1 as a general state-of-the-art of generic wind turbine control. Publication 4, is the short-circuit calculation tool utilized to analyze asymmetrical faults in chapter 6. Publication 5 includes asymmetrical fault studies covered mainly in chapter 2, 6 and 7. Publication 6 covers the LOS problem and the proposed PLL frequency based solution placed in chapters 2, 3, 4 and 5.

P1. Mufit Altin, Ömer Göksu, Remus Teodorescu, Pedro Rodriguez, Birgitte Bak-Jensen, and Lars Helle, "Overview of recent grid codes for wind power integration," International Conference on Optimization of Electrical and Electronic Equipments, Romania, May 2010

P2. Ömer Göksu, Remus Teodorescu, Pedro Rodriguez, and Lars Helle, "A Review of the State of the Art in Control of Variable-Speed Wind Turbines," 9th International Workshop on Large-Scale Integration of Wind Power into Power systems, Quebec, Canada, October 2010

P3. Andrzej Adamczyk, Mufit Altin, Ömer Göksu, Remus Teodorescu, and Florin Iov, "Generic 12-Bus Test System for Wind Power Integration Studies," EPE Joint Wind Energy and T&D Chapters Seminar, Aalborg, Denmark, June 2012

P4. Ömer Göksu, Remus Teodorescu, Birgitte Bak-Jensen, Florin Iov, and Philip Kjær, "An Iterative Approach for Symmetrical and Asymmetrical Short-Circuit Calculations with Converter-Based Connected Renewable Energy Sources. Application to Wind Power," IEEE Power & Energy Society General Meeting, San Diego, USA, July 2012

P5. Ömer Göksu, Remus Teodorescu, Claus Leth Bak, Florin Iov, and Philip Kjær, "Impact of Wind Power Plant Reactive Current Injection during Asymmetrical Grid Faults," IET Journal of Renewable Power Generation, accepted.

P6. Ömer Göksu, Remus Teodorescu, Claus Leth Bak, Florin Iov, and Philip Kjær, "Instability of Wind Turbine Converters during Current Injection to Low Voltage Grid Faults and PLL Frequency Based Stability Solution," IEEE Transactions on Power Systems, under review.

Chapter 2

Identified Problems during Grid Faults

In this chapter, identified problems, when conventional method for current reference generation is employed during asymmetrical and symmetrical grid faults, are given. It is shown that during asymmetrical grid faults, if the wind power plant is injecting pure positive sequence reactive current, the positive sequence voltage is boosted as desired; but negative and non-faulted phase voltages are also boosted. The loss of synchronism (LOS) problem, which is observed during severe symmetrical faults, is described and shown with simulations. It is shown that, depending on the wind turbine current injection, i.e. active and reactive current magnitudes, and the voltage magnitude at the faulted bus, the wind turbines can lose their synchronism with the fundamental frequency (e.g. 50Hz) of the grid.

2.1 Problems Observed during Asymmetrical Grid Faults

As a conventional method (CM) complying with the grid code requirement of reactive current injection, modern WTs are injecting pure positive sequence (symmetrical) currents boosting positive sequence voltage. The magnitude of the reactive current is limited to current capacity (e.g. 1pu) of the wind turbine, whereas the conventional power plants (CPP) can inject higher values (e.g. 3pu). Positive sequence reactive current injection by WPPs helps the grid voltage via boosting the positive sequence voltage, in case of low voltage faults. However, as will be shown below, when this conventional method is employed in case of asymmetrical faults, which is injection of pure positive sequence current and keeping negative sequence current as zero, all three phases, including the non-faulty phase(s) are boosted. Since negative sequence current injection of WPP is kept as zero, which means that WPP behaves as open circuit in

negative sequence, negative sequence voltage is not attenuated and propagates towards the WPP. Though only positive sequence current is injected, it is observed that negative and zero sequence voltages are additionally boosted at the fault point, due to coupling. Consequently, higher negative sequence voltage and higher phase overvoltages are observed towards WPP.

Comparison of three cases are given in figure 2.1; in the first case response of a CPP based on synchronous generators to a SLG fault (at phase-"a") is shown, in the second case CPP is supplanted by a WPP, which is injecting zero current during the fault, in the third case WPP is injecting pure positive sequence current in accordance with the CM. The voltage magnitudes and phase angles are obtained from time-domain simulations. In both cases power plants are connected radially to the main grid via 20km long overhead lines. As observed from figure 2.1-(a) and (c), in positive sequence both power plants are boosting the positive sequence voltage by means of supplying fault currents. As expected, CPP can boost the positive sequence voltage more than the WPP, due to high current capability of CPP.

Comparing the phase voltages in figure 2.1(b) and 2.1-(c), it is observed that with the use of CM, which is injecting pure positive sequence currents, non-faulty phases ("b" and "c") are boosted from 1.08pu to 1.13pu at the faulted point, and from 0.95pu to 1.04pu at PCC, unnecessarily above rated. Additionally, even though only positive sequence reactive current is injected, negative sequence voltage at the faulted bus increases from 0.28pu to 0.30pu due to the coupling. Hence, high negative sequence voltages and phase overvoltages are observed in the power system, with the use of CM.

In zero sequence, which is not shown in figure 2.1 for clarity, both CPP and WPP give the same response since they both employ dYN transformers, which are grounding the neutral of the grid side, and also isolating the zero sequence networks of power plant and the grid side. Hence zero sequence currents flow, and zero sequence voltage is attenuated towards the power plants in both cases.

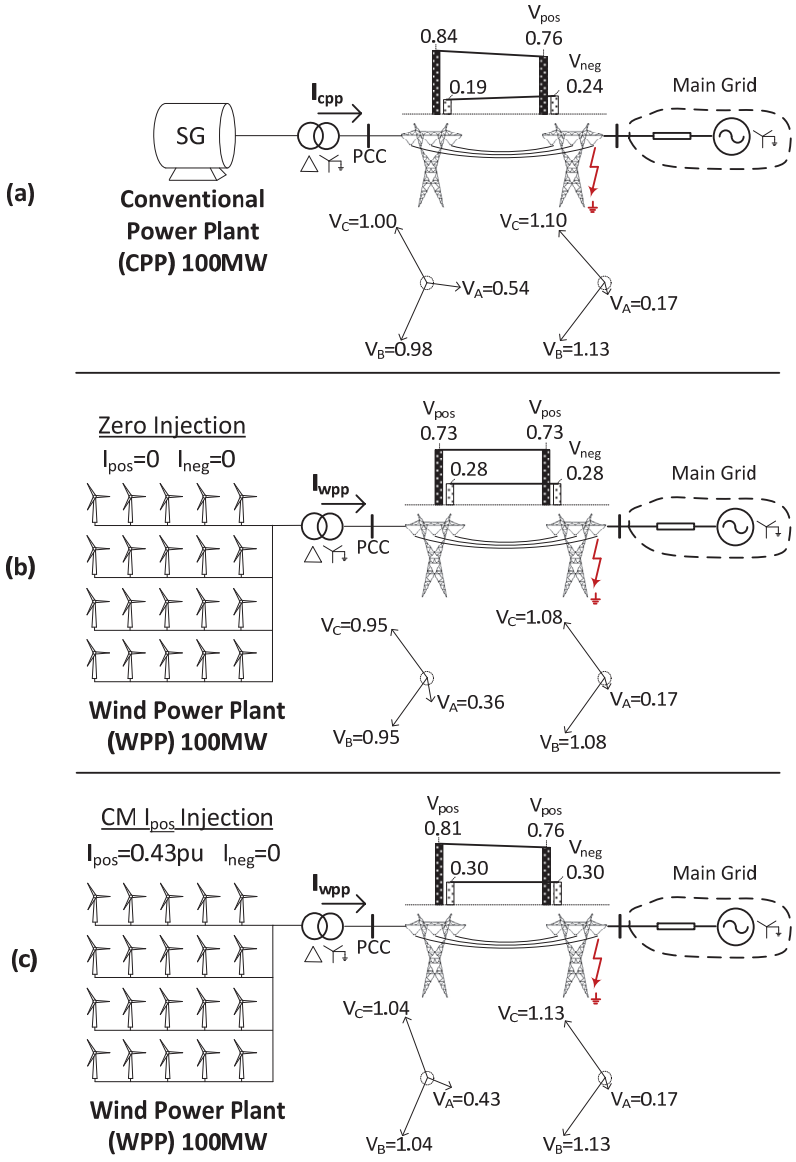

Figure 2.1 SLG response of (a) CPP, (b) WPP with zero current, (c) WPP with CM.

Detailed analysis of the identified problems, and control solutions during asymmetrical faults will be given in chapter 6 and 7, respectively. In the following part of this chapter and consequent chapters (3, 4, and 5), analysis of problems and solutions for the symmetrical faults will take place.

2.2 Loss of Synchronism during Symmetrical Grid Faults

2.2.1 Simulation Case

Structure of a generic WPP, utilized in this chapter, is shown in figure 2.2. The WPP has a rating of 100MW and composed of 20 of FSCWTs each having 5MW ratings. The WPP is aggregated as a single wind turbine with equivalent of collector grid. The wind turbine is performing grid synchronization and current control action at the low voltage side of the WT transformer. The impedance between the WT control terminal and the PCC has a magnitude of 0.21pu with and X/R of 8, which is composed of the WT transformer, collector grid, and the WPP main transformer. The PCC is connected to the main grid via a 20km line, which has impedance of 0.1pu with X/R of 4. The main grid is represented with its Thevenin equivalent with impedance of 0.1pu and X/R of 10 (SCR is 10).

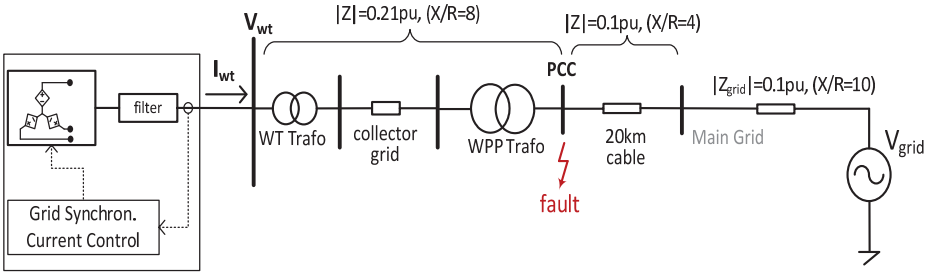

Fig. 2.2 Aggregated WPP diagram and Thevenin equivalent grid of simulation study.

Within the simulation cases in this section, a symmetrical short-circuit fault is created at the PCC point, where the fault impedance is adjusted to have remaining voltage magnitudes as 2%, also 10% and 25% of the rated during the faults. The fault is created at time is equal to 1 second and removed at time is equal to 1.4 second, as will be seen in the following simulation results.

The grid synchronization algorithm, PLL, implemented within the WT is shown in figure 2.3 below. As well-known, within the PLL, a frequency signal is calculated, which is integrated to obtain the phase angle of WT terminal voltage, θ_{wt}. The estimated angle θ_{wt} is used within the current control algorithms to obtain active and reactive current components and to generate necessary voltage at the converter output.

For observation of a clean frequency signal without transients a Low-Pass Filter, which has a cut-off frequency of 30Hz, is applied to the raw frequency signal in simulation results.

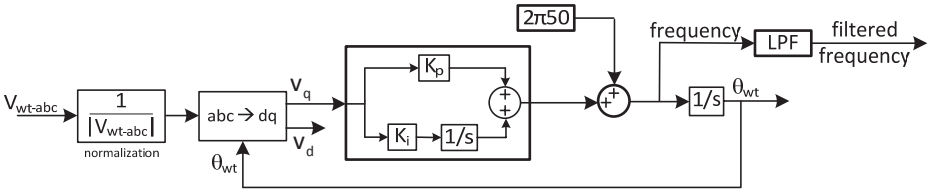

Fig. 2.3 Generic PLL structure.

Three fault cases, cases 1 to 3, where the PCC voltage drops to 2% of the rated, are shown in the following sections.

In case-1 (figure 2.4), the WT is injecting pure reactive current with magnitude of 1pu during the low voltage fault. In this case, the WT frequency, which is the frequency of the voltage at the WT terminals calculated by the PLL, drops down close to 0Hz during the fault. In other words, frequency of the voltage and current generated by the WT drop down to 0Hz; though the frequency at the faulted point (PCC) is still around 50Hz. This event is called as Loss of Synchronism (LOS) - frequency fall, which will be studied in the following chapters.

In case-2 (figure 2.5), the WT is injecting 1pu reactive current and 0.125pu active current during the low voltage fault. However, for certain reasons, which will be given in the next chapters, the WT frequency stays stable (synchronized to the grid) around 50Hz in this case.

In case-3 (figure 2.6), the WT injects highly active current of 0.65pu magnitude and still 1pu reactive current, which results in total current magnitude of 1.2pu, i.e. WT injects more than the rated 1pu value during fault. In this case of highly active current injection the frequency of the voltage at the WT terminal increases towards very high values, such as 100 Hz, due to the reasons that will be explained in the following chapters. This event is called as LOS – frequency rise.

In section 2.2.5, results of these simulation cases and six more cases with higher PCC voltages during the faults, is summarized in a single figure, showing whether stable

operation around 50Hz or LOS is observed. It is important to mention that in case of zero current injection during the fault, which is not shown here, WT stays synchronized to 50Hz. Hence the LOS is observed only if current injection during fault is accomplished by wind turbines.

2.2.2 Fault Case-1: Loss of Synchronism – Frequency Fall

As observed in the last subfigure of figure 2.4, for a severe fault and pure reactive current injection case, frequency calculated and used within the PLL of wind turbine decreases towards zero, therefore voltage and current generated by the WT have low frequency as observed in third and fourth subfigures.

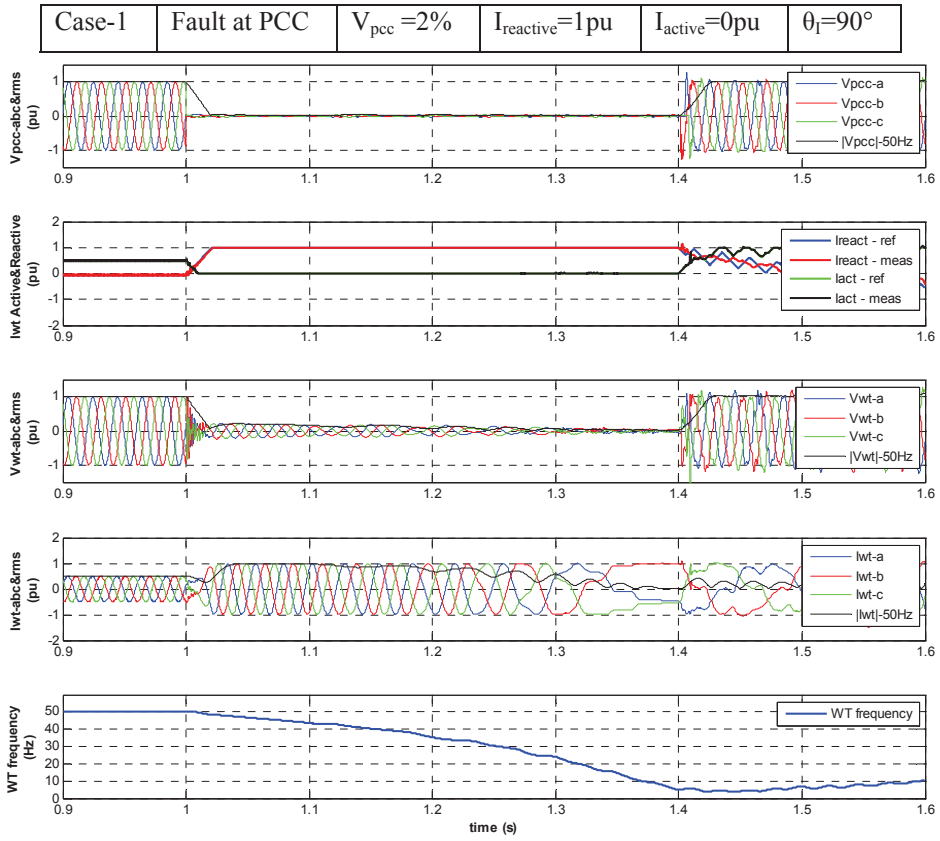

Fig. 2.4 Case-1: Loss of Synchronism – Frequency Fall.

2.2.3 Fault Case-2: Synchronized to 50Hz

As observed in the last subfigure of figure 2.5, for a severe fault and injection of a current with specific active and reactive components, LOS is not experiences and the frequency calculated and used within the PLL of the wind turbine remains around 50 Hz, where the reasons are explained in the following chapters.

Case-2	Fault at PCC	V_{pcc} =2%	$I_{reactive}$=1pu	I_{active}=0.125pu	θ_I=83°

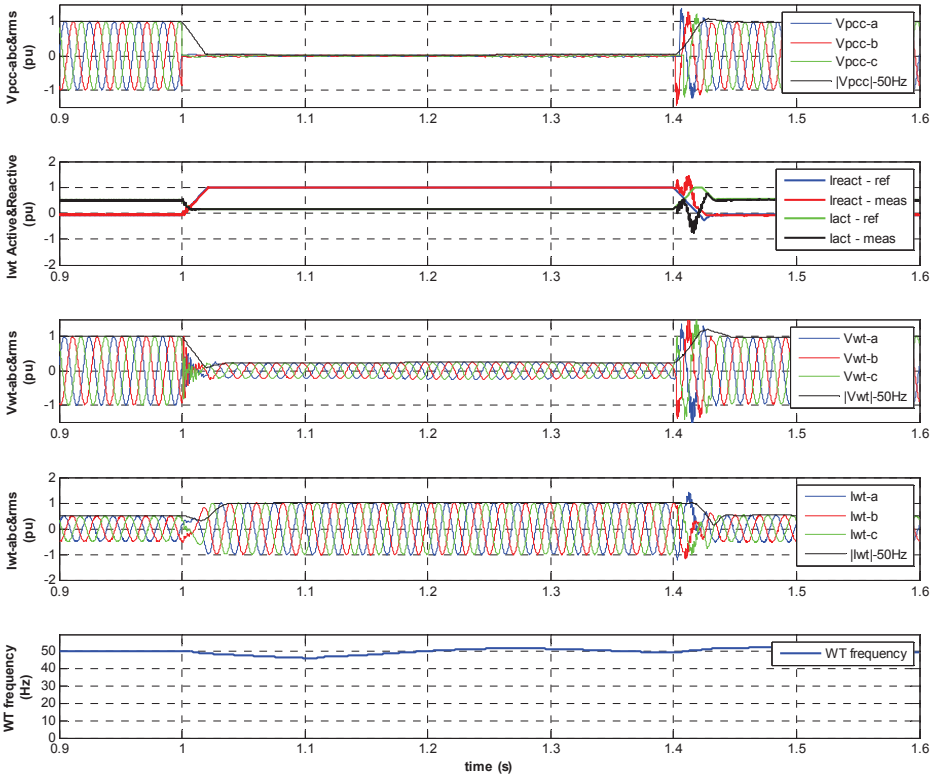

Fig. 2.5 Case-2: Stable operation – synchronized to 50Hz.

2.2.4 Fault Case-3: Loss of Synchronism – Frequency Rise

As observed in the last subfigure of figure 2.6, for a severe fault and injection of high active current component together with 1pu reactive component case, the frequency calculated and used within the PLL of the wind turbine increases towards high values (e.g. 100Hz), therefore voltage and current generated by the WT have high frequency as observed in third and fourth subfigures.

Case-3	Fault at PCC	V_{pcc}=2%	$I_{reactive}$=1pu	I_{active}=0.65pu	θ_I=57°

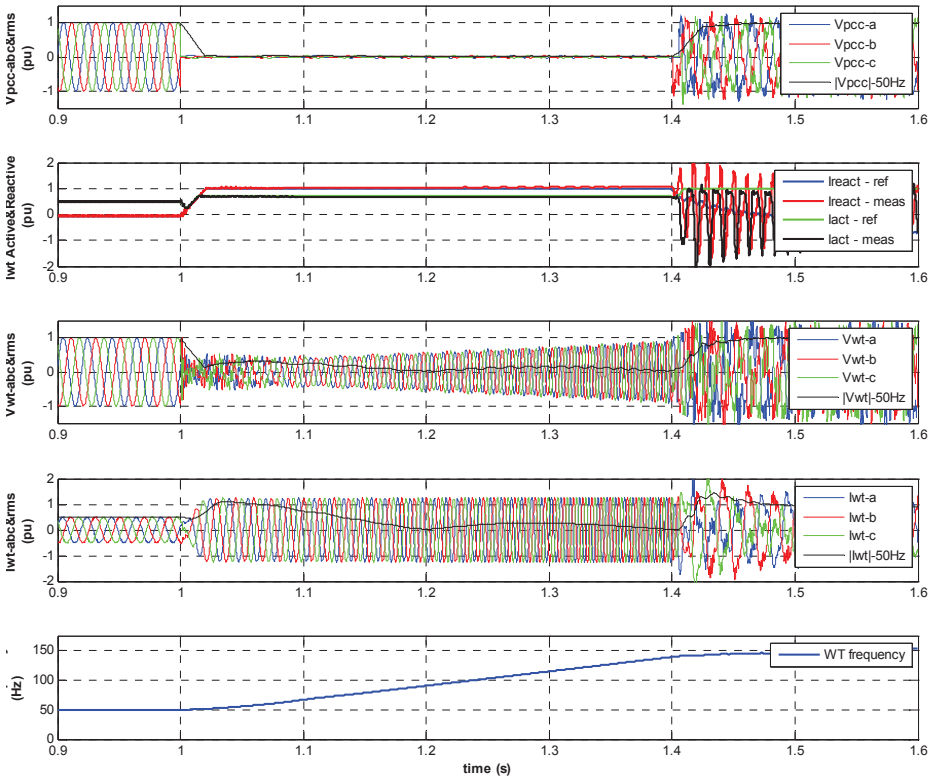

Fig. 2.6 Case-3: Loss of Synchronism – Frequency Rise.

2.2.5 Fault Cases with 0.1pu and 0.25pu PCC Voltages

In addition to three cases (1 to 3) of previous sections with results given in figures 2.4 to 2.6, where the PCC voltage was dropping to 2% of the rated value, six more cases (4 to 9) are simulated. In cases 4 to 6, PCC voltage drops to 10%; and in cases 7 to 9, PCC

voltage drops to 25% of the rated value. The simulation results for cases 4 to 9 are not shown to save space and since similar time-domain results (LOS as frequency fall/rise or stable operation at 50Hz) are observed. The overall results of total nine cases are given in figure 2.7. As seen in figure 2.7 case-6, LOS is observed also when the PCC voltage is 10% of rated and high active current is injected accompanying the 1pu reactive current.

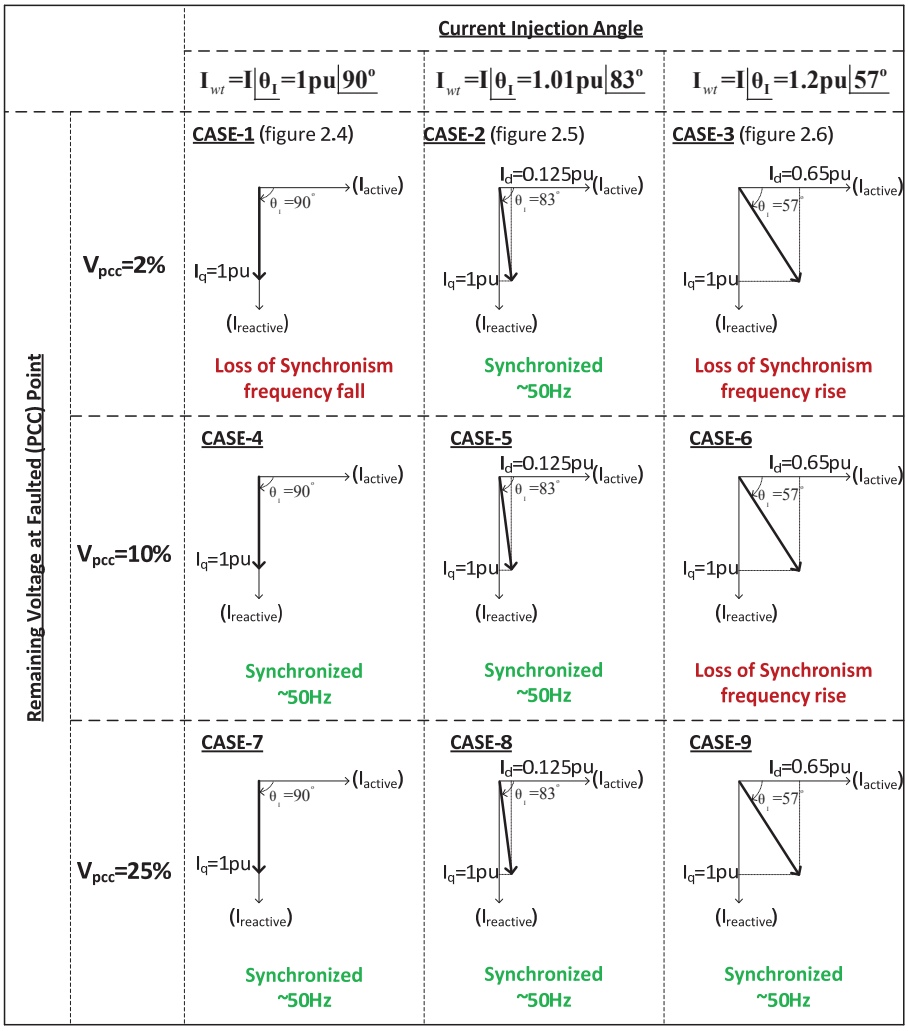

Fig. 2.7 Results with respect to active and reactive current components and PCC voltage.

As given in the previous figures, during the LOS events, frequency of the WT deviates from the fundamental 50Hz frequency of the grid. It is interesting but proven to be true (with simulation and experiment results in following chapters) that the frequency of the voltage at the WT terminal becomes 0Hz (DC) or larger than 100 Hz while the faulted grid point (in this case PCC) voltage is still at 50 Hz. Phase voltages from previous results are given in figures 2.8 and 2.9 to clearly show the mentioned events.

It is seen in figure 2.8 that during the LOS – frequency fall event, the WT voltage drops almost to 0Hz (DC signal) while the PCC voltage is still around 50Hz. Similarly in figure 2.9, during the LOS – frequency rise event, the WT voltage is above 100Hz, while the PCC voltage is still at 50Hz. Inevitably, the current injection from the WT, which has 0 or 100 Hz frequency, cause some amount of distortion at the PCC voltage as observed in figures 2.8 and 2.9.

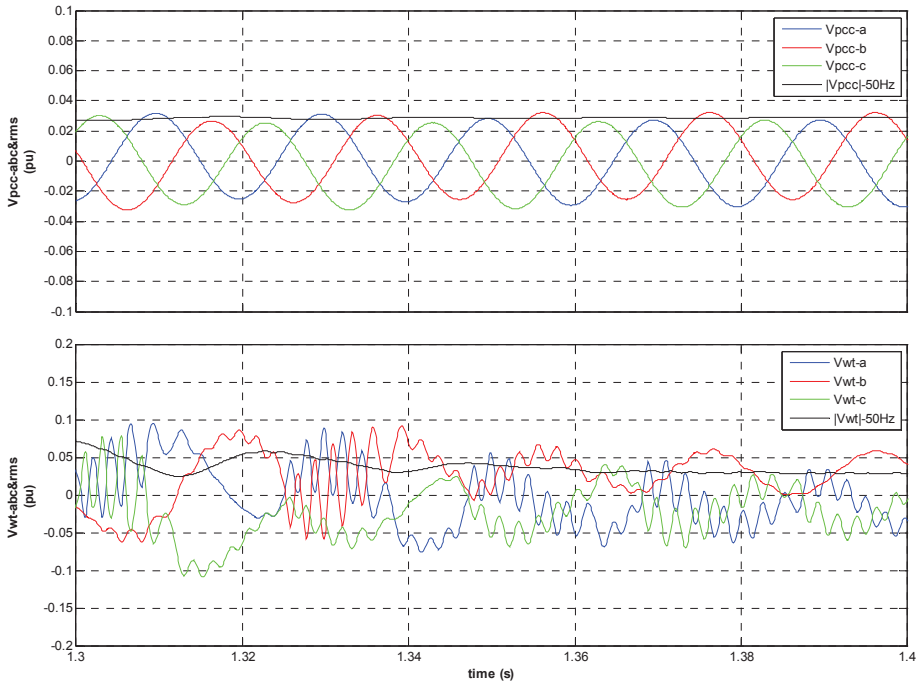

Fig. 2.8 Trace of PCC and WT voltages in figure 2.4 (between 1.3 and 1.4 seconds)

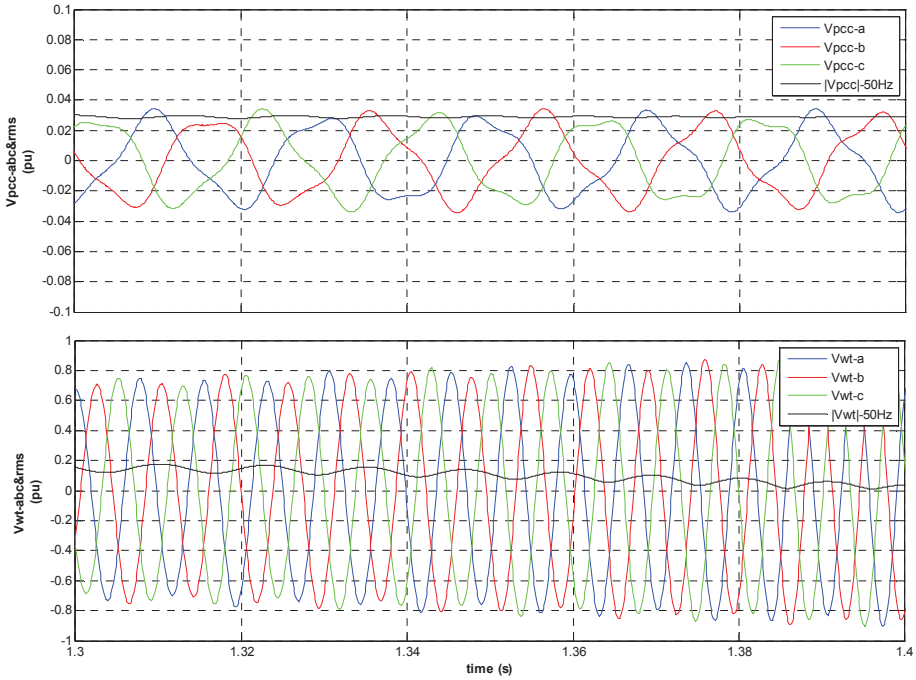

Fig. 2.9 Trace of PCC and WT voltages in figure 2.6 (between 1.3 and 1.4 seconds)

As a summary of the results in figure 2.7, it can be commented that LOS occurs in some specific cases depending on the remaining voltage at the faulted bus (PCC) and the active-reactive current magnitudes. Being not shown here, it has been observed that the occurrence of the LOS event also depends on the characteristics (magnitude and angle) of the impedance between the WT and the faulted point (e.g. PCC). It is important to state that in case of zero current injection during the fault, which is not shown here; WT stays synchronized to 50Hz. Also, for the faults occurring on the line between the PCC and main grid, or at the bus where the line is connected to the main grid, similar LOS events have been observed.

In practical wind turbines in a real WPP, or the protection units within WPP would trip if such a frequency deviation is measured during a fault. Additionally, as observed in figures 2.4 and 2.6, if a LOS event occurs during the fault, WT is not able to restore its normal 50Hz operation even after the fault is cleared and PCC voltage recovers.

2.2.6 PLL with Saturation and Anti-Windup Algorithm

The PLL structure shown in figure 2.3 does not include any saturation block within its PI controller or at the calculated frequency signal output. In practical saturation blocks are employed for the integrator blocks and a limit is applied to the calculated frequency. When the output of the integrator is limited to the saturation value, the state of the integrator also needs to be limited to the saturation value, i.e. an anti-windup algorithm is needed, to avoid windup of integrator. The described saturation blocks are included in the PLL structure in Figure 2.10 below. As an example, the frequency signal can be limited to be maximum 55Hz and minimum 45Hz.

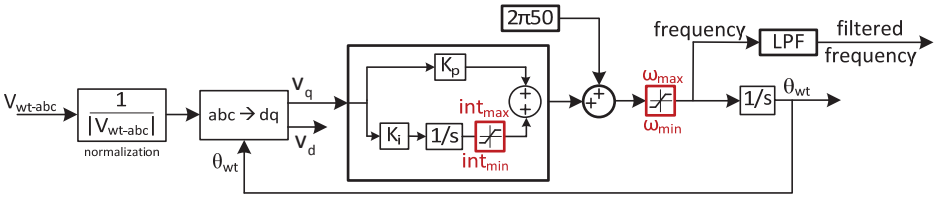

Fig. 2.10 PLL structure with saturation and anti-windup algorithms.

The impact of PLL saturation blocks on the LOS problem will be handled again in chapter 4 and 5. It should be stated here that the LOS –frequency fall/rise events are observed for cases 1, 3, and 6 (of figure 2.7), also when the PLL structure with saturation functions in Figure 2.10 is employed. However, when the saturation blocks are employed, the frequency falls or rises until the limit values, e.g. 45 Hz or 55Hz, while the PCC voltage is still around 50Hz.

2.2.7 Physical Understanding of LOS

In order to better explain LOS event physically, figure 2.11 is given below. As seen in the figure, when a severe (solid) fault close to PCC or at the PCC occurs, WPP experiences a very low grid voltage and as explained above, LOS occurs during current injection from wind turbines to the low voltage. The WPP side of the network behaves like “isolated” from the main grid side, which continues with 50Hz unless it is an unstable system. As shown in figure 2.11-(b), in such a fault case the wind turbine is injecting current to the low voltage at the faulted point through impedance Z (R+jX),

which is composed of the impedance of the WT transformer, WPP collector grid, WPP transformer, and the connection line. During severe grid faults the faulted point voltage drops down close to zero and wind turbines are injecting controlled active and reactive currents to a resistive inductive (R-X) impedance load with a very low voltage behind. As will be shown in the next chapters, if active and reactive current references are not convenient with the impedance characteristics, LOS occurs as shown in this chapter. In the following chapters analysis of the LOS and novel control methods will be proposed to provide stable operation of the WPP side of the network avoiding LOS.

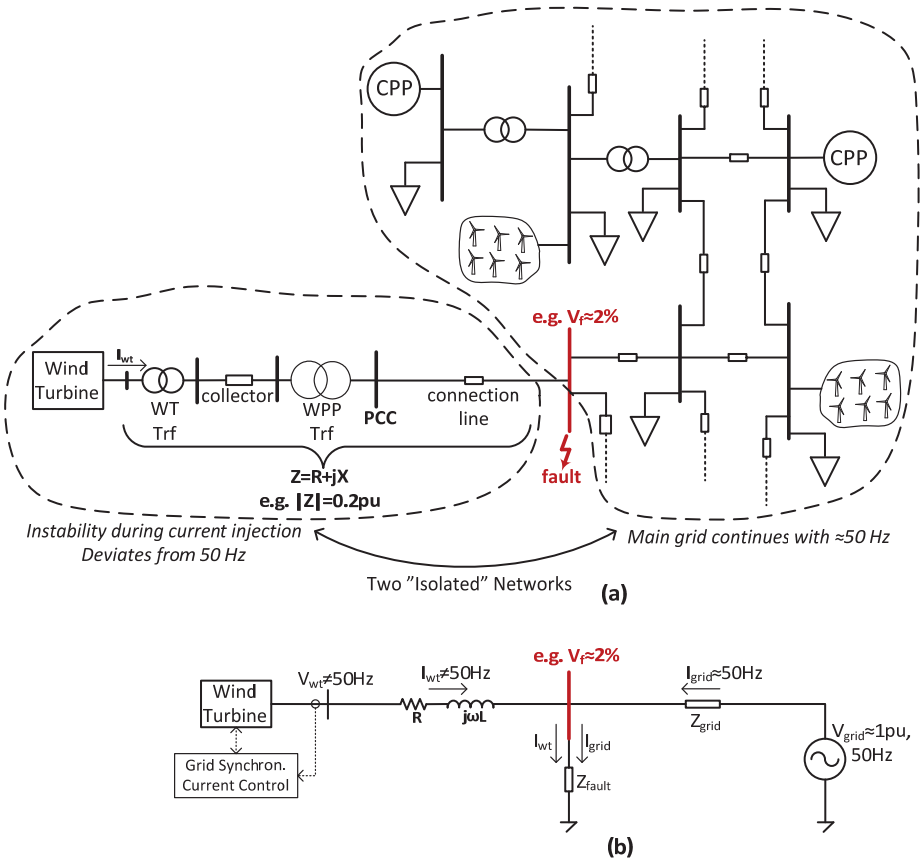

Fig. 2.11. Representative (a) two "isolated" networks during current injection to severe faults, (b) with Thevenin equivalent of main grid.

2.3 Conclusion

According to recent grid codes, wind turbines are required to inject reactive currents during faults proportional to the voltage drop at their connection terminals, even for severe faults, where the voltage drops down to zero, and also for asymmetrical faults. In this chapter, details of the identified problems, which occur with the use of the conventional current reference generation methods during asymmetrical and severe symmetrical faults, are given.

In order to show the dependency of the LOS event to the active and reactive current injection and PCC voltage, nine different cases have been simulated. Throughout the following chapters, simulations results will be analyzed with theory and verified with experimental results. In the next chapter, active and reactive current transfer limits will be derived. In chapter 4, where the LOS event will be analyzed, the results of these nine cases will be correlated with the active and reactive current transfer limits.

Chapter 3

Active and Reactive Current Transfer Limits

In this chapter, a basic but fundamental theory; active and reactive current transfer limits between two buses are explored as a function of voltage magnitude at the receiving bus, and the line impedance between the buses. It is shown that when active and reactive current control (vector control) is performed to inject current through impedance, certain current transfer limits exist, which have not been considered before. The derived limits play an important role to understand the Loss of Synchronism (LOS) phenomenon occurring during active and reactive current injection from wind turbines to severe symmetrical grid faults. The impact of taking the resistance of the line into account especially for low voltage situations is emphasized. The correlation of derived active and reactive current transfer limits to a WPP case and to the grid code requirements are given at the end.

3.1 Active and Reactive Power Flow between Two Buses

For a better understanding of current limits, active and reactive power transfer limits between two buses, which is a well-known classical power system theory, is given first.

3.1.1 Power Flow on a Line neglecting the Resistance

Two buses, which are connected through a line, with voltages V_1 and V_2 and their phasor diagram are shown in figure 3.1 below. Since transmission lines in a power system are highly inductive with low resistance, as a general approach, resistive component of the line is neglected when power-angle characteristics are derived.

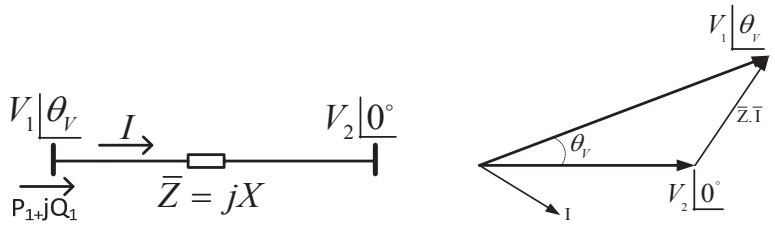

Fig. 3.1 Power flow on a lossless line; single-line diagram and phasor diagram.

Neglecting the resistive component of the line, active and reactive power-angle characteristics at the sending end (V_1) of the diagram above is defined as (3.1) and (3.2) below, which are well-known from classical power system theory.

$$P_1 = \frac{V_1 V_2}{X} \sin\theta_V \tag{3.1}$$

$$Q_1 = \frac{V_1^2 - V_1 V_2 \cos\theta_V}{X} \tag{3.2}$$

In figure 3.2, power-angle characteristics are drawn for a healthy situation with V_1 and V_2 having rated magnitudes of 1pu with a line of Z=j0.4pu. In figure 3.3, voltage V_2 drops down to 0.05pu and V_1 drops down to 0.3pu, still being higher than V_2. In figure 3.4, voltage V_2 drops to zero while V_1 is 0.3pu.

As seen from (3.1), (3.2) and figure 3.3, and well-known from power system theory, active power limit flow from sending end substantially decreases for low voltage situations. As seen from figure 3.4, when the sending end (V_1) voltage is 0.3pu and the receiving end (V_2) voltage is zero, active power flow becomes zero and a certain amount of reactive power flows. Active and reactive power equations for zero V_2 are given below;

$$V_2 = 0 \quad \Rightarrow \quad P_1 = 0 \quad \text{and} \quad Q_1 = \frac{V_1^2}{X} \tag{3.3}$$

Remark 3.1:

Observing figure 3.4 and (3.3), where reactive power is flowing from sending end, without supplying any active power flow, a comment like “pure reactive power can be supplied to a zero voltage bus through a line without supplying any active power” can be done, which is incorrect since the resistive component of the line has been neglected

in the calculations. However, practically lines do have non-zero resistive component, of value depending on the line characteristics and temperature. In the next section, power-angle characteristics are derived considering the resistive component of the line.

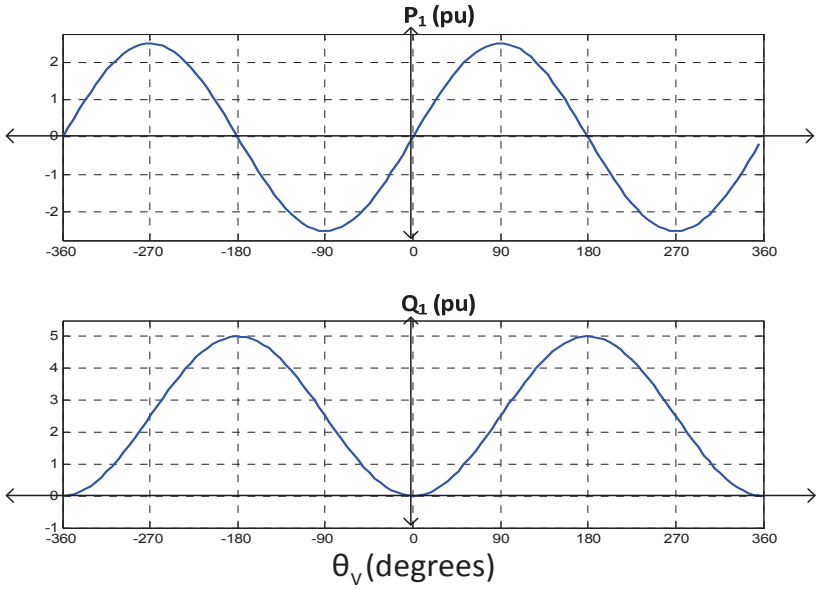

Fig. 3.2 Power -angle characteristics for V_1=V_2=1pu and Z=j0.4pu

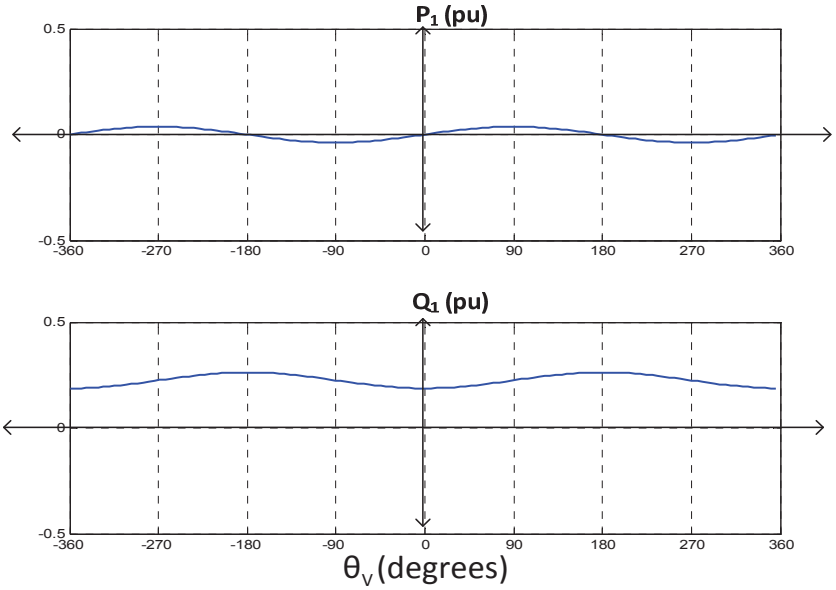

Fig. 3.3 Power -angle characteristics for V_1 =0.3pu, V_2=0.05pu, and Z=j0.4pu

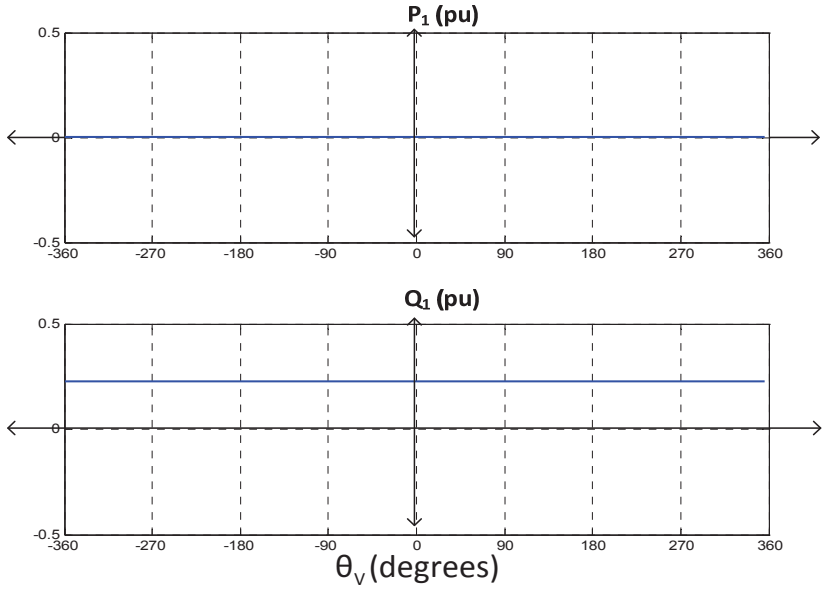

Fig. 3.4 Power -angle characteristics for V_1=0.3pu, V_2=0pu, and Z=j0.4pu

3.1.2 Power Flow on a Line considering the Resistance

In this section power flow characteristics between two buses is derived while taking the resistive component of the line into account. Two buses, which are connected through a line, with voltages V_1 and V_2 and their phasor diagram are shown in figure 3.5 below.

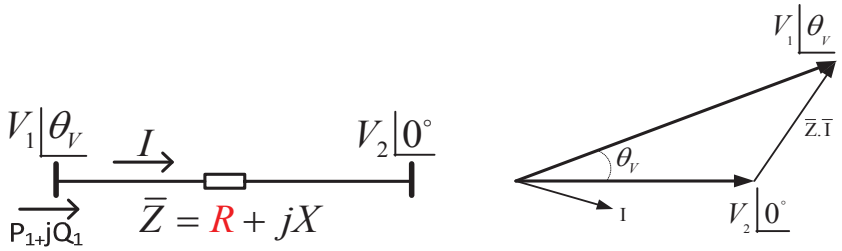

Fig. 3.5 Power flow on an inductive/resistive line; single-line diagram and phasor diagram.

Active and reactive power equations with consideration of the line resistance are given below, where Z represents magnitude of the impedance;

$$P_1=\frac{V_1V_2X}{Z^2}\sin\theta_V+\frac{V_1^2R}{Z^2}-\frac{V_1V_2R\cos\theta_V}{Z^2} \tag{3.4}$$

$$Q_1=\frac{V_1^2X}{Z^2}-\frac{V_1V_2X\cos\theta_V}{Z^2}-\frac{V_1V_2R\sin\theta_V}{Z^2} \tag{3.5}$$

In the following three figures, power-angle characteristics are drawn for different bus voltage magnitudes for a line having an impedance as 0.08pu+j0.4pu, i.e. with an X/R ratio of 5. In figure 3.6, power-angle characteristics are drawn for a healthy situation with V_1 and V_2 having identical magnitudes of 1pu. In figure 3.7, voltage V_2 drops down to 0.05pu and V_1 drops down to 0.3pu, still being higher than V_2. In figure 3.8, voltage V_2 drops to zero while V_1 is 0.3pu.

As seen from (3.4) and figure 3.7, and well-known from power system theory, active power flow substantially decreases for low voltage situations. However, in this case, where line resistance is taken into account, active power takes values larger than zero for any angle (θ_V) value. Similarly, in figure 3.8, where the sending end (V_1) voltage is 0.3pu and receiving end (V_2) voltage is zero, certain amount of reactive power, but also a non-zero amount of active power flow are observed. Active and reactive power equations for zero V_2 are given below;

$$V_2=0 \quad \Rightarrow \quad P_1=\frac{V_1^2R}{Z^2} \quad \text{and} \quad Q_1=\frac{V_1^2X}{Z^2} \quad \Rightarrow \quad \frac{P_1}{Q_1}=\frac{R}{X} \tag{3.6}$$

It is obvious that when the receiving end voltage, V_2, is zero, the active and reactive power flowing from sending end to the receiving end is dissipated as active (I^2R) and reactive (I^2X) power losses on the resistance and reactance of the line.

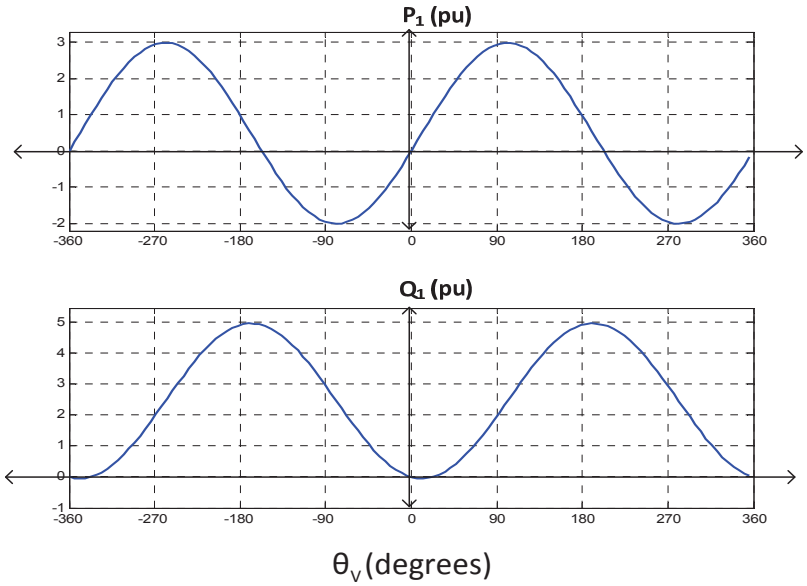

Fig. 3.6 Power -angle characteristics for V_1=V_2=1pu and Z=0.08+j0.4pu

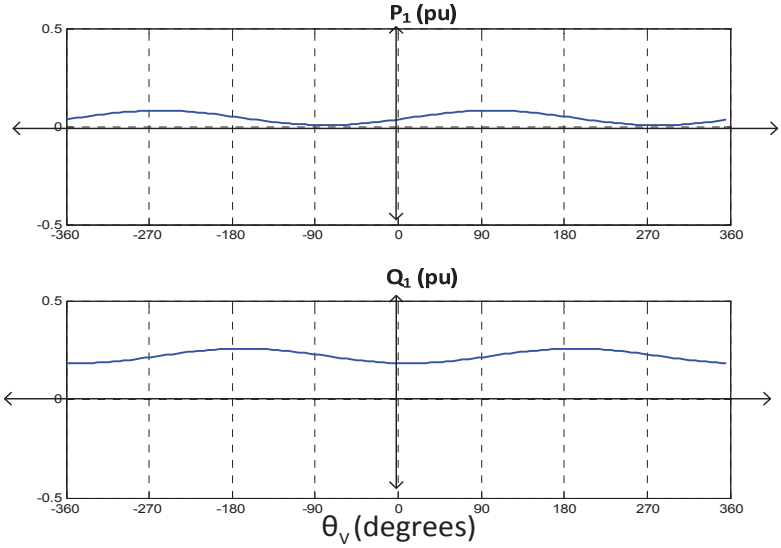

Fig. 3.7 Power -angle characteristics for V_1=0.3pu, V_2=0.05pu, and Z=0.08+j0.4pu

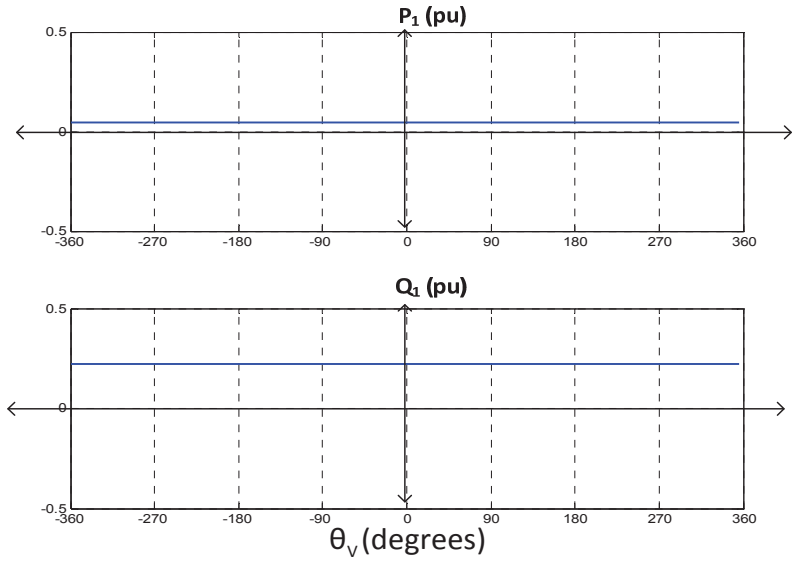

Fig. 3.8 Power -angle characteristics for V_1=0.3pu, V_2=0pu, and Z=0.08+j0.4pu

Following remarks can be done based on the observations above;

Remark 3.2:

Observing figures 3.7 and 3.8 it can be stated that in case of very low (or zero) receiving end voltage; for reactive power flow from sending end (i.e. $V_1 > V_2$), active power injection cannot be zero. Referring to the remark 3.1 in previous section, it is important to note that, pure reactive power flow from sending end requires a voltage, which is not very low (neither zero), at the receiving end.

In order to provide reactive power flow from sending end (i.e. $V_1 > V_2$) a certain amount of non-zero active power supply from the sending end is required. An explanation for this situation can be that; the amount of active power loss (arising with the reactive power flow) on the resistive component of the line has to be compensated by the sending end, since this amount cannot be supplied by the receiving end, which has very low (or zero) voltage.

Remark 3.3:

Similar to the remark 3.2, for active power flow from sending end, reactive power injection cannot be zero. The reason for this situation is that the reactive power loss

(arising with the active power flow) on the inductive component of the line has to be compensated by the sending end, since it cannot be supplied by the receiving end, which has very low (or zero) voltage.

Remark 3.4:

Observing figure 3.7, where V_2 is very low, and especially figure 3.8 and (3.6), where V_2 is zero, it can be stated that for a fixed amount of reactive power injection, active power injection cannot be lower or higher than a fixed amount. Similarly, for a fixed amount of active power injection, reactive power injection cannot be lower or higher than a fixed amount. As seen in (3.6), proportionality between active and reactive power injection when V_2 is zero, depends on the line X/R characteristics, i.e. the line characteristics dictates the dependency between active and reactive power.

These remarks play important role in order to help understanding of the active/reactive current transfer limits in the following parts.

3.2 Active and Reactive Current Flow between Two Buses

Since the focus of this thesis is on the current injection by wind turbines, current transfer characteristics from one bus to another bus through impedance are analyzed in this part. First, the current-angle characteristics are given, and then the active/reactive current transfer limits as a function of the receiving bus voltage magnitude and line impedance (R+jX) are derived.

3.2.1 Current - Angle Characteristics

The current is defined as the active and reactive currents injected from the sending end (V_1) as shown in figure 3.9 below. Current-angle characteristics can be easily obtained as (3.7) and (3.8) below using power-angle characteristics (3.4) and (3.5) from previous section;

$$I_{active} = \frac{P_1}{V_1} = \frac{V_2 X}{Z^2}\sin\theta_V + \frac{V_1 R}{Z^2} - \frac{V_2 R\cos\theta_V}{Z^2} \tag{3.7}$$

$$I_{reactive} = \frac{Q_1}{V_1} = \frac{V_1 X}{Z^2} - \frac{V_2 X\cos\theta_V}{Z^2} - \frac{V_2 R\sin\theta_V}{Z^2} \tag{3.8}$$

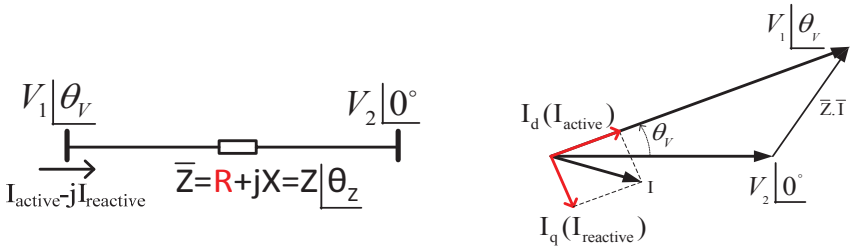

Fig. 3.9 Current flow on an inductive/resistive line; single-line diagram and phasor diagram

As observed in figure 3.10, for a line with impedance Z=0.08+j0.4, when sending end voltage V_1 drops to 0.3pu and the receiving end voltage V_2 to 0.05pu, the active current gets non-zero values for any angle, θ_V. In figure 3.11, when V_2 drops down to zero, a fixed amount of active and reactive current flows, similar to the previous power flow in figures 3.7 and 3.8.

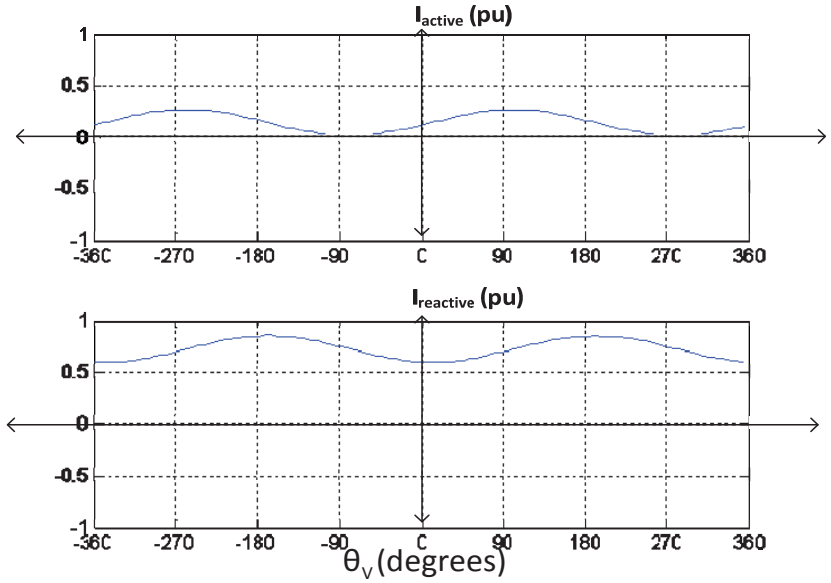

Fig. 3.10 Current -angle characteristics for V_1=0.3pu, V_2=0.05pu, and Z=0.08+j0.4pu

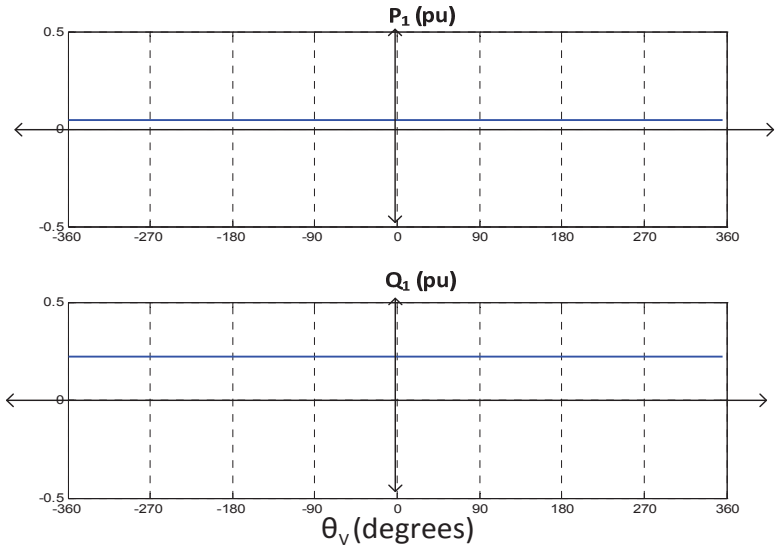

Fig. 3.11 Current -angle characteristics for V_1=0.3pu, V_2=0pu, and Z=0.08+j0.4pu

Based on (3.7) and (3.8), for V_2=0 and V_1>0, active and reactive currents can be obtained as (3.9) below;

$$V_2 = 0 \quad \Rightarrow \quad I_{active} = \frac{V_1 R}{Z^2} \quad \text{and} \quad I_{reactive} = \frac{V_1 X}{Z^2} \quad \Rightarrow \quad \frac{I_{active}}{I_{reactive}} = \frac{R}{X} \tag{3.9}$$

It is obvious that when the receiving end voltage, V_2, is zero, the active and reactive currents flowing from sending end to the receiving end creates only active (I^2R) and reactive (I^2X) losses on the resistance and reactance of the line.

Remark 3.5:

Observing figure 3.10, where V_2 is very low, and especially figure 3.11 and (3.9), where V_2 is zero, it can be stated that for a fixed amount of reactive current injection, active current injection cannot be lower or higher than a fixed amount. Similarly, for a fixed amount of active current injection, reactive current injection cannot be lower or higher than a fixed amount. As seen in (3.9), proportionality between injected active and reactive currents when V_2 is zero, depends on the line X/R characteristics, i.e. the line dictates the dependency between active and reactive currents.

3.2.2 Derivation of Active and Reactive Current Transfer Limits

In previous sections power-angle and current-angle characteristics are analyzed, however power and current equations were based on given V_1 and V_2, and varying θ_V. However, wind turbines are injecting controlled active and reactive currents (as vector control) at their terminals. For instance, when the receiving end voltage V_2 (e.g. PCC voltage) drops to a low voltage value, active and reactive currents are injected from the sending end V_1 (WT terminal). Hence, it is more than necessary to analyze the active and reactive current injection operating points as a function of (low) voltage magnitude at the receiving end (V_2) and the line impedance (R+jX). In order to derive the active and reactive current operating points, single-line diagram in figure 3.12 and phasor diagram in figure 3.13-(a) are utilized. Since active and reactive currents are injected with reference to V_1, the V_1 voltage is located on the horizontal axis, and controlled current phasor with respect to V_1 is shown with current angle θ_I. With the positive value of θ_I and I_q (reactive current) the wind turbine is injecting reactive power (overexcited operation, equivalent to capacitive behavior).

In order to find the magnitude limit for a current injection with angle θ_I, the diagram in figure 3.13-(b) is used, similar to the one given in [56]. Regarding the constraint that magnitude of V_2 is fixed, a circle with radius equal to the magnitude of V_2 voltage is drawn. Then, V_2 voltage is found via locating the voltage phasor on the impedance (ZI) such that the tip of the ZI is on the circle and the end of the ZI is on the V_1 reference axis, while keeping the angle of ZI with respect to V_1 fixed at θ_I–θ_Z. As expected, magnitude of V_1 is varied while locating ZI. In the following parts, for every current angle, i.e. θ_I from 0° to 360°, the limit value for the current magnitude is found, while keeping constant V_2 value and Z (R+jX). It is important to note that the impedance includes a resistive component, i.e. θ_Z<90°, in the following phasor diagrams.

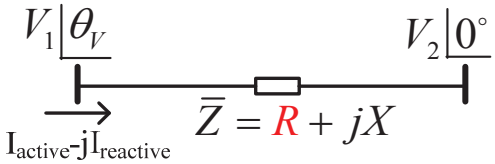

Fig. 3.12 Single line diagram used for derivation of current limits.

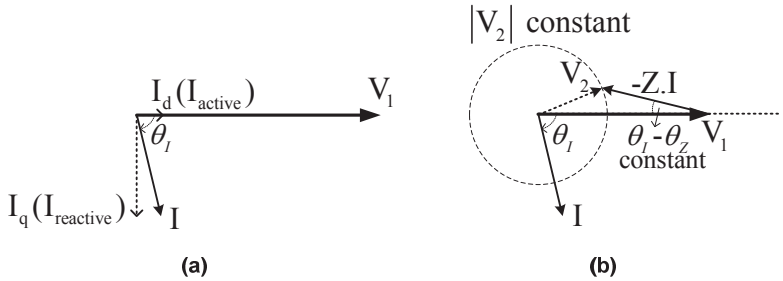

Fig. 3.13 Current phasor (a) and methodology (b) to derive limits.

Current magnitude limit for θ_I=90° (pure reactive):

As the first step, using methodology described above, current magnitude limit is derived for pure reactive current injection, i.e. θ_I=90°, below.

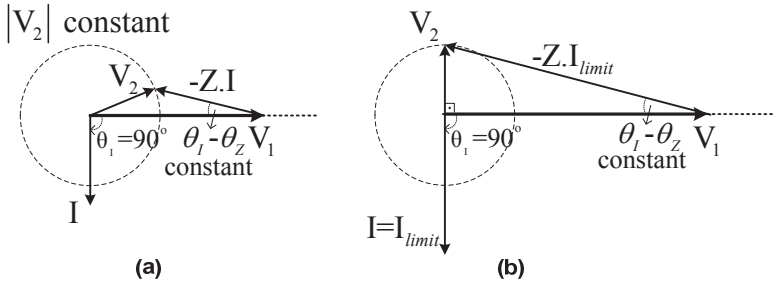

Fig. 3.14 Current transfer limit for θ_I=90° (pure reactive).

As seen in figure 3.14-(a), with a low current magnitude an operating point can be found. However, when the current magnitude reaches a level, called as I_{limit}, as shown in figure 3.14-(b), the angle difference between V_1 and V_2 becomes 90°. This is the point where the largest phasor ZI can be located with the constraint of constant V_2 magnitude and fixed at $\theta_I - \theta_Z$. Figure 3.15 is given to better explain this statement. If the current magnitude becomes larger, magnitude of the phasor ZI becomes larger as expected. However, with this large magnitude of ZI phasor and fixed angle with respect to V_1, θ_I–θ_Z, the ZI phasor can only be located between V_1 reference line and reference line-2, shown in figure 3.15. Therefore, the tip of the ZI phasor cannot intersect with the V_2 circle, which implies that a larger V_2 is required, which means that there is not

any operating point with $I > I_{limit}$ and $\theta_I=90°$. In other words, for the current injection angle, $\theta_I=90°$, the current transfer limit is found as in figure 3.14-(b) and (3.10).

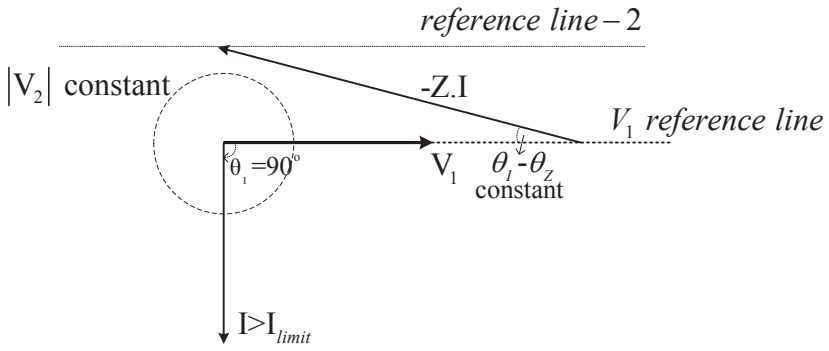

Fig. 3.15 Out of transfer limit situation for $I > I_{limit}$ and $\theta_I=90°$.

The current transfer limit for $\theta_I=90°$ can be calculated from figure 3.14-(b), as below;

$$\theta_I=90^o \Rightarrow V_2=Z.I_{limit}.\sin(\theta_I-\theta_Z) \Rightarrow I_{limit}=\frac{V_2}{Z.\cos(\theta_Z)} \Rightarrow I_{limit}=\frac{V_2}{R} \quad (3.10)$$

Remark 3.6:

Observing figure 3.15, when the pure reactive current magnitude is larger than the limit value given in (3.10), an operating point cannot be found, due to small magnitude of V_2. This means that for a very low receiving end voltage, it is not possible to inject unlimited pure reactive current with zero active current, which was also commented for pure reactive power in remark 3.2 and 3.5 in previous sections.

It is also important to note that this situation arises due to resistive (R) component of the line. If R was zero, an operating point would always be found, i.e. limit would be infinity in (3.10). However, since it is not practically possible to have R as zero, it is not possible to have operating point with pure reactive current larger than the limit in (3.10).

Observing (3.10), it can be commented that, when the receiving end voltage drops to very low values and/or resistive component becomes larger, limit value becomes smaller.

The limit value obtained in this section is imposed on the active/reactive current axes in figure 3.16 below. This plot is filled throughout this section for all current angles.

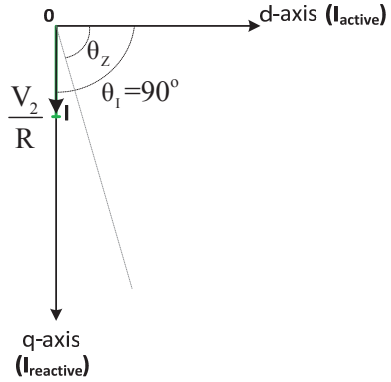

Fig. 3.16 Active/reactive current transfer limits

Current magnitude limit for $90° > \theta_I > \theta_Z$:

From figure 3.17-(a) to 3.17-(b), magnitude of current is increased while keeping the angle constant at θ_I until the phase difference between V_1 and V_2 reaches 90°, which is largest current magnitude with a possible operating point. As explained in the previous part, any current larger than this magnitude would require a higher V_2 magnitude.

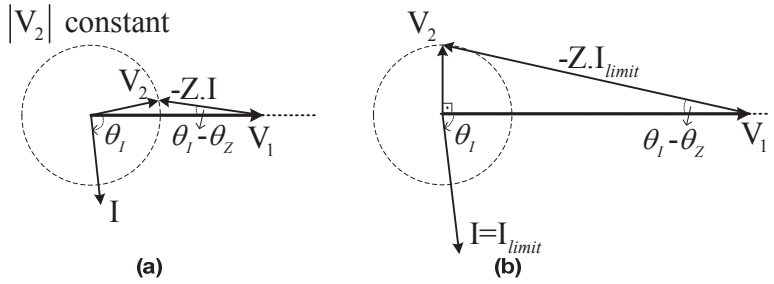

Fig. 3.17 Current magnitude limit for $90° > \theta_I > \theta_Z$.

Following the same methodology as previous case, the current transfer limit as a function of V_2, Z and θ_I, for $90°>\theta_I>\theta_Z$ is found from figure 3.17-(b) as;

$$90^o > \theta_I > \theta_Z \quad \Rightarrow \quad V_2 = Z.I_{limit}.\sin(\theta_I - \theta_Z) \quad \Rightarrow \quad I_{limit} = \frac{V_2}{Z.\sin(\theta_I - \theta_Z)} \qquad (3.11)$$

The derived limit is added to the active/reactive current axes as in figure 3.18. The possible operating points are shown as the green-shaded area. It is important to note that the formula of I_{limit} in (3.11) results in a straight line while θ_I is varying between 90° and θ_Z.

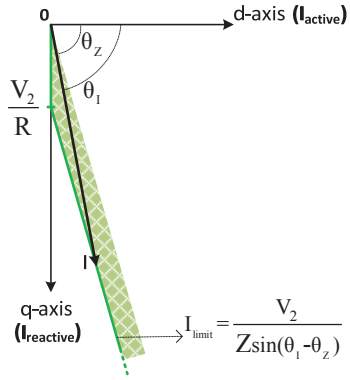

Fig. 3.18 Active/reactive current transfer limits-2.

Remark 3.7:

It is important to note that for a fixed current injection angle as in figures 3.14 and 3.17, the angle difference between the sending end (V_1) and receiving end (V_2) voltage increases, which reaches 90° at the limit point. Also for a fixed current magnitude, this angle difference between two bus voltages increase in proportion with the deviation of the current angle from the impedance angle, θ_Z. This remark will be important for the small-signal stability analysis in the next chapter.

Remark 3.8:

Observing the current phasor and the receiving end voltage V_2 phasor in figures 3.14-(a) and 3.17-(b), it is seen that current phasor has a component anti-phase with V_2; which implies that active power is absorbed from the V_2 bus. This means that, for highly (or pure) reactive current injection, the current phasor at the receiving end bus takes a form of highly active, but as consumption. Observing figure 3.14-(b), when the limit is reached for pure reactive current, there is only active current (consumption) at the receiving end bus. This means that the reactive power supplied by the V_1 bus is

consumed as I^2X loss on the line, and the I^2R loss (arising with the reactive current flow) is absorbed from the V_2 bus.

Current magnitude limit for $\theta_I = \theta_Z$:

In figure 3.19, magnitude of current is increased while keeping the angle constant equal to the impedance angle, $\theta_I=\theta_Z$. Different from the previous injection angles, when the current is injected with the angle of the impedance (θ_Z), a limit such as in figures 3.14-(b) or 3.17-(b) is not reached. There is always an operating point, and there is not a limit for the current transfer with this angle.

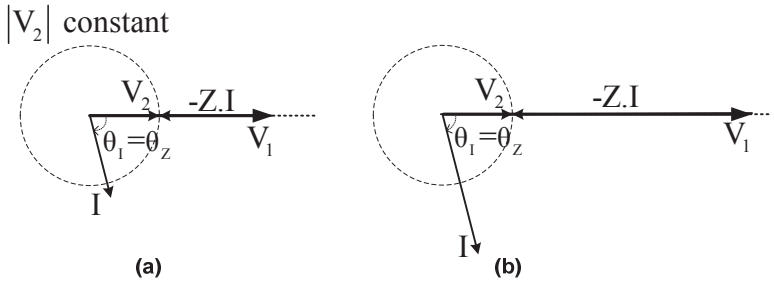

Fig. 3.19 Current magnitude limit for $\theta_I = \theta_Z$.

It should be noted that, as observed in figure 3.19, V_1 magnitude is increasing with increasing current magnitude. Hence, at some point V_1 would reach high values, which means that there would be a limit due to voltage limitations at the sending end V_1. However, in case of fault conditions, due to low voltage at V_2 and limited current ratings, V_1 would not increase above rated value; hence mentioned current limit due to voltage limit is not shown here for clarity.

The current injection, which is not limited when current has the angle of the impedance, is imposed to the active/reactive current operating point plot as in figure 3.20.

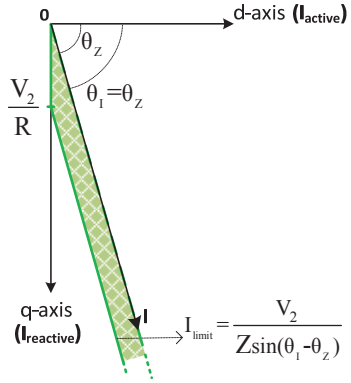

Fig. 3.20 Active/reactive current transfer limits-3.

Current magnitude limit for $\theta_Z > \theta_I > 0°$:

In figure 3.21, magnitude of current is increased while keeping the angle constant at θ_I until the phase difference between V_1 and V_2 reaches 90°, which is largest current magnitude with a possible operating point. As explained in the previous part, any current larger than this magnitude would require a higher V_2 magnitude. Different from the previous cases, where highly reactive (overexcited/capacitive) current was being injected and V_1 was increasing with increasing current magnitude, here V_1 magnitude is decreasing with increasing current since highly active current is injected

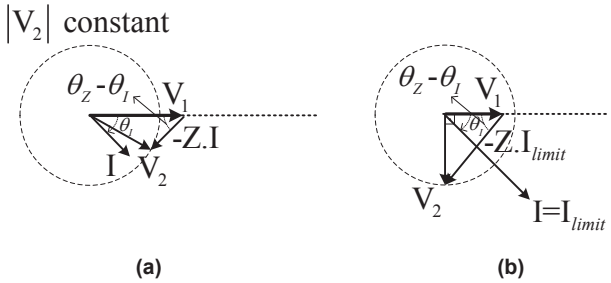

Fig. 3.21 Current magnitude limit for $\theta_Z > \theta_I > 0°$.

Following the same methodology as previous case, the current magnitude limit for $\theta_Z > \theta_I > 0°$ is found from figure 3.21-(b) as;

$$\theta_Z > \theta_I > 0^o \quad \Rightarrow \quad V_2 = Z \cdot I_{limit} \cdot \sin(\theta_Z - \theta_I) \quad \Rightarrow \quad I_{limit} = \frac{V_2}{Z.\sin(\theta_Z - \theta_I)} \qquad (3.12)$$

The derived limit is imposed to the active/reactive current operating point plot as in figure 3.22. The possible operating points are shown as the green-shaded area.

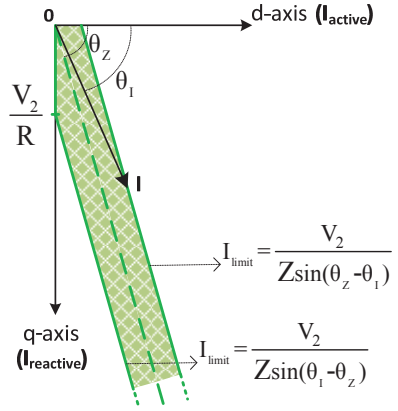

Fig. 3.22 Active/reactive current transfer limits-4.

<u>Current magnitude limit for $\theta_I = 0°$ (pure active):</u>

In figure 3.23, magnitude of current is increased while keeping the angle constant at $\theta_I = 0°$ (pure active) until the phase difference between V_1 and V_2 reaches 90°, which is the largest current magnitude with a possible operating point. It should be noted that V_1 drops down towards zero since pure active current is being injected.

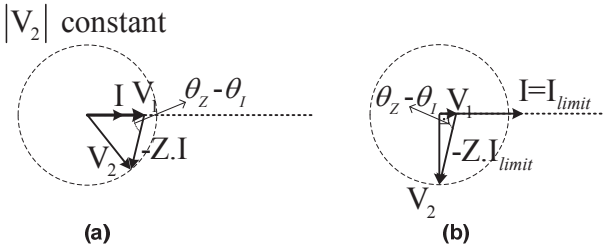

Fig. 3.23 Current magnitude limit for $\theta_I = 0°$ (pure active).

Following the same methodology as previous case, the current magnitude limit for $\theta_I = 0°$ is found from figure 3.23-(b) as;

$$\theta_I=0^o \quad \Rightarrow \quad V_2=Z.I_{limit}.\sin(\theta_Z-\theta_I) \quad \Rightarrow \quad I_{limit}=\frac{V_2}{Z.\sin(\theta_Z)} \quad \Rightarrow \quad I_{limit}=\frac{V_2}{X} \qquad (3.13)$$

Remark 3.9:

Observing figure 3.23, it is seen that an operating point cannot be found, when the pure active current magnitude is larger than the limit value given in (3.13). This means that for a very low receiving end voltage, it is not possible to inject unlimited pure active current with zero reactive current, which was also commented for active power transfer in remark 3.3 and 3.5 in previous sections.

Observing (3.13), it can be commented that, when the receiving end voltage drops to very low values and/or inductive component becomes larger, pure active current limit value becomes smaller, which is a well-known concern for active power injection to a weak grid. The derived limit is imposed to the active/reactive current operating point plot as in figure 3.24. The possible operating points are shown as the green-shaded area.

As seen in figure 3.23, with increasing active current magnitude, the angle difference between V_1 and V_2 reaches 90°, which is known as the maximum transferrable active power point in power system theory. However, as increasing reactive power injection increases the active power transfer limit, increasing reactive current can increase the active current transfer limit, as shown in figure 3.24 below.

Remark 3.10:

Observing the current phasor and the receiving end voltage V_2 phasor in figure 3.21-(a), the reactive current component of the current phasor with respect to V_2 voltage decreases as highly active current is injected. This means that due to high active current, high I^2X reactive loss on the line arises, causing less reactive power at the receiving end.

Observing the current phasor and the receiving end voltage V_2 phasor in figures 3.21-(b) and 3.23-(a), it is seen that current phasor has a component leading V_2; which implies that (underexcited) reactive power is absorbed from the V_2 bus. This means that, for highly (or pure) active current injection, the current phasor at the receiving end bus takes a form of highly reactive, but as consumption (underexcited). Observing figure 3.23-(b), when the limit is reached for pure active current, there is only reactive

current (underexcited) at the receiving end bus. This means that the active power supplied by the V_1 bus is consumed as I^2R loss on the line, and the I^2X loss (arising with the active current flow) is absorbed from the V_2 bus.

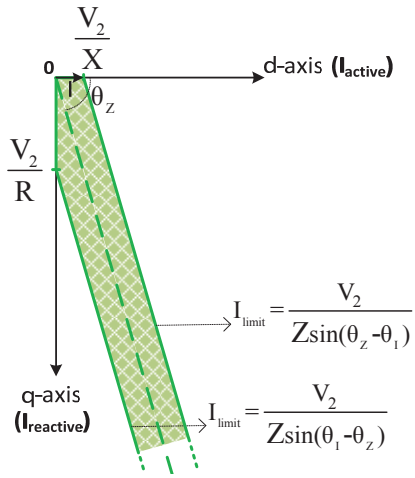

Fig. 3.24 Active/reactive current transfer limits-5.

Current magnitude limit for $270°+\theta_Z>\theta_I>90°+\theta_Z$ (active and reactive power consumption):

In figure 3.25, magnitude of current is increased while keeping the angle constant at θ_I, where the injected current is causing active power consumption and underexcited operation (reactive power consumption). Though such an operating point is quite uncommon for a wind turbine during low voltage situations, transfer limits are explored for the sake of completeness. As seen in figure 3.25, for such an injection angle, V_1 drops to zero with a certain current magnitude, which is the largest current with a possible operating point.

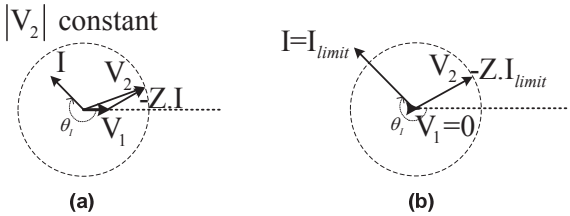

Fig. 3.25 Current magnitude limit for $270°+\theta_Z>\theta_I>90°+\theta_Z$

The current magnitude limit for this region of operation can be calculated as (3.14) below.

$$270^{o}+\theta_Z > \theta_I > 90^{o}+\theta_Z \quad \Rightarrow \quad V_2=Z.I_{limit} \quad \Rightarrow \quad I_{limit}=\frac{V_2}{Z} \tag{3.14}$$

The derived limit is imposed to the active/reactive current operating point plot as in figure 3.26. The possible operating points are shown as the green-shaded area.

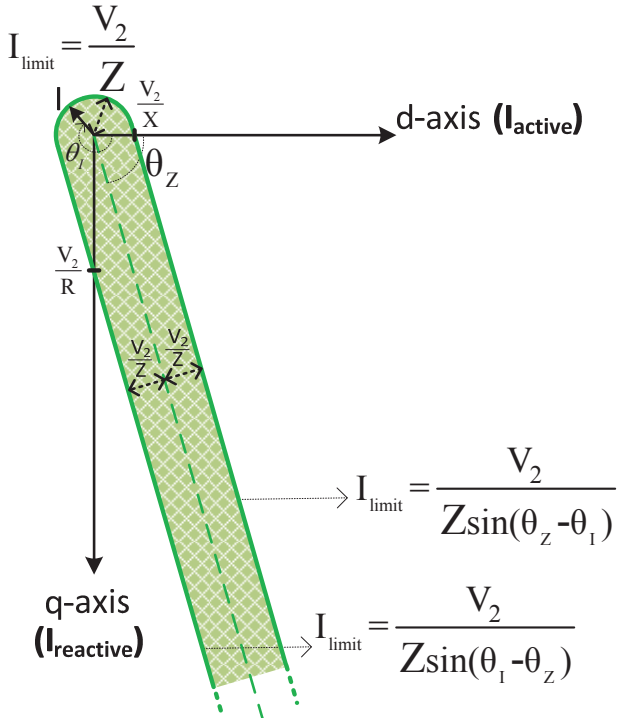

Fig. 3.26 Resultant active/reactive current transfer limits.

As seen in the resultant active and reactive current transfer limits in figure 3.26, the valid operating points are like a band with a width depending on the receiving end voltage (V_2) and impedance magnitude (Z), and the inclination angle of the band depending on θ_Z ($\tan^{-1}(X/R)$) of the impedance. As explained above, for any current outside this region a valid operating point does not exist. In figure 3.27, the current limits are drawn for a lossless (R=0) line, which is not practically existing; as seen below theoretically no limit exists for pure reactive current for a lossless line.

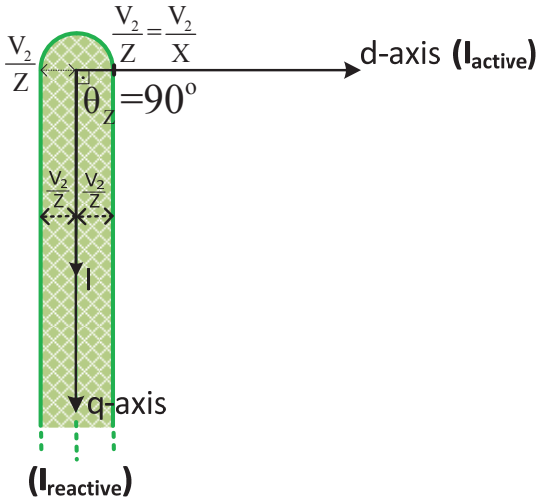

Fig. 3.27 Active/reactive current transfer limits for a lossless line.

3.2.3 Summary of Current Transfer Limit Equations

Summary of the resultant current transfer limit equations are given below, such that for a given current injection angle (active and reactive components), the maximum current magnitude at this injection angle can be calculated, as a function of receiving end voltage magnitude (V_2) and impedance characteristics (R+jX), as below. Various ways to define transfer limits can be derived from these equations.

$$\theta_I \begin{cases} 90^o+\theta_Z > \theta_I > 270^o+\theta_Z \quad \Rightarrow \quad I_{limit}=\dfrac{V_2}{Z.\sin(\left|\theta_Z-\theta_I\right|)} \\ 270^o+\theta_Z > \theta_I > 90^o+\theta_Z \quad \Rightarrow \quad I_{limit}=\dfrac{V_2}{Z} \end{cases} \tag{3.15}$$

$$\theta_I=90^o \text{(pure reactive)} \Rightarrow I_{limit}=\frac{V_2}{Z.\sin(\left|90^o-\theta_Z\right|)} \Rightarrow I_{limit}=\frac{V_2}{Z.\cos(\theta_Z)} \Rightarrow I_{limit}=\frac{V_2}{R}$$

$$\theta_I=0^o \text{(pure active)} \Rightarrow I_{limit}=\frac{V_2}{Z.\sin(\left|0^o-\theta_Z\right|)} \Rightarrow I_{limit}=\frac{V_2}{Z.\sin(\theta_Z)} \Rightarrow I_{limit}=\frac{V_2}{X}$$

$$\theta_I=\theta_Z \text{(imp. angle)} \Rightarrow I_{limit}=\frac{V_2}{Z.\sin(\left|0^o\right|)} \Rightarrow I_{limit}=\frac{V_2}{Z.0} \Rightarrow I_{limit}=\infty$$

3.3 Correlation of Current Transfer Limits with Wind Turbine Current Injection

In the previous sections, the current transfer limits from a bus to another bus through a line has been derived. In order to correlate these limits with the case of current injection from wind turbines during faults, below diagram in figure 3.28 is shown, where a WPP is represented as a single aggregated wind turbine, with the same parameters in figure 2.2 from chapter 2.

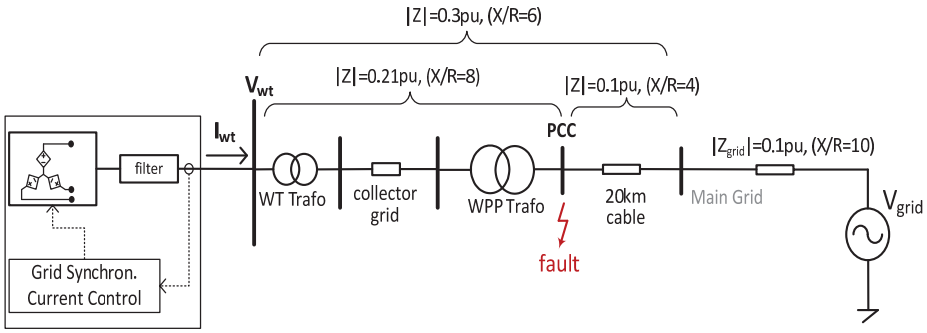

Fig. 3.28 WPP diagram and Thevenin equivalent grid.

In case of a short-circuit fault at PCC, the current flow between WT and the faulted location can be represented with the below single line diagram, where Z represents the impedance between the WT terminal and faulted point (PCC), and V_f represents the voltage at the faulted point (PCC).

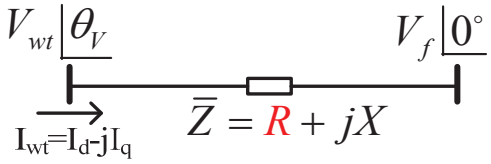

Fig. 3.29 Current flow from WT to a low voltage fault.

The magnitude of the voltage at the faulted bus (PCC) mainly depends on the fault impedance and the grid impedance (grid strength). For a severe fault, faulted bus voltage can drop to very low values close to zero (e.g. 5%). As given in figure 3.28, the impedance between WT and PCC is Z=0.026pu+j0.208pu. In figure 3.30, current

transfer limits are drawn for three different remaining voltages at PCC as 25%, 10% and 2%, together with a WT current magnitude (1pu) circle. While applying the theory of current transfer limits for the WPP current injection, the faulted bus voltage is assumed to have constant magnitude during the fault. The WPP current injection impact (boost or attenuation) on the (remaining) voltage at the faulted bus is neglected, which is analyzed in the appendix in detail.

As observed in figure 3.30, for decreasing voltage at the faulted point (PCC), the current transfer band becomes narrower. As summarized in table I below, when the PCC voltage is high enough, any current can be injected since the band is wider than WT current magnitude rating, i.e. 1pu or 1.25pu. However, when the voltage goes low, a current within rated magnitude can be out of transfer limits for certain injection angles. For example, when the PCC voltage is 10% as in figure 3.30-(b), pure or highly reactive currents can be injected, whereas highly active currents cannot be injected.

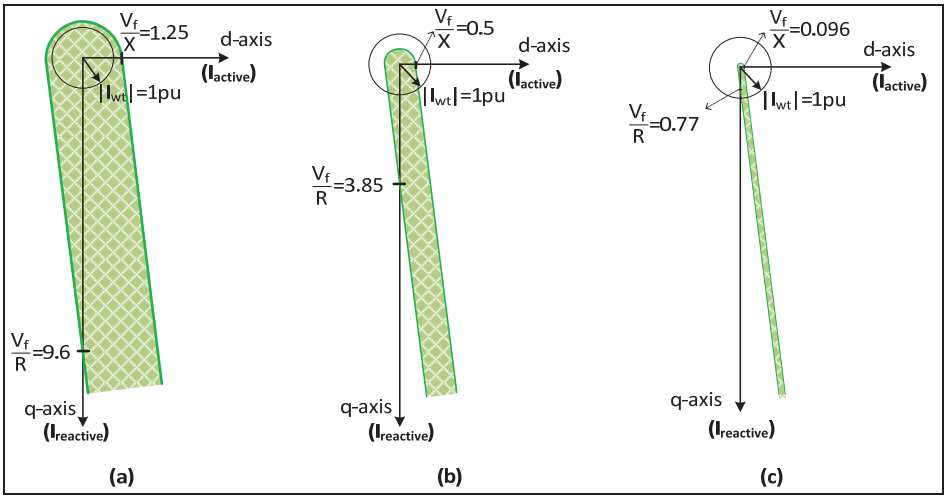

Fig. 3.30 Current transfer limits for V_{pcc}=25% (a), V_{pcc}=10% (b), V_{pcc}=2% (c)

When the PCC voltage is very low, e.g. 2% as in figure 3.30-(c), the band becomes almost a line and current injection angle needs to be close to the impedance angle.

Table 3.1 Current injection versus voltage magnitude at PCC

	I_{wt}=-j1pu (pure reactive)	**I_{wt}=1pu (pure active)**	**I_{wt}=0.86-j0.5pu (highly active)**	**I_{wt}=0.12-j0.99pu (highly reactive)**
V_{pcc}=25%	inside limits	inside limits	inside limits	inside limits
V_{pcc}=10%	inside limits	out of limit	out of limit	inside limits
V_{pcc}=2%	out of limit	out of limit	out of limit	inside limits

Referring to the grid code FRT and reactive current injection (RCI) requirements; assuming that the WPP shown in figure 3.28 is injecting pure reactive current of 1pu during a low voltage fault, the maximum current that can be injected, i.e. intersection of the transfer limit band with the reactive current axis (y-axis), depends on the resistance value between the WT and the faulted point. In other words, the minimum faulted bus voltage magnitude, where the WT can inject 1pu pure reactive current can be found based on (3.10), as in (3.16) below;

$$\theta_I=90^o \quad \Rightarrow \quad I=1pu\angle 90^o=I_{limit} \quad \Rightarrow \quad I_{limit}=\frac{V_f}{R}=1pu \quad \Rightarrow \quad V_f=R\ pu \qquad (3.16)$$

For the WPP in figure 3.28; the minimum FRT voltage levels at the PCC, for injection of pure 1pu reactive current, are shown below for two different cases as; for the case when the fault occurs at PCC and for the case when the fault occurs at the end of 20km cable where the WPP is connected to the main grid. When the fault is at PCC, the resistance of the impedance, R, between WT and the faulted point (PCC) is 0.026pu; hence, based on (3.16), WT can inject pure reactive current of 1pu when the PCC voltage is above 0.026pu (2.6%) as shown in figure 3.31-(a). When the fault is at the main grid connection point (end of 20km line), the impedance, R, between WT and the faulted point is 0.05pu. Hence, WT can inject pure reactive current of 1pu when the voltage is above 0.05pu (5%) at the faulted bus, which results in the voltage at PCC be observed as 10% of the rated voltage with 1pu reactive injection, as shown in figure 3.31-(b).

For the voltage sags below the values shown in figure 3.31, pure reactive current cannot be injected by the wind turbine, irrespective of the performance and stability of the WT control algorithms, since such an operating point does not exist. Pure reactive

current injection within these regions should either be avoided by some means, or problems arising, which are studied throughout this thesis, should be considered and solved with the proposed methods given in the following chapters of this thesis.

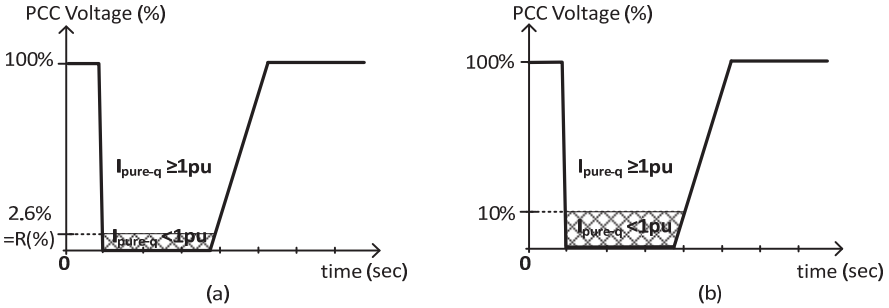

Fig. 3.31Minimum PCC voltage for WPP (figure 3.28) injecting 1pu pure reactive current (a) fault at PCC (b) fault at main grid connection point.

Remark 3.11:

Observing figure 3.31 (a) and (b), it is seen that the minimum PCC voltage required for pure 1pu reactive current injection from wind turbine is changing with the location of the fault. As explained above; for a fault at PCC it is 2.6%, and for a fault at the end of connection line it is 10%. Hence, for a WPP it is difficult to specify certain limits since it is difficult to differentiate between two cases without knowing where the fault is occurring.

The impedance between the WT and the faulted point mainly depends on the WT transformer, WPP collector network, WPP main transformer, and connection cable (if exists). Hence for a WPP with long collector network cables (due to distant location of wind turbines) or a long connection cable (most likely exists for off-shore WPP) impedance would be high and the current limit band would be narrower. It is also important to note that, impedance between the wind turbine and the faulted point (which might be PCC or points further towards main grid) might vary with the temperature of the cables. It can be commented that for high wind conditions, i.e. high power generation, cables' resistance would increase with increasing cable temperature

due to cable loading, and the impedance characteristics would change to be more resistive; making the limit for pure reactive current smaller.

In this section the active and reactive current limits are correlated with the WPP current injection via taking the wind turbine bus (V_{wt}) as the sending end (V_1) and the faulted bus (V_f) as the receiving end (V_2). However, the active/reactive current transfer limits in this chapter are derived based on current flow between two buses, which can be any bus, not necessarily the wind turbine bus and the faulted bus. Hence, for a case that active and reactive currents are controlled at the PCC bus of a WPP, the limits still apply via taking the PCC bus as the sending end and the faulted point as the receiving end. If the fault is occurring at PCC, then the Z value between sending end (PCC) and faulted point (again PCC) is zero and any current can be injected without limit. However if fault is remote from PCC, for instance at the end of the connection cable where the WPP is connected to the main grid, for pure 1pu reactive current injection at the PCC bus, the minimum voltage at the faulted bus has to be 2.4%, due to 0.024pu resistance of the connection cable. With 1pu reactive current injection, the voltage at the PCC bus is observed as 9.7% in this case, as shown in figure 3.32 below.

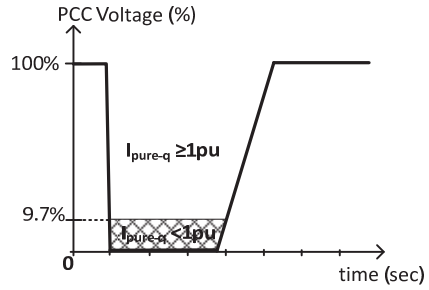

Fig. 3.32Minimum PCC voltage for WPP (figure 3.28) injecting 1pu pure reactive current at PCC and fault occurring at main grid connection point.

Hence, WPP level current control at PCC improves to avoid limitations of current transfer, if fault is at PCC. However, limits still apply if the fault is remote from PCC, which will be discussed in chapter five.

The minimum PCC voltages shown in figures 3.31 and 3.32 are given for pure reactive current injection. However, as will be shown in the following chapters, if the current is not injected as pure reactive, but with an angle close to impedance angle within the transfer limits, then injection can be possible for lower (even zero) PCC voltage magnitudes.

3.4 Two Operating Points Phenomenon

As observed in the derived current transfer limits in (3.15) and also in figure 3.26, a current with magnitude smaller than V_f/Z, is always within the transfer limits, for any current injection angle, as shown in (3.17) and blue-shaded area in figure 3.33.

$$I<\frac{V_f}{Z} \quad \Rightarrow \quad I<I_{limit} \quad \text{for} \quad 0^o < \theta_I < 360^o \tag{3.17}$$

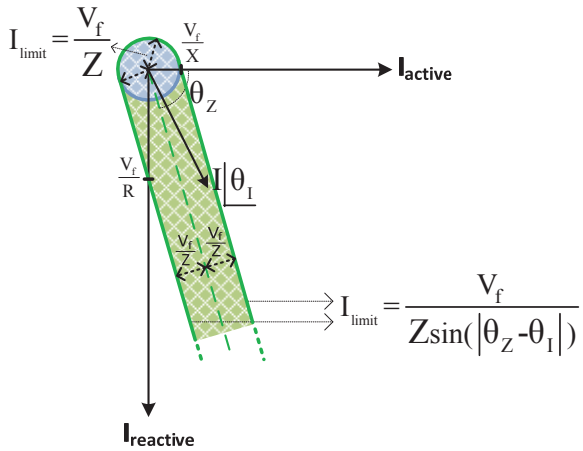

Fig. 3.33 Resultant active/reactive current transfer limits.

Hence, any current injection from the wind turbine with magnitude smaller than V_f/Z (in the blue-shaded area) is definitely within the transfer limits. Currents larger than V_f/Z, can be inside (the green-shaded area) or outside the transfer limits depending on the active and reactive combination, i.e. injection angle.

Another issue for the current larger than V_f/Z is shown in figure 3.34 and 3.35 below. When the current magnitude is larger than V_f/Z, which means that the voltage drop on

the impedance (ZI) is larger than the receiving end V_f voltage, two operating points exist for the same active/reactive current injection; one with θ_V smaller than 90° as in figure 3.34-(a), and another one with θ_V larger than 90°as in figure 3.34-(b), where θ_V is the phase angle difference between the V_f and V_{wt} voltages. As observed in 3.34 and 3.35, the operating point with θ_V larger than 90° results in a very low V_{wt} voltage, compared to the operating point with θ_V smaller than 90°. In figure 3.34-(a), high active and reactive power is supplied from V_{wt} (due to higher V_{wt} voltage) and current lags V_f such that reactive power is supplied to the V_f point (overexcited operation); however in figure 3.34-(b), low active and reactive power is supplied from V_{wt} (due to lower V_{wt} voltage) and current leads V_f such that reactive power is absorbed from the V_f point (underexcited operation). This means that when θ_V is larger than 90°, reactive power is supplied from both ends (V_f and V_{wt}) which is dissipated on the reactance of the line between. It is also important to note that for the operating points with θ_V larger than 90°, voltage at any point between WT and faulted point is smaller than any of V_f or V_{wt}.

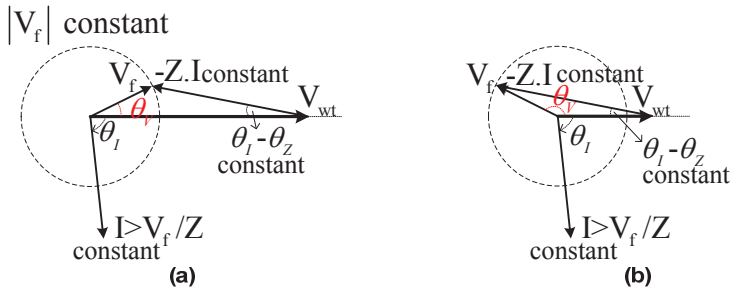

Fig. 3.34 Two operating points with the same current; θ_V smaller (a) and larger (b) than 90°.

As stated above, two operating point issue is occurring for any current with magnitude larger than V_f/Z, thus it also occurs when the current has the same angle of the impedance as in figure 3.35. The existence of two operating points doesn't change current transfer limits derived in this chapter. It is only showing that for the currents in the green-shaded area, there are two operating points for each current, which is still inside the current transfer limits. It will be shown in following chapters that the

operating point with θ_V larger than 90° is not a stable operating point that the system cannot stay at this operating point. It is also important to keep in mind that as seen in the current transfer limits (figures 3.14, 3.17, 3.21, 3.23) above, at the limit points the phase angle difference θ_V between V_f and V_{wt} reaches 90°. It will be shown that during the loss of synchronism events, such a limit point will be reached and operating point will become like in figure 3.34-(b) or 3.35-(b) for transients during frequency fall/rise.

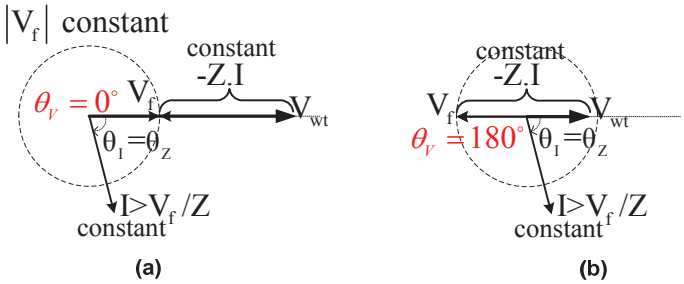

Fig. 3.35 Two operating points with the same current; θ_V equal to 0° (a) and 180° (b).

In summary, if the current magnitude is smaller than V_f/Z, in other words inside the blue-shaded area in figure 3.33, it is definitely inside the transfer limits, with one operating point solution with θ_V smaller than 90°. However, in this case current injection would be very small (or even zero) for severe faults and/or high impedance cases, which would not be acceptable considering grid code requirements. For instance, for the WPP in figure 3.28, if the current injection is kept to be smaller than V_f/Z in order to guarantee operation within current transfer limits, for a fault at PCC with remaining voltage of 5% the current that can be injected has a magnitude of 0.238pu due to 0.21pu Z magnitude (0.238=0.05/0.21). Such a limited current injection scheme will be evaluated in chapter five as a reference solution.

3.5 Conclusion

In this chapter, active and reactive current transfer limits between two buses connected with a line are explored. It is shown that active and reactive current transfer limits do exist similar to the active and reactive power transfer limits, which are well-known from power system theory.

The correlation of the derived transfer limits with the WPP current injection during low voltage faults is given. It is shown that, when the receiving end (faulted point) voltage is very low, the current transfer limit from the sending end (e.g. wind turbine) becomes smaller. Outside the transfer limits a "valid" operating point does not exist. The meaning of invalid operating point and what happens if the wind turbine tries to inject a current out of the defined transfer limits will be analyzed in the next chapter.

It is important to note that the active and reactive current transfer limits derived here is exploring an underestimated phenomenon for wind turbines' current injection during low voltage faults, which has been omitted in the wind power studies before. In the previous studies, it has been assumed that the wind turbine can inject any controlled current from its terminals irrespective of the fault level at the PCC. However, as shown in this chapter, limits apply due to low voltage at the grid side and due to the impedance between WT and PCC, and some currents "cannot" be injected. The theory of current limits derived in this chapter will be verified with simulation and experiment results in the following chapters.

It should be noted that the transfer limits derived in this chapter are "steady-state" limits, such that the limits can be exceeded during short-time transients. It is important to realize that any current out of the defined transfer limits cannot be flowing, which means that there is not any operating point out of the transfer limits in steady-state period of a low voltage fault.

The derived current limits can be utilized for other applications, such as current injection from a STATCOM to a low voltage bus, or HVDC or WPP current injection to a weak grid, including non-faulted operation (when the grid side voltage is at rated). The derived current transfer limits are based on phasor theory; hence can be applied for positive sequence voltages and currents, but also for negative sequence and zero sequence as well.

Chapter 4

Analysis of Loss of Synchronism (LOS) during Symmetrical Faults

In this chapter, Loss of Synchronism (LOS), which was identified in chapter 2, is analyzed. The correlation of LOS occurrence with the active and reactive current transfer limits, which have been derived in chapter 3, is shown. The reasons and dynamics of LOS - frequency fall and rise events during low voltage faults are explored with large-signal and small-signal stability analysis, verified with EMT simulations and experimental results of a grid-connected converter.

4.1 Correlation of Observed LOS and Current Transfer Limits

The active and reactive current transfer limits have been derived in chapter 3. It is shown that, especially for severe symmetrical faults, where the grid voltage drops down close to zero, and for high impedance between the WT and the faulted point (e.g. PCC), strict current transfer limits exist. However it is known that, these transfer limits, which sets dependency between active and reactive current components, have not been considered within conventional control methods. Hence, while the WPP is injecting active and reactive currents during low voltage faults based on conventional control methods, the referenced currents may easily be out of the transfer limits, which might cause LOS events shown in chapter 2. In order to see the relation between LOS events in chapter 2 and the current transfer limits in chapter 3, figure 4.1 is given. In figure 4.1, the transfer limits in figure 3.30 are imposed on the results from figure 2.7. As seen in figure 4.1, the observed LOS events are consistent with the transfer limits, such that

the LOS events are occurring for cases 1, 3, and 6 where the current references are out of the transfer limits (green-shaded areas).

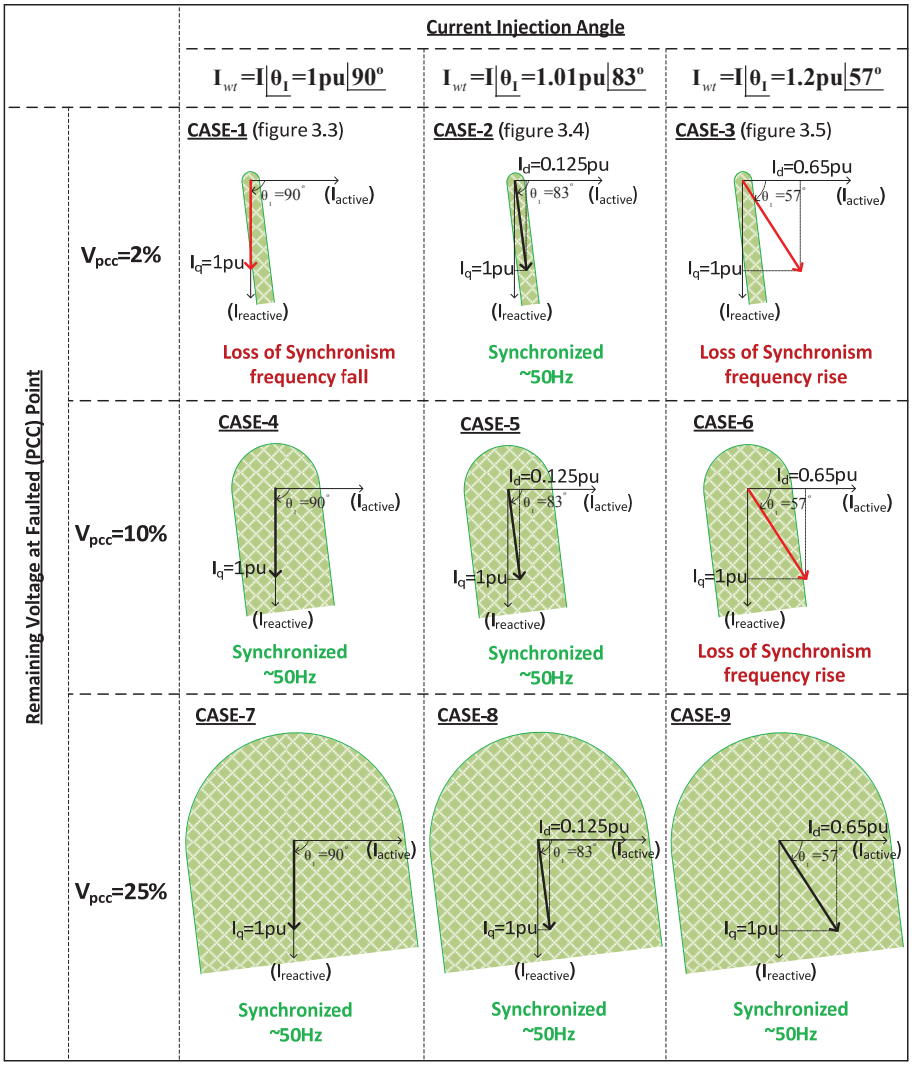

Fig. 4.1 Correlation of Observed LOS and Current Transfer Limits.

The LOS events in this study are observed when the current references are out of the current transfer limits, such that the WT is referenced to operate at a point where a valid operating point does not exist. An analogy can be given from classical power

system theory; such that the conventional synchronous generator accelerates during a low voltage fault if the synchronous generator is given an input mechanical power higher than the electrical power transfer limit.

4.1.1 Response of WT to Non-transferrable Current Reference

As shown in active and reactive current transfer limits between two buses in chapter 3, when the receiving end (PCC) voltage is very low (e.g. 2%) the active and reactive current flow is mainly dictated by the X/R ratio of the impedance between the two buses. Based on figure 3.11 and (3.9), when the receiving end voltage is very low (e.g. smaller than 2%), the transferrable current has the angle of the impedance between two buses (between WT and PCC bus).

$$V_f \approx 0 \quad \Rightarrow \quad \frac{I_{active}}{I_{reactive}} = \frac{R}{X} \quad \Rightarrow \quad \theta_I = \theta_Z \tag{4.1}$$

In such a severe fault case the WT current angle is dictated by the grid impedance irrespective of the referenced current; in other words the grid dictates the current to stay within the band of the current transfer limits. Hence, active and reactive current references cannot be realized. The simulation case from chapter 2, figure 2.2 is executed again for a severe fault occurring at PCC point, where the PCC voltage drops to 1% of the rated. It should be remembered that in this case the impedance between WT and PCC had X/R ratio of 8, which implies an impedance angle of 83°. The case, with pure reactive current reference, is shown in figure 4.2 below. As observed in second subfigure, active and reactive current references are realized. However, the measured active and reactive current references are calculated based on the angle estimated by the PLL. In order to see the actual active and reactive current components, phase-"a" voltage and current are shown in third subfigure. Around time equal to 1.06 second, where the WT operates at a quasi stationary point around 45Hz, the zero crossing time difference between phase-"a" voltage and current is found to be 5 millisecond, which implies that the phase difference of 81°. Even though the angle of the current reference was given as 90°, the actual current is dictated by the grid to be inside the current transfer band. In the fourth subfigure, the V_d and V_q signals within the PLL are shown. As known, the PI compensator of the PLL acts on the error, the V_q

signal, to lock the measured voltage to V_d, i.e. d-axis. As seen in fourth subfigure, before the fault at time equal to 1 second, PLL is able to keep the V_q signal at zero, which means that the estimated angle is correct. However, during the fault, there occurs a sustained (negative) V_q error, which cannot be compensated. Thus, the current regulator is able to realize the current reference with respect to the estimated d&q axes but the estimated d&q axes by PLL are incorrect. It should be noted that the sustained estimation error of the PLL arises due to the given current reference, which is out of the current transfer limits. The referenced current and the transfer limits are shown in figure 4.4-(a), and the resultant quasi steady-state phasor diagram showing actual current phasors together with the referenced and transfer limits is given in figure 4.4-(b).

The results of case with 1pu reactive end 0.65pu active current reference during a severe fault at PCC, where the voltage drops to 1% of the rated, is given in figure 4.3. Similar to the previous case, the referenced active and reactive currents cannot be realized and the actual current angle is observed as 85°, though the reference is 57°. A sustained (positive) V_q signal, i.e. PLL error, is observed during the fault. The referenced current and the transfer limits are shown in figure 4.5-(a), and the resultant actual current phasors together with the referenced and transfer limits are shown in figure 4.5-(b).

It is shown that a current reference out of the transfer limits causes a sustained PLL estimation error. When the sustained estimation error is continuously integrated by the integrator of the PLL, a fall or rise of frequency is observed as in chapter 2 and here. As discussed in section 2.2.6, in practical saturation is applied for the integrator and calculated frequency within the PLL. However, limiting the frequency to a value (e.g. 45Hz or 55Hz) doesn't change the fact that the sustained estimation error occurs. In the next chapter implementation of the saturation and anti-windup algorithms for the PLL and impact will be evaluated.

It should be kept in mind that, the sustained estimation error arises due to the current reference out of the transfer limits. Hence, the LOS is an issue related to the "inconvenient" active and reactive current references and causes loss of control of active and reactive currents, i.e. loss of vector control.

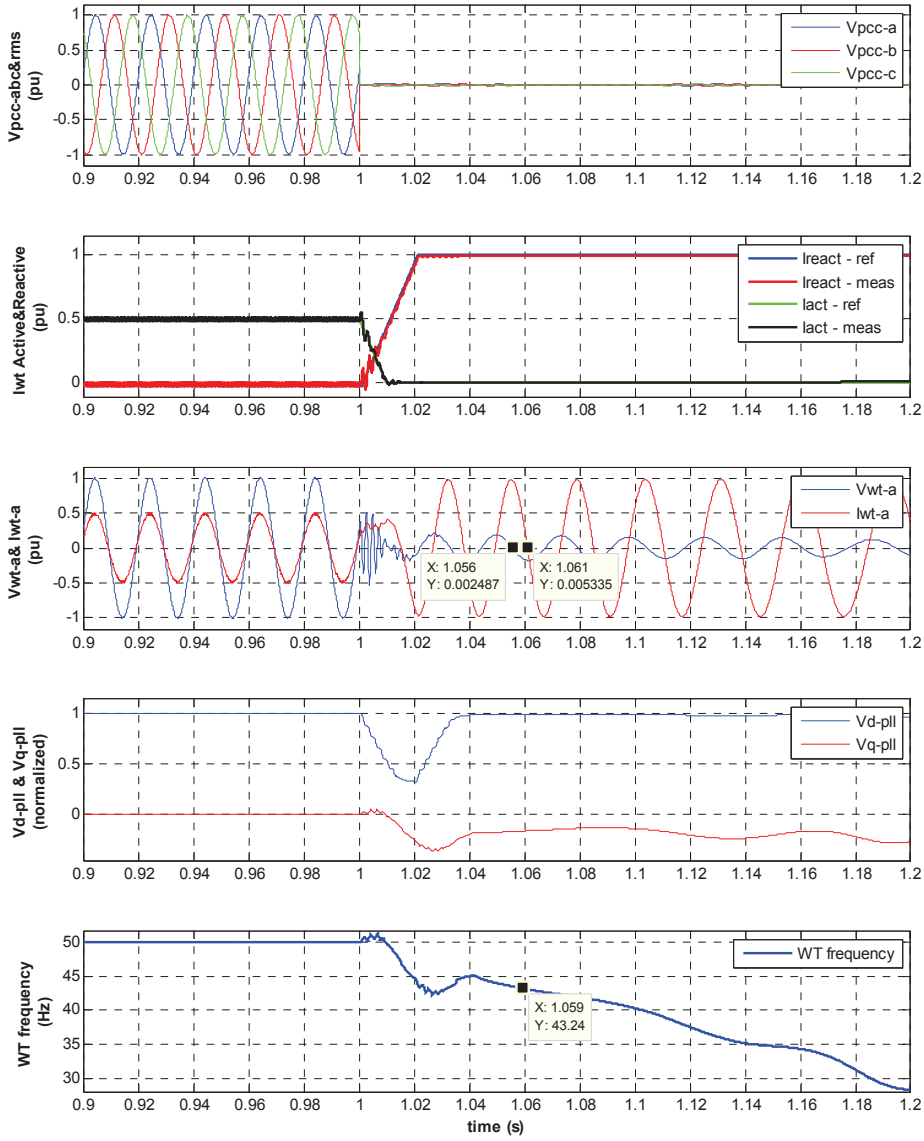

Fig. 4.2 WT response during LOS – frequency fall event.

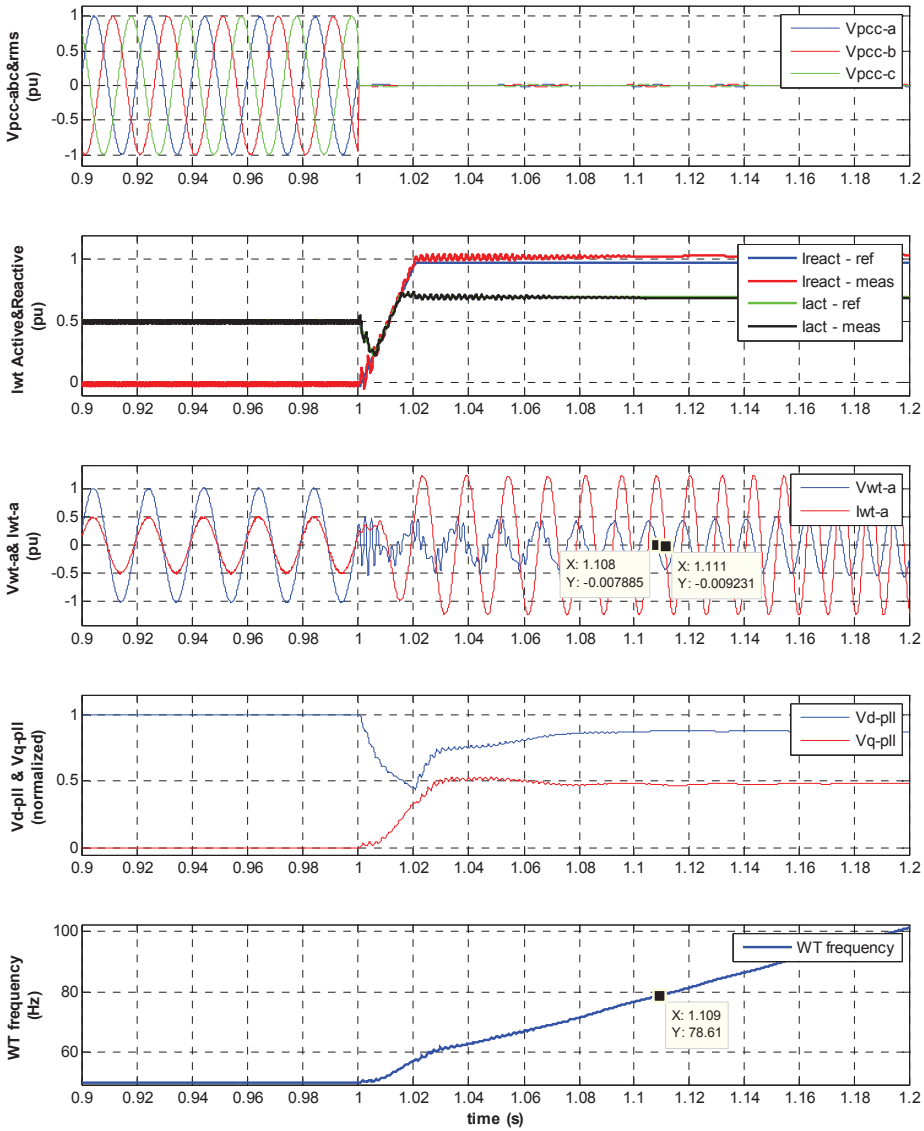

Fig. 4.3 WT response during LOS – frequency rise event.

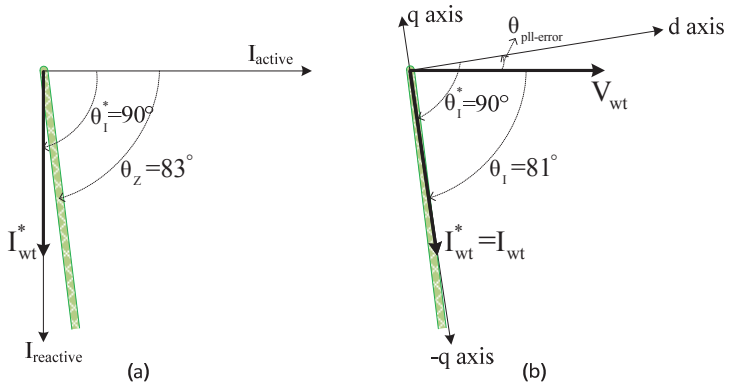

Fig. 4.4 Current transfer limits and (a) pure reactive reference current phasor, (b) WT voltage and actual current – causing sustained negative PLL error and LOS frequency fall.

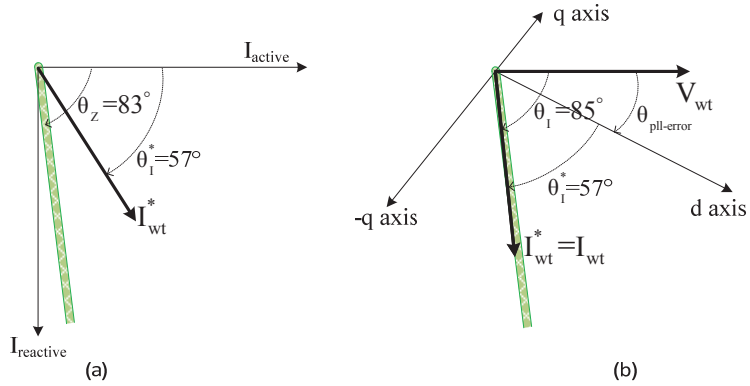

Fig. 4.5 Current transfer limits and (a) highly active reference current phasor, (b) WT voltage and actual current – causing sustained positive PLL error and LOS frequency fall.

Based on the current transfer limits, an equation for the change of frequency of the WT can be obtained empirically as below, where Ki is the integral gain of the PLL. The V_q signal magnitude disappears with the use of the normalization block for measured phase voltages in the PLL.

$$\frac{df_{wt}}{d_t} = K_i V_q = K_i \sin(\theta_{pll\text{-}error}) = K_i \sin(\theta_Z - \theta_I^*) \tag{4.2}$$

4.2 Large-Signal Stability Analysis of PLL during LOS

The analysis of the LOS is done using the WPP structure in figure 4.6 below, which is aggregated as a single wind turbine and used in the previous cases. As done in the previous cases, a symmetrical severe fault at PCC point (alternatively at the point where the WPP is connected to the main grid) is considered.

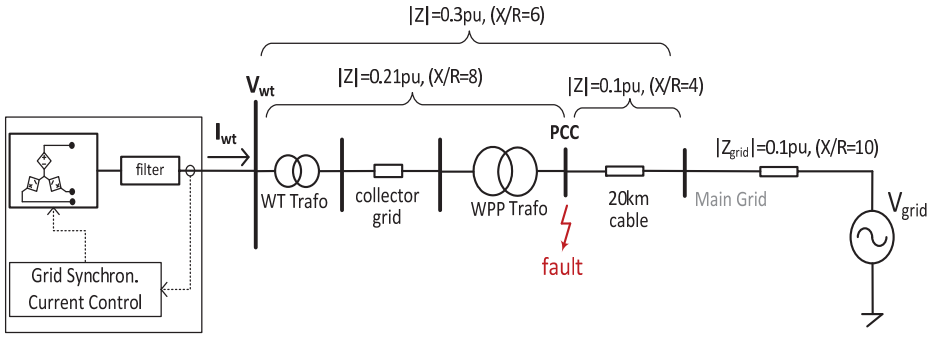

Fig. 4.6 WPP structure used in large-signal stability analysis.

Voltage at the faulted point (e.g. PCC) is assumed to be constant (i.e. constant V_f) and the impedance between the wind turbine and the faulted point is represented as Z (R+jX) as shown in figure 4.7. In this case the grid-side voltage becomes the faulted point voltage V_f with phase angle θ_f.

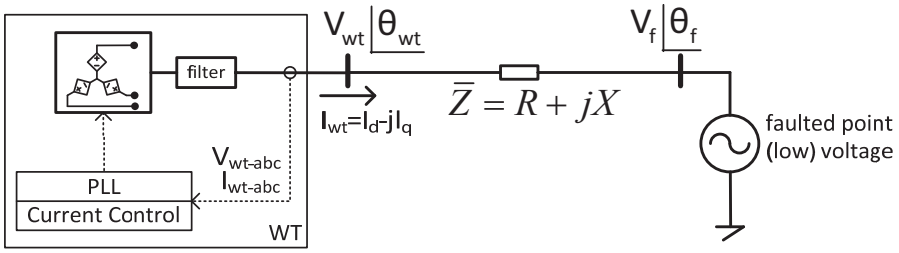

Fig. 4.7 Current injection during fault.

Based on the separation principle the voltage at the wind turbine terminal V_{wt}, where the phase voltages and currents are measured for feedback to PLL and current control, can be obtained as superposition of two sources; the grid side (faulted point) voltage V_f

and the current injection by the wind turbine, as shown in figure 4.8, similar to the approach in [79]. The saturation blocks, which were shown in PLL structure in figure 2.10, are not shown for simplicity in this case.

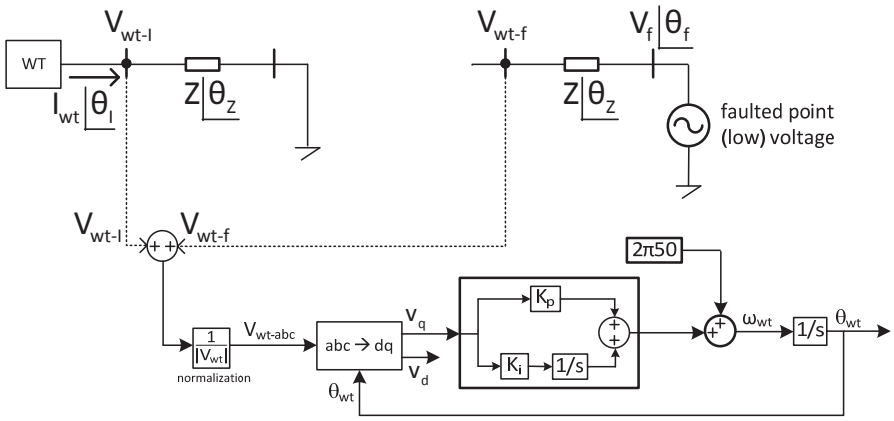

Fig. 4.8 Wind turbine voltage during fault as superposition of two sources [79].

The wind turbine feedback voltage can be written as composition of two voltages as in (4.3) to (4.5) below;

$$V_{wt} = V_{wt\text{-}I} + V_{wt\text{-}f} \tag{4.3}$$

$$V_{wt\text{-}I} = Z\underline{|\theta_Z} \cdot I_{wt}\underline{|\theta_I} \tag{4.4}$$

$$V_{wt\text{-}f} = V_f\underline{|\theta_f} \tag{4.5}$$

The phasor diagram showing the active and reactive current injection, together with wind turbine and faulted point voltages is given in figure 4.9.

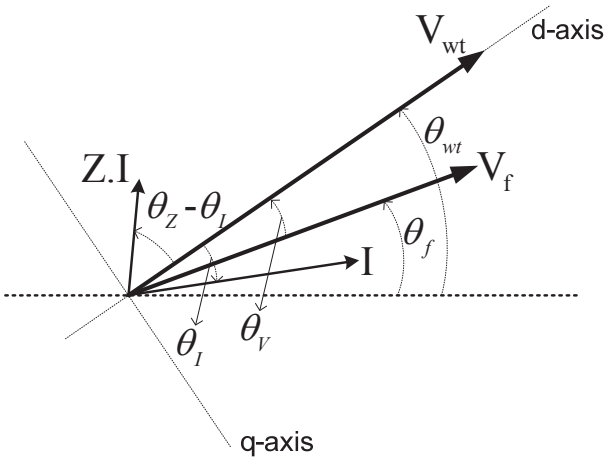

Fig. 4.9 Phasor diagram showing wind turbine voltage, current and fault point voltage.

The q-axis component of the wind turbine voltage, which is error input of the PI compensator within PLL, can be written in terms of the q-axis components of the two sources; grid-side (faulted point) voltage and the voltage drop on the impedance due to the injected current (ZI), as in (4.6) to (4.8);

$$V_{q-} = \sin(\theta_V) \cdot V_f \tag{4.6}$$

$$V_{q+} = \sin(\theta_Z - \theta_I) \cdot Z \cdot I_{wt} \tag{4.7}$$

$$V_q = V_{q-} + V_{q+} \tag{4.8}$$

The grid angle reference that is tracked in this case is the angle of the faulted pointed voltage, which represents the grid voltage in the faulted network, and the frequency of the main grid is the frequency at the faulted point. The mathematical model of the PLL for a quasi-stationary operating point, where the grid (faulted point) frequency ω_f, and wind turbine frequency, ω_{wt}, can have different values (due to possible LOS), is shown in figure 4.10 below [79]. The feedback sourcing from the grid (faulted point) voltage V_{q-} provides the necessary negative feedback for the PLL to track the grid phase angle θ_g, which is θ_f in the faulted case. However, the feedback sourcing from the current injection,V_{q+}, behaves as a positive feedback, which can be considered as a disturbance to the stability of the PLL. The angle and magnitude of the impedance Z is taken as a

function of the wind turbine frequency. The angle of the injected current, θ_I, is based on the active and reactive current magnitudes and independent of the wind turbine frequency.

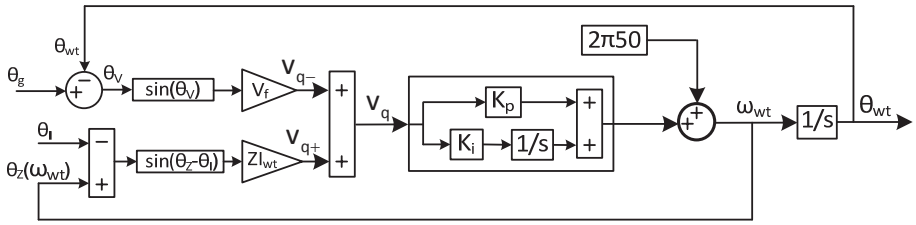

Fig. 4.10 Quasi-stationary model of the PLL [79].

The large signal stability of the PLL requires a negative feedback magnitude larger than the positive feedback as given in (4.9) and (4.10);

$$\left|V_{q-}\right| > \left|V_{q+}\right| \tag{4.9}$$

$$\left|V_f \sin(\theta_V)\right| > \left|ZI_{wt} \sin(\theta_Z - \theta_I)\right| \tag{4.10}$$

The constraint for current magnitude can be written as in (4.11) for θ_V equal to ±90°;

$$\frac{V_f}{Z\sin\left|(\theta_Z - \theta_I)\right|} > I_{wt} \tag{4.11}$$

It is interesting to see that the large-signal stability limit for the PLL is found to be the same as the current transfer limits from chapter 3, figure 3.26 and equation (3.15). As also seen in (4.10), large-signal stability depends on the current injection angle θ_I, such that injection angle same as impedance angle reduces the positive feedback component (V_{q+}) to zero, providing stability. The global large-signal stability requirement is given in (4.12), which is the counterpart of the blue-shaded circle in figure 3.33 in chapter 3, such that when the voltage drop on the impedance is smaller than the faulted point voltage magnitude, stability is provided for any injection angle.

$$\frac{V_f}{Z} > I_{wt} \tag{4.12}$$

As observed in (4.10) and phasor diagram in figure 4.9 above, the large-signal stability limit is reached when θ_V reaches ±90°; similar to the cases in chapter 3 (figures 3.14,

3.17, 3.21, 3.23). As observed in the previous cases, a frequency deviation (fall or rise) from the main grid (faulted point) frequency during a LOS implies that the angle difference θ_V goes beyond ±90° and causes phase jumps at the wind turbine voltage with respect to the faulted point voltage.

It will be shown in the following parts with small-signal stability analysis that the instability can also be observed before θ_V reaches ±90°, due to sensitivities for the operating points with θ_V close to ±90°.

For the current magnitudes causing large-signal instability, which are found to be the same as current transfer limits, LOS occurs as observed in previous cases. During the LOS, the positive feedback magnitude becomes larger than the negative feedback magnitude causing sustained PLL error V_q. As discussed in the preceding section compensation (proportional plus integration) of sustained error causes deviation of the wind turbine frequency. Based on the sustained error magnitude, neglecting the negative feedback (due to low V_f) and the transient contribution from the proportional compensator, the rate of change of frequency is calculated as below;

$$V_q = V_{q-} + V_{q+} = V_f \sin(\theta_V) + ZI_{wt} \sin(\theta_Z - \theta_I) \tag{4.13}$$

$$\omega_{wt} = 2\pi 50 + (K_p + \frac{K_i}{s})V_q \tag{4.14}$$

$$\frac{d\omega_{wt}}{d_t} = K_i V_q = K_i ZI_{wt} \sin(\theta_Z - \theta_I) \tag{4.15}$$

Approximating the V_{wt} voltage magnitude as the voltage drop on the impedance, ZI, for very low fault voltages, the V_q signal is divided by ZI magnitude due to the normalization function within PLL, in figure 4.8, yielding the rate of change of frequency as;

$$\frac{d\omega_{wt}}{d_t} = K_i \sin(\theta_Z - \theta_I) \tag{4.16}$$

For the case in figure 4.2 (case-1 in figure 2.4), where the current reference was given as 90° to an impedance of 83°, the rate of change of frequency (with a PLL K_i of 3000) is calculated to be around -58Hz/sec, which can also be seen in figure 4.2.

$$\frac{df_{wt}}{d_t} = \frac{K_i \sin(\theta_Z - \theta_I)}{2\pi} = \frac{3000 \times \sin(83-90)}{2\pi} = -58 Hz/\sec \quad (4.17)$$

It is important to note that during LOS-frequency fall, the impedance characteristics (magnitude and angle) change considerably due to change of frequency. Since the frequency is falling towards zero the reactance component (X) magnitude decreases towards zero, causing the impedance to become pure resistance with zero angle ($\theta_Z(\omega_{wt})=0°$); which in turn increases error magnitude causing exponentially increasing of rate of change (fall) of frequency. Similarly for the case in figure in 4.3 (case-3 in figure 2.6), where the current reference was given as 57° to an impedance of 83°, the rate of change of frequency (with a PLL K_i of 3000) is calculated to be around +209Hz/sec.

$$\frac{df_{wt}}{d_t} = \frac{K_i \sin(\theta_Z - \theta_I)}{2\pi} = \frac{3000 \times \sin(83-57)}{2\pi} = +209 Hz/\sec \quad (4.18)$$

In this case rise of frequency cause the impedance to become pure reactance ($\theta_Z(\omega_{wt})=90°$), again causing exponentially changing frequency. Rate of change of frequency value gives the chance to evaluate the impact of a LOS event during a low voltage fault. For instance, for the cases given previously, considering typical fault duration of 150ms, the frequency would deviate around -9Hz for the fall event and 31.5Hz for the rise event. This implies that a considerable frequency deviation would occur, which should be avoided by solutions as will be given in the following chapters. Such a rate of change of frequency can represent the "inertia" of the wind turbine during LOS event, and would be beneficial to analyze how fast the LOS and frequency deviation would occur.

4.3 Experimental Verification of the Simulation Results

In this section, a grid-connected converter, which is representing an aggregated WPP and injecting active/reactive current during a low voltage fault, is experimentally investigated. The experimental setup is shown in Figure 4.11 below. The converter's dc side is connected to a dc power supply, with 650Vdc. The current transfer limits and LOS are verified based on the remaining voltage at the faulted point and the impedance between the controlled point (WT) and the faulted (PCC) point. The PLL is

implemented with a saturation limit, which is kept high as 0Hz minimum and 60Hz maximum, in order observe the frequency fall/rise during LOS substantially. Three cases are created similar to the cases 1 to 3 in chapter 2 and section 4.1. In case-1 pure reactive current, in case-2 a combination of active and reactive current, and in case-3 high active current is injected by the converter. As seen in Figure 4.11, the experimental setup has relatively low impedance magnitude (Z=0.018pu+j0.036pu) with a low X/R ratio of 2 (θ_Z=63°) between the WT terminal and the PCC, where the fault is created.

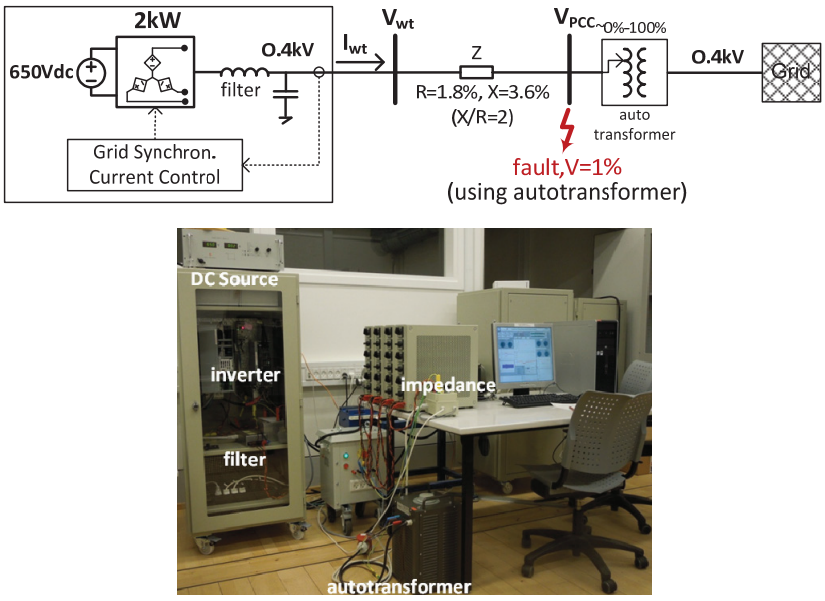

Fig. 4.11 Experimental setup.

The voltage sag at the bus called as PCC is created by use of the autotransformer, which can drop the voltage down to 0.01pu (1% of the rated).

In the experimental case-1, shown in Figure 4.12, pure 1pu reactive current is referenced to the wind turbine when the voltage sag is created at time equal to 2.2 second. As expected, LOS – frequency fall occurs, similar to the simulation case-1 (figure 2.4) in chapter 2. As seen in first subfigure, the vector control algorithm is realizing the active and reactive current references, with respect to the angle estimated by the PLL. However, as explained in above parts, PLL estimation is incorrect as also

seen in third subfigure that the V_q component remains as a non-zero negative value during the current injection. Due to the sustained PLL error, negative V_q, the frequency calculated by the PLL, thus frequency of the voltage and current generated by the converter, falls down to zero (dc).

In the experimental case-2, shown in Figure 4.13, current reference with 0.375pu active and 0.75pu reactive components, which are having the same ratio as X/R ratio of the impedance, is given to the wind turbine at time equal to 3.15 second. The current reference and the impedance have the same angle of 63°. Hence, LOS does not occur and converter stays synchronized at 50Hz, similar to the simulation case-2 (figure 2.5) in chapter 2. As seen in third subfigure, the PLL error V_q is kept around zero in this case.

In the experimental case-3, shown in Figure 4.14, the WT has 1pu active current reference and 1pu reactive current is referenced when the voltage sag is created at time equal to 2.75 second, causing highly active current reference, which has angle of 45°, smaller than the impedance angle of 63°. As expected, LOS – frequency rise occurs, similar to the simulation case-3 (figure 2.6) in chapter 2, since the current reference angle is lower than impedance angle. As seen in first subfigure, the vector control algorithm is realizing the active and reactive current references, with respect to the angle estimated by the PLL. However, as explained in above parts, PLL estimation is incorrect during LOS, as also seen in third subfigure that the V_q component remains as a non-zero positive value during the LOS. Due to the sustained PLL error, positive V_q, the frequency calculated by the PLL, thus frequency of the voltage and current generated by the converter, rises towards 60Hz.

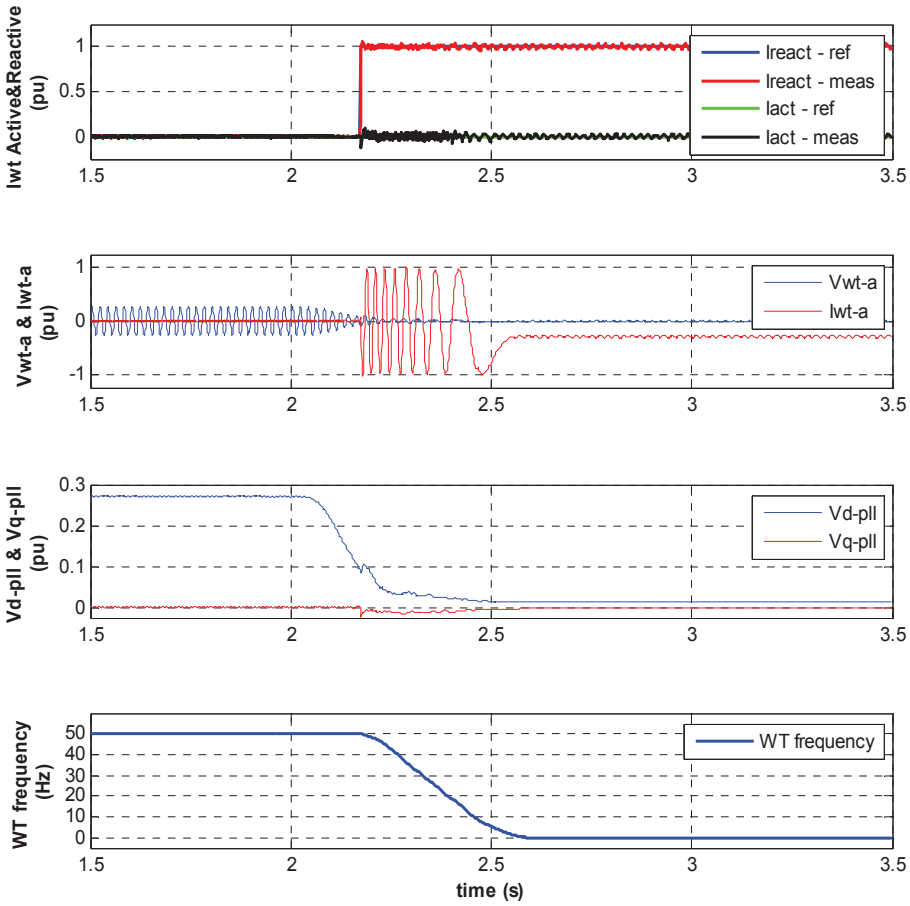

Fig. 4.12 Experimental case-1: Loss of Synchronism – Frequency Fall.

Based on (4.15), the rate of change of frequency is calculated as -150Hz/sec, as also observed in Figure 4.12.

$$\frac{df_{wt}}{d_t} = \frac{K_i V_q}{2\pi} = \frac{K_i \sin(\theta_Z - \theta_I)}{2\pi} = \frac{2000 \times \sin(63-90)}{2\pi} = -150 Hz/\sec \qquad (4.19)$$

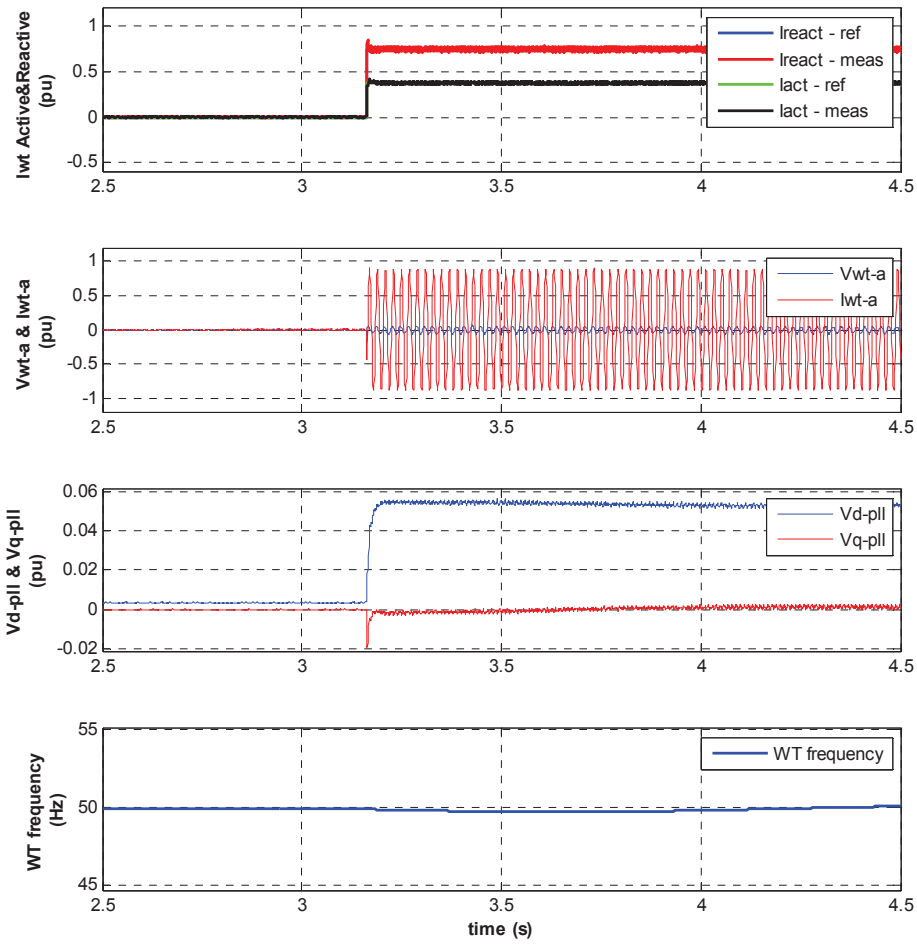

Fig. 4.13 Experimental case-2: Stable operation – synchronized to 50Hz.

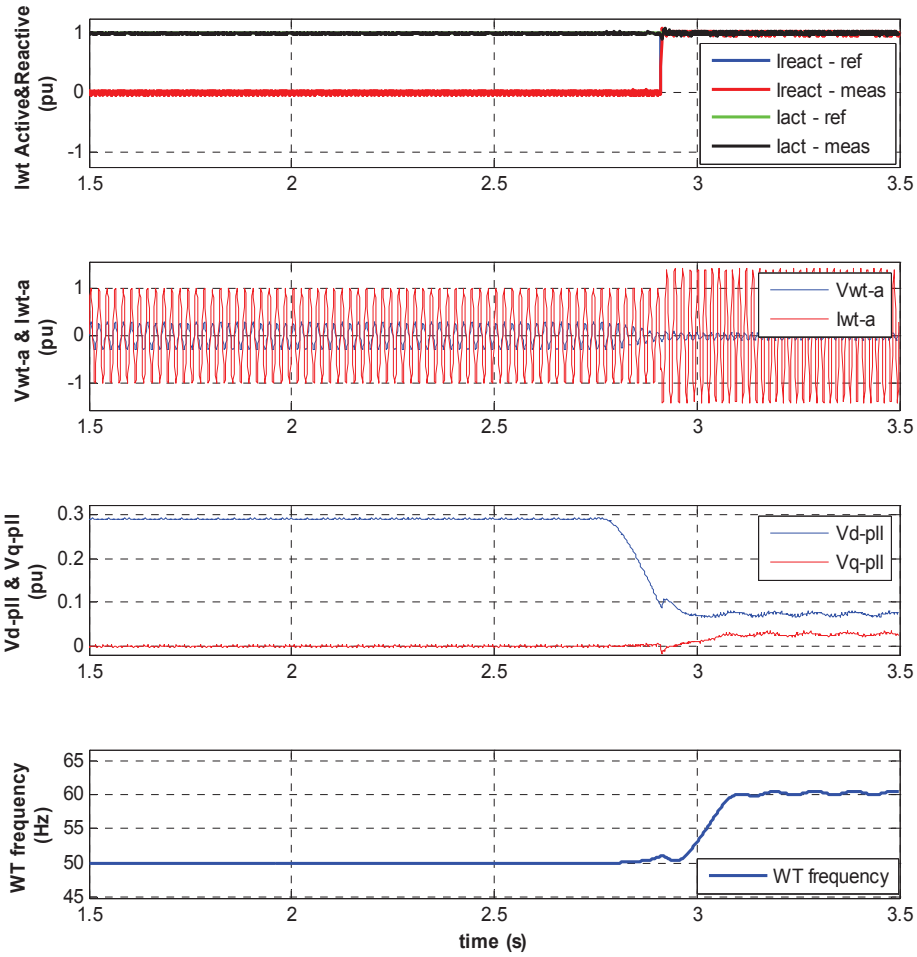

Fig. 4.14 Experimental case-3: Loss of Synchronism – Frequency Rise.

Based on (4.15), the rate of change of frequency is calculated as +100Hz/sec, as also observed in Figure 4.14.

$$\frac{df_{wt}}{d_t} = \frac{K_i V_q}{2\pi} = \frac{K_i \sin(\theta_Z - \theta_I)}{2\pi} = \frac{2000 \times \sin(63-45)}{2\pi} = +100 Hz/\sec \qquad (4.20)$$

4.4 Small-Signal Stability Analysis within Transfer Limits

Small-signal stability of a system is a measure of its stability against small-signal disturbances, when the system is operating at a steady-state point. Hence, small-signal stability of the WT can be analyzed if the WT is at a valid operating point. However, as discussed above, the LOS events in this study are observed (cases 1, 3, and 6) when the current references are out of the current transfer limits, such that the WT is referenced to operate at a point where a valid operating point does not exist, which is shown to cause large-signal stability. Hence, small-signal stability analysis cannot be conducted for the LOS cases 1, 3, and 6. However, the non-problematic cases with current references within the transfer limits (cases 4, 5, 7, 8, and 9) are shown to be operating stable. It is shown that using the generic current regulator and grid synchronization (PLL) structures and tuning them in accordance with the grid and wind turbine performance requirements, the wind turbine is able to inject current references when the references are within the transfer limits. As known from literature, small-signal stability of the wind turbine is a concern when the grid voltage is very low and/or the grid impedance is high (weak grid). Also, as will be seen in the next chapter, some of the proposed solutions in this thesis are based on modifying the current references to be inside the transfer limits. Hence, it is beneficial to analyze small-signal stability of the wind turbine for current injection within the transfer limits. It should be kept in mind that even though the wind turbine has small-signal stability for the current references within the transfer limits, the wind turbine inevitably experiences LOS when referenced currents are out of the transfer limits.

The model in figure 4.10 is utilized for small-signal stability analysis, as done in [79]. In this study, small-signal stability analysis is done only for the faulted case without any local loads at PCC, where the fault is occurring at PCC, as shown in figure 4.6 above. The large-signal negative and positive feedback terms are linearized at an operating point (with current injection within transfer limits) and at an operating frequency (of the wind turbine), ω_{op}, to reach small-signal model. The negative feedback terms are linearized as below;

$$V_{q-}=V_f \sin(\theta_V) \tag{4.20}$$

$$\tilde{V}_{q-}=V_f \cos(\theta_V) \tag{4.21}$$

The θ_V angle at the operating point can be obtained by solving the below equality based on current injection magnitude (I_{wt}) and angle (θ_I).

$$V_f \sin(\theta_V)=I_{wt} Z \sin(\theta_Z-\theta_I) \tag{4.22}$$

It is important to note that, when the difference between impedance angle (θ_Z) and current angle (θ_I) increases, the phase angle difference (θ_V) between wind turbine voltage and faulted point voltage increases, such that 90° the transfer limit is reached. Due to cosine term in (4.21), operating points with θ_V larger than 90° result in a negative gain at the negative feedback of the PLL, which will be shown to cause instability. The positive feedback terms are linearized as below;

$$V_{q+}=I_{wt}\left|Z(\omega_{wt})\right|\sin(\theta_Z(\omega_{wt})-\theta_I) \tag{4.23}$$

$$\tilde{V}_{q+}=I_{wt}\left[\left|Z(\omega_{wt})\right|+k_Z\tilde{\omega}_{wt}\right]\sin(\left|\theta_Z(\omega_{wt})-\theta_I\right|+k_\theta\tilde{\omega}_{wt}) \tag{4.24}$$

$$\tilde{V}_{q+}=I_{wt}\left[\left|Z(\omega_{wt})\right|+k_Z\tilde{\omega}_{wt}\right]\left[\sin(\left|\theta_Z(\omega_{wt})-\theta_I\right|)+k_\theta\tilde{\omega}_{wt}\right] \tag{4.25}$$

$$k_Z=\left.\frac{\sigma\left|Z(\omega_{wt})\right|}{\sigma\omega_{wt}}\right|_{\omega_{wt}=\omega_{op}}=\left.\frac{\sigma\sqrt{R^2+(\omega_{wt}L)^2}}{\sigma\omega_{wt}}\right|_{\omega_{wt}=\omega_{op}}=\frac{L^2\omega_{op}}{\sqrt{R^2+(\omega_{op}L)^2}}=\frac{L^2\omega_{op}}{\left|Z(\omega_{op})\right|} \tag{4.26}$$

$$k_\theta=\left.\frac{\sigma\left|\theta_Z(\omega_{wt})-\theta_I\right|}{\sigma\omega_{wt}}\right|_{\omega_{wt}=\omega_{op}}=\left.\frac{\sigma\tan^{-1}\left(\frac{\omega_{wt}L}{R}\right)}{\sigma\omega_{wt}}\right|_{\omega_{wt}=\omega_{op}}=\frac{L}{R\left(1+\left(\frac{\omega_{op}L}{R}\right)^2\right)}=\frac{RL}{\left|Z(\omega_{op})\right|^2} \tag{4.27}$$

The operating point frequency ω_{op} is taken as fundamental frequency (50Hz) in the calculations in this section.

$$\tilde{V}_{q+}=I_{wt}\underbrace{\left[\left|Z(\omega_{op})\right|k_\theta+\sin(\left|\theta_Z(\omega_{op})-\theta_I\right|)k_Z\right]}_{K_{+FB}}\tilde{\omega}_{wt}=I_{wt}K_{+FB}\tilde{\omega}_{wt} \tag{4.28}$$

Substituting k_z and k_θ from (4.26) and (4.27) into (4.28), the positive feedback gain term (4.29) is obtained;

$$K_{+FB}=\left|Z(\omega_{op})\right|\frac{RL}{\left|Z(\omega_{op})\right|^2}+\sin(\left|\theta_Z(\omega_{op})-\theta_I\right|)\frac{L^2\omega_{op}}{\left|Z(\omega_{op})\right|}=\frac{L}{\left|Z(\omega_{op})\right|}\left(R+\sin(\left|\theta_Z(\omega_{op})-\theta_I\right|)L\omega_{op}\right) \quad (4.29)$$

The small-signal model of the PLL is obtained as in figure 4.15 below [79]. As stated above, for θ_V larger than 90° the negative feedback gain gets negative value, causing small-signal instability as shown below. The transfer function at the operating point around fundamental frequency (50Hz) is obtained as in (4.30).

$$\frac{\tilde{\omega}_{wt}}{\tilde{\theta}_g}=\frac{s\left(K_p\cos(\theta_V)V_f s+K_i\cos(\theta_V)V_f\right)}{s^2(1-K_pI_{wt}K_{+FB})+s\left(K_p\cos(\theta_V)V_f-K_iI_{wt}K_{+FB}\right)+K_i\cos(\theta_V)V_f} \quad (4.30)$$

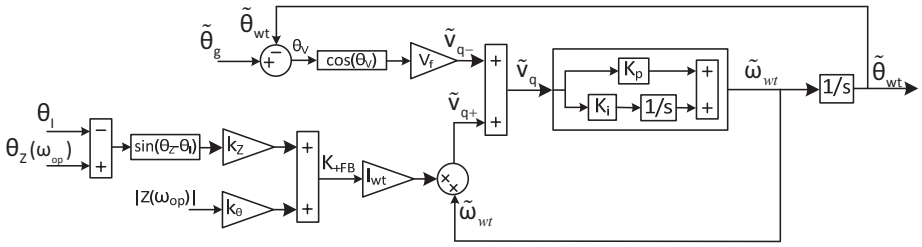

Fig. 4.15 Small-signal model of PLL [79].

The transfer function in (4.30) can give measure of frequency behavior during a fault with current injection from wind turbine against a small disturbance in the grid phase angle (e.g. as a result of a load disconnection on the grid side). Based on the characteristic equation in the denominator of the transfer function in (4.30), the small-signal stability criteria can be obtained as in (4.31);

$$\frac{\left(K_p\cos(\theta_V)V_f-K_iI_{wt}K_{+FB}\right)}{(1-K_pI_{wt}K_{+FB})}>0 \quad (4.31)$$

Assuming that the wind turbine current is around 1pu and the proportional constant K_p is not larger than $1/K_{+fb}$, the denominator in (4.31) is positive; yielding the stability criteria in (4.32), which is expanded as in (4.33);

$$K_p \cos(\theta_V) V_f > K_i I_{wt} K_{+FB} \tag{4.32}$$

$$K_p \cos(\theta_V) V_f > K_i I_{wt} \frac{L}{|Z(\omega_{op})|} \left(R + \sin(|\theta_Z(\omega_{op}) - \theta_I|) L \omega_{op} \right) \tag{4.33}$$

Interpreting (4.33), it can be commented that for higher V_f values, or smaller current magnitudes, stability can be provided easily, as same was also commented in chapter 3 with the current transfer limits approach. It is important to note that when the current injection angle is same as the impedance angle, the second term on the right hand side of (4.33) is eliminated but still small-signal instability can occur depending on the controller gains, fault voltage and impedance characteristics. When the current angle deviates from the impedance angle, θ_V angle increases as given in (4.22); thus the right hand side term increases due to the sine term and left hand side term decreases due to the cosine term, which in turn increases risk of instability. In other words, for increasing deviation of the current angle from the angle of the impedance, the angle difference between WT voltage and faulted voltage, θ_V, increases (refer figure 4.17); increasing small-signal instability risk, and moves towards ±90° to the current transfer limit (i.e. large-signal instability). As stated above, for any operating point with θ_V larger than ±90° the left hand side term gets negative values causing small-signal instability, such that the wind turbine cannot operate with this angle as stated in chapter 3.

For the system given in figure 4.6 closed-loop poles are calculated for different operating points, with varying current injection angle, for a PCC voltage of 0.05pu. The results are given in table 4.1 below. It should be noted that the case with θ_V equal to 95° can only be obtained with a current magnitude larger than V_f/Z, as discussed in chapter 3. As seen in table 4.1, unstable poles in right half-plane are observed when the current angle deviates from impedance angle and θ_V increases towards ±90°.

Table 4.1 Poles calculated for different operating points

V_f=0.05pu, I_{wt}=1pu, Z=0.21pu, θ_Z=83° (X/R=8)		
θ_I	**resulting θ_V**	**poles**
82.9°	0°	s1,2= –17.8162 ± 18.3067i
89.8°	-30°	s1,2= –16.3310 ± 18.8402i
76°	30°	s1,2= –16.3310 ± 18.8402i
69.15°	85°	s1,2= – 0.0652 ± 9.1803i
69.12°	87°	s1,2= 0.8954 ± 7.0977i
69.1°	90°	s1= 0.4, s2= 4.25
69.15°	95°	s1= –6.2, s2= 17

The nine cases given in chapter 2 and 4 are summarized in table 4.2 for their small-signal stability analysis results with the calculated closed-loop poles. The non-problematic cases in figure 4.1 are shown to have stable closed-loop poles, as expected.

Table 4.2 Poles calculated for cases in figure 4.1

Z=0.21pu, θ_Z=83° (X/R=8)				
Case	**V_{pcc} (pu)**	**$I\lfloor\theta_I$**	**resulting θ_V**	**poles**
1	0.02	$1pu\lfloor 90^o$	N/A	large-signal instability
2	0.02	$1.01pu\lfloor 83^o$	0°	$s_{1,2}$= –7.7529 ± 15.4046i
3	0.02	$1.2pu\lfloor 57^o$	N/A	large-signal instability
4	0.05	$1pu\lfloor 90^o$	-15°	$s_{1,2}$= – 17.6012 ± 18.5918i
5	0.05	$1.01pu\lfloor 83^o$	0°	$s_{1,2}$= – 17.8162 ± 18.3067i
6	0.05	$1.2pu\lfloor 57^o$	N/A	large-signal instability
7	0.25	$1pu\lfloor 90^o$	-6°	s_1= –80.3, s_2= –23.2
8	0.25	$1.01pu\lfloor 83^o$	0°	s_1= –77.2, s_2= –23.3
9	0.25	$1.2pu\lfloor 57^o$	26°	s_1= –96.7, s_2= –22.7

In figure 4.17, root loci for varying θ_V are given for the system in figure 4.6. As observed in table 4.1, the closed-loop poles ($\sigma+j\omega_d$) move to the right-half plane causing small-signal instability for increasing θ_V angle. Not being shown here, the root loci change considerably with the faulted point (PCC) voltage, such that for lower (e.g. 0.02pu) faulted point voltage cases, closed-loop poles move towards the right-half plane increasing the risk of small-signal instability.

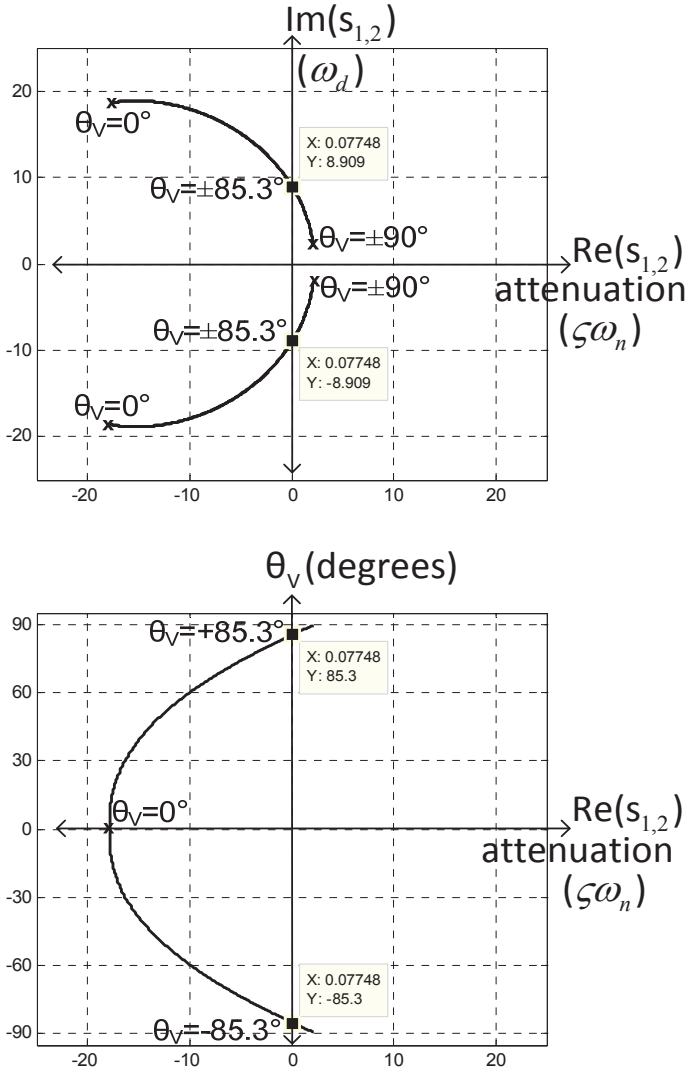

Fig. 4.16 Root loci for varying θ_V, for V_f =0.05pu, for system in figure 4.6.

From figure 4.17 and previous discussions, it can be commented that the system becomes unstable before θ_V reaches ±90°, which is the large-signal stability limit. Hence, within the current transfer limits, small-signal stability limits exist due to sensitivities for operating points close to ±90°. This statement is shown in figure 4.17, where the deviation of the current angle from the impedance angle is projected to the deviation of the wind turbine voltage from the reference voltage (V_f). As seen in figure 4.17, a small-signal stability limit can be applied within the current transfer limits, based on a desired value of damping and attenuation value. Additionally, the small-signal stability margin of the system can be improved via designing and tuning the PLL of the system accordingly. As will be seen in the next chapter, in this study stability of the wind turbine is aimed via modifying the current references to be within transfer limits to avoid LOS occurrence. Large-signal instability limit is considered and such a small-signal stability limit is not applied. However the small-signal model given in this section will be utilized for design and tuning of the frequency based controller in the next chapter.

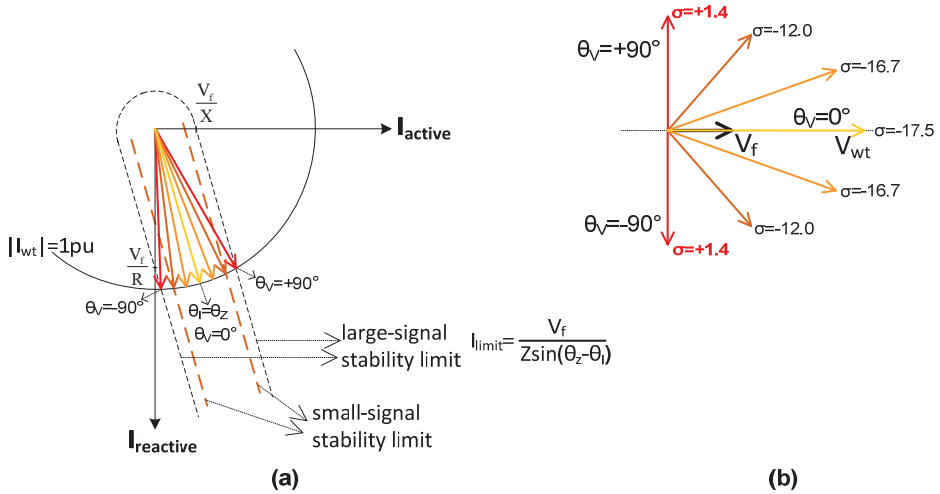

Fig. 4.17 Small-signal stability limit – representative attenuation values.

The LOS frequency fall/rise can be explained in various ways. As explained in chapter 3, during very low voltage faults the current from the wind turbine has to be injected convenient to the angle of the impedance between the wind turbine and the faulted point (e.g. PCC). Otherwise the active and reactive power losses on the impedance are not compensated effectively, which is the basis of the current transfer limits, and LOS occurs. In another explanation, an inconvenient current reference (highly active or highly reactive out of the transfer limits) drives the angle difference between the wind turbine voltage and the faulted point, θ_V, beyond ±90°, which is the basis of the large-signal stability limit, and LOS occurs; such that the frequency falls (or rise) causing the θ_V decrease (or increase) with respect to the reference angle continuously.

Two cases with θ_V larger than ±90° should not be mixed; as explained in chapter 3, for currents within the transfer limits (with an angle close to the impedance angle) but larger than V_f/Z, θ_V can go beyond ±90° as a transient, and decrease back since this point is not a stable operating point. However, for a current reference out of transfer limits (with an angle deviated from the impedance angle), θ_V goes beyond ±90° and continuously moves during LOS event. As will be shown in the next chapter, the solutions in this thesis will be proposed to modify the current references to stay within limits close to the impedance angle avoiding large-signal and small-signal instability.

4.5 Conclusion

The LOS – frequency fall/rise has been analyzed in this chapter and shown that the LOS is occurring when the current reference is out of the current transfer limits specified in chapter 3. It is shown that the loss of control of vector control and also deviation from fundamental grid (50Hz) frequency are shown to be main results of LOS. The reason for the frequency fall/rise during LOS is found to be mainly due to sustained error in the estimation of the PLL, and integration of the error resulting in frequency change.

As given in this chapter LOS is resulting in loss of vector control and frequency deviation. Loss of vector control means that the WT is not able to inject the referenced

active and reactive current references. As a result, grid code compliance would be violated. Moreover, if the actual active current becomes high causing active power injection to the grid without control, the dc link might become discharged during the fault, if the wind speed is low. Additionally, loss of control of vector control might create problems during the recovery period of the fault, due to uncontrolled active and reactive currents.

Deviation from the fundamental grid frequency means phase difference between the grid voltage and the wind turbine voltage. Such a phase difference can cause adverse effects to the grid that the grid voltage might be attenuated during the fault. Phase difference can cause transient problems when the wind turbine is re-synchronizing to the main grid after the fault. Hence, the LOS has to be avoided.

It is observed that wind turbines' current injection during severe symmetrical faults is driving the PLL towards instability. As stated in [79], despite substantial amount of research on advanced PLL design, instability of PLL in case of weak grid connections and low voltage faults, and impact of the PLL structure on the WT stability and power system stability have not been studied sufficiently in literature.

As shown in this chapter, the LOS is occurring due to "inconvenient" current references, which are out of transfer limits during the fault. An analogy was made to acceleration of a synchronous generator during a fault due to high input mechanical power and low output transfer limits. As well-known, for a synchronous generator without fast acting valves, it is quite difficult to modify the input mechanical power within the short duration of the fault, to avoid acceleration. However, it is quite possible for a converter-connected wind turbine to modify the current references within short duration of the fault, to avoid LOS, which will be basis of the proposed solutions in the next chapter.

Chapter 5

Proposed Solutions for Loss of Synchronism

In this chapter, proposed solutions for Loss of Synchronism (LOS) are given, reviewing the state-of-the-art solutions in the beginning. First, impact of PLL settings on the occurrence of LOS is shown and evaluated as a partial solution. Then, limiting the current injection during severe faults is given as a fundamental reference. Two methods to prevent LOS while injecting active and reactive currents are proposed; namely, current injection based on grid X/R characteristics and the novel PLL frequency based current injection. WPP level implementation issues are also discussed. A comparison of five injection schemes is provided at the end.

5.1 State-of-the-Art Solutions

Mainly due to distant location of wind resources from central areas, wind power plants are connected to low short-circuit capacity buses, and also due to continuously increasing installed capacity of renewable energy sources, more weak grid situations are encountered. Issues related with weak grid connection of wind power plants and response of wind turbines during severe faults have been studied thoroughly in the literature both by academia and industry. Specifically the problems occurring due to power or current injection during low voltage faults and with high impedance connection, which resembles the LOS problem given in this thesis, have been handled only in few studies, which are reviewed below. In [80]-[83], the weak grid problem is handled mainly for non-faulted grid cases. Only in [56], specifically the stability problem during low voltage faults is handled.

Active Current Reduction:

In [56], the problem of instability, which is highly relevant with the LOS studied in this thesis, is called as "transient stability problem" occurring specifically during low voltage faults. In accordance with the grid codes, priority is given to reactive current injection, while active current is injected as the remaining current capacity of the wind turbine. In [56], active and reactive current transfer limits have been derived, similar to the limits in this thesis; however the limits derived in [56] and in this thesis are not consistent with each other completely. In [56], based on the limits derived, it is claimed that the instability is occurring for high active current injection during very low voltage faults. An algorithm, called as "voltage dependent active current reduction" is proposed such that when the voltage is very low during fault, the active current is reduced to avoid the instability.

Active current reduction action of the proposed algorithm is shown in figure 5.1 as imposed on the limits derived in this thesis. Two fault cases, where the wind turbine with 1.25pu current capacity is referenced to inject 1pu reactive current and 0.75pu active current during faults, are shown. In the case of figure 5.1-(a), the voltage at the faulted bus is dropping to 20% of the rated, and in figure 5.1-(b) PCC voltage drops to 10%. As seen in figure 5.1-(a), the algorithm is successfully modifying the current reference from point "a" towards points "b", "c" or "d", which are inside the transfer limits, as a result the instability is avoided successfully. However, for more severe fault cases as in figure 5.1-(b) (or higher impedance and more resistive connection with lower X/R ratio), which are not covered within [56], the proposed algorithm cannot guarantee that current reference to be within the transfer limits. In other words, the active current can be reduced from point "e" in figure 5.1-(b), towards "g", which is within limits but also to "f" or "h", which are outside transfer limits. Hence the "voltage dependent active current reduction" algorithm can work for faults, where the voltage drops to low values such as 20%, and for inductive networks with high X/R ratio; but can become insufficient for severe faults, where the voltage drops to very low values (e.g. less than 10%) or highly resistive connection with low X/R ratios.

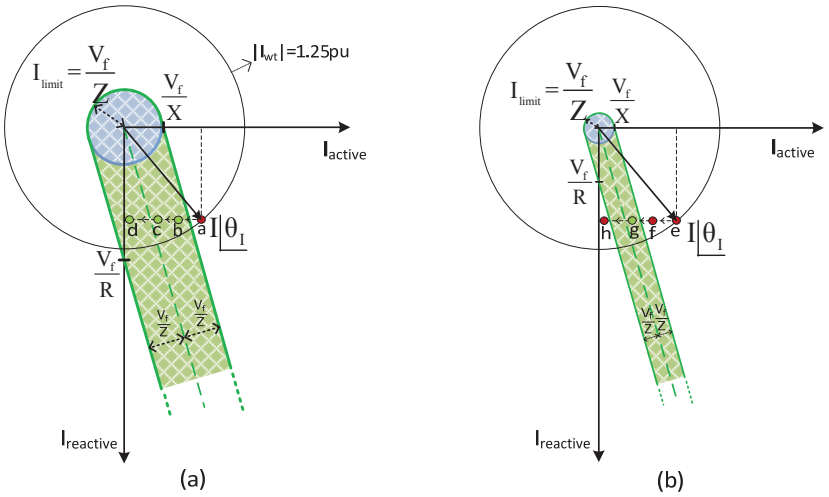

Fig. 5.1 Active current reduction action for (a) 20% PCC voltage, (b) 10% PCC voltage.

In [56], instability analysis and transfer limits are accomplished for active and reactive current injection from wind turbine terminals towards PCC, without specifying the type of the turbine as DFIG or Full-Converter, since the active reactive current control can be realized for both. However, impact of instability situation is simulated and assessed for DFIG, and effects are stated, such as called by "pole-slippage" which is stated to cause mechanical stress on the machine [56].

Limitation of Power Angle:

In [80], the stability is considered not only for fault cases but also non-fault cases, and primarily for active power injection. The priority of reactive current injection during fault is not considered. The instability is proposed to be avoided via limiting the power injection below the maximum transferrable value, which is calculated online based on the well-known power-angle characteristic equation.

$$P_{wt}=\frac{V_{wt}V_{grid}}{X}\sin\theta_V \tag{5.1}$$

As well-known, the maximum transferrable power is reached when the phase angle difference between the wind turbine voltage and the grid voltage, becomes 90°. Such a situation is shown in figure 5.2, which is in current-angle form, similar to the figure 3.17.

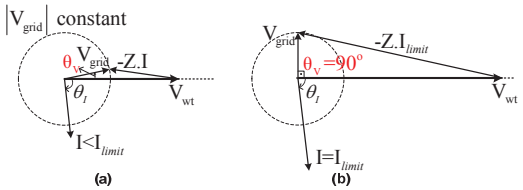

Fig. 5.2 Power-angle limitation.

In [80], the maximum transferrable power is calculated and active power injection is reduced in conjunction with the aim of staying within limits. This action is similar to the "active current reduction" in [56], but for the non-fault case. In [80], the necessary angle and grid voltage magnitude information is obtained via estimations using voltage and current measurements at the wind turbine terminals at two instants of time. Additionally, in order to have higher stability margin, the maximum power transfer limit is calculated for an angle difference value chosen to be lower than 90°, for instance 70°. However, this algorithm has the disadvantage that any instability due to reactive power (current) injection is not considered and the proposed solution is to cease injection, which would not be acceptable considering grid code requirements.

Current Limitation Based on PLL Estimation Error:

In [81] a method, which is focusing on how to detect a possible instability as quick as possible, is proposed. It is claimed that in addition to the WT terminal voltage as in [56] and [80], error of the PLL (V_q voltage signal) have to be used as signals to detect possible instability. Any significant variation as terminal voltage drop and/or increase in PLL error, are used as signals for possible instability detection. Similar to [81], the proposed action to avoid instability is to limit the injection, which is a disadvantage considering the reactive current injection required by the grid codes.

Loss of Angle Stability of Weak-Grid-Connected Wind Turbines:

In [82] Loss of (Angle) Stability (LOS) during healthy (non-faulty) conditions is studied; however, it is stated that instability occurs due to a small disturbance in healthy conditions or a large disturbance such as a fault. It is stated that when the VSC is considered as a voltage source, angle instability can occur if the angle difference between the VSC and grid voltage reaches 90 degrees. The source of instability is shown to be high grid impedance (mostly reactance is considered), in other words low SCR connections. The relation of grid strength and the limits for instability is discussed. A "Voltage Control System (VCS)" is proposed to keep the WT inside the stable operating points despite the fluctuating wind conditions. In order to avoid instability a sequence of actions; fast identification of LOS event, stopping the power feed-in and restoring slowly back (post-LOS control), is proposed. As described above, reactive current injection during low voltage faults, which is the main scope of this thesis, is not covered in [82].

In addition to above studies, the instability problem is handled in [83] for VSC and LCC based HVDC converters, and also for renewable (e.g. wind) power plants are included in the scope as aggregated single converters. Specifically post-fault instability due to a change in the grid (line disconnection) is referred to be the source of instability. Also faulty and healthy (non-faulty) conditions but of a weak grid are covered. The converters are assumed to be injecting high active power (which would be valid for a HVDC converter or a WPP during recovery of a fault; but invalid for a WPP during fault, where primarily reactive current is injected). Instability is referred as "voltage" and "transmission angle instability" occurring due to exceeding maximum transferrable power. If the converter continues injecting active power via injecting active current, the voltage at the output terminals decreases and DC link voltage decreases, which cause active power to decrease after a level of injection. After that level, change of active power becomes negative for positive change of active current. The solution is suggested to measure dP/dt and dI/dt continuously, such that when these signals have opposite signs, the active power reference is decreased in order to avoid instability. In this study, LOS during reactive current injection to low voltage faults is not covered.

Active Current Control during Grid Faults:

In [84], a new method for active current reference control during grid faults, which is based on the X/R characteristics of the impedance within WPP and voltage observed at the PCC bus, is proposed to obtain a current, which is called "optimal", at the PCC. The conventional method is described to inject reactive current as required by the grid codes (e.g. 0.9pu) and also active current (e.g. 0.4pu) in accordance with the power production of the wind turbine. It is shown that for low voltage faults (V_{pcc}<20%) and/or high impedance (especially high reactance) between the wind turbine and PCC, the injected wind turbine current takes form of reduced (even zero or negative) reactive component at PCC. This situation is mentioned in remark 3.10 of this thesis to be originated mainly from reactive (I^2X) loss on the impedance, and referring the figure 3.21, the below phasor diagram in figure 5.3 is given to better explain the situation. As seen in figure 5.3-(a), when highly active current is injected from the wind turbine, due to low faulted point (PCC) voltage and/or due to high impedance, the PCC voltage angle deviates from WT; as a result reactive component of current at PCC decreases, even towards zero such that only active current is supplied to grid for an increased current magnitude. In figure 5.3-(b), it is seen that for even higher magnitudes of current, the current starts leading the PCC voltage such that reactive power is absorbed from the grid (underexcited operation). As also explained above and in chapter 3, this situation is mainly due to reactive (I^2X) loss on the impedance arising due to excessively high active current injection.

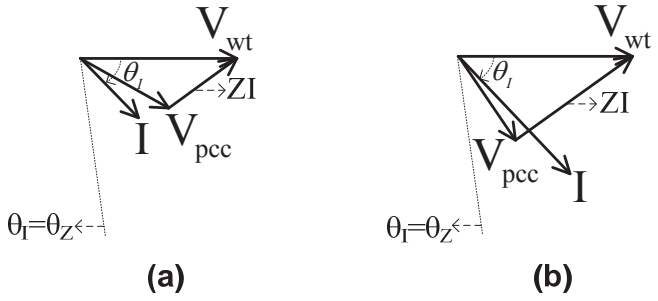

Fig. 5.3 Decreasing reactive current at PCC with high active current injection from WT.

In [84], a method is proposed such that the active current injection from wind turbine is adjusted (decreased relative to what is injected by conventional method) to a specific value defined by X/R of the impedance and the PCC voltage as in (5.2) below;

$$I_{active} = \frac{R}{X}\left(I_{reactive} - \frac{V_{pcc}}{Z} \right) \tag{5.2}$$

The action of proposed method is shown as imposed on the current transfer limits derived in this thesis as in figure 5.4. As seen in figure 5.4-(a), the proposed method is bringing the highly active current reference of conventional method towards an angle close to the impedance angle. This method seems similar to the one in [56], except in [56] active current reference was reduced based on voltage without any specific target angle, whereas in [84] the active current is adjusted to a specific angle, which can also work for highly reactive current references. As seen in figure 5.4-(b), with the use of proposed method, the current with respect to PCC voltage takes a form of high reactive which is also desired by the grid codes, solving the issue shown in figure 5.3 above.

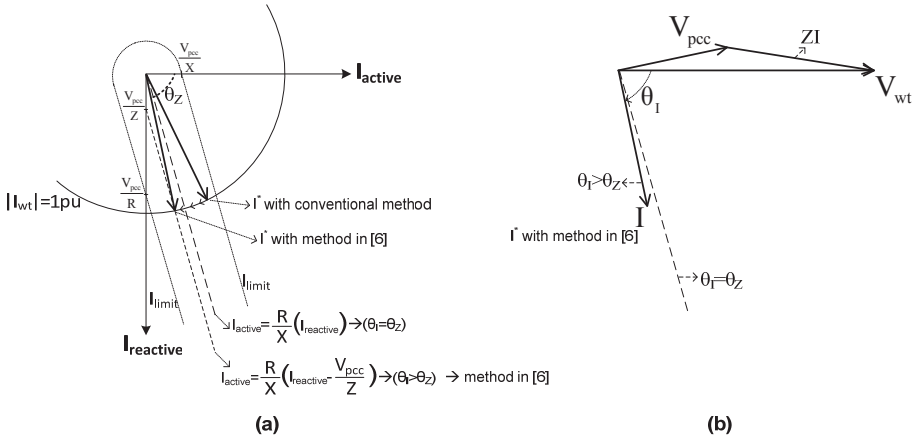

Fig. 5.4 Active current reference control based on X/R and PCC voltage.

In [84], LOS is not considered and results are shown for a moderately severe fault with 10% remaining voltage at PCC. Nevertheless, as mentioned above, the proposed method brings the current reference close to the impedance angle, which can help to solve the LOS. However the method in [84] provides highly reactive current at PCC, which would still cause LOS when a severe fault occurring remote from PCC, as

mentioned in section 3.3 and shown figure 3.32 in chapter 3. Additionally, as will be discussed below, for very severe faults (e.g. 2% PCC voltage) the precision requirement for X/R value estimation becomes very critical that makes the X/R based methods insufficient to avoid LOS. In [84], the proposed method is tested against X/R estimation deviances for a fault with 10% PCC voltage, without considering the impact of severity of the fault on allowed deviances. Additionally, the method in [84] requires information of PCC voltage during faults, which is stated to be calculated using the minimum RMS voltage value measured at the wind turbine terminals.

Maximum Voltage Increase with Optimum Current Angle:

In [23], weak (high impedance) and low X/R grid cases are studied both for faulted and post-fault periods. It is shown that when the current at the PCC of a WPP is injected with the angle of the impedance of the grid, highest voltage increase at the PCC is obtained. This situation is represented in figure 5.5 below for a current injection with constant magnitude and varying angle from WPP. The grid voltage here can be considered as the voltage at the faulted point, which is a point remote from PCC. Similarly in first part of [56], similar conclusion has been made, such that during a fault at PCC, the highest PCC voltage increase can be obtained when the PCC current is injected with the angle of the grid impedance. However in related part of [56] only a special case that the fault impedance is having the same angle with the grid impedance is analyzed. In practical fault impedance can have quite different characteristics than the grid impedance. Additionally in [8] and [9], impact of active current injection additional to the reactive current injection during fault is shown to improve the voltage nearby PCC.

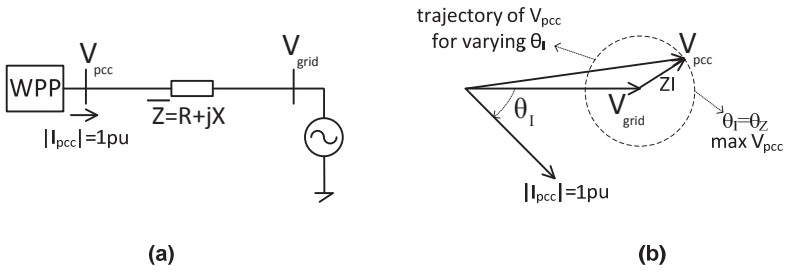

Fig. 5.5 Maximum voltage increase at PCC.

As seen in figure 5.5 and as was also shown in figure 3.19 in chapter 3 of this thesis, at such an operating point, the sending end (PCC) voltage and receiving end (grid side) voltage are in phase with each other, which also helps to avoid LOS. Hence such an injection scheme can help to reduce risk of LOS, however LOS is not considered and aimed to be solved within these proposed X/R based studies. Moreover, as also commented above for [84], X/R based methods suffer from precision requirement of X/R value. In these studies, new methods are proposed based on the X/R of the grid in order to provide higher voltage boost at wind turbine and PCC terminals, whereas the wind turbines are assumed to be working properly without any LOS.

Most of the state-of-the-art solutions for weak grid and low voltage fault stability problems are proposing to limit or cease current injection during fault. In the following sections of this thesis, novel algorithms are proposed, which can inject currents without creating instability.

5.2 Impact of PLL Settings to LOS

As given in chapter 4, the source of LOS is “inconvenient” current references which are out of current transfer limits, and resulting in estimation error within PLL. As shown in chapter 2 to 4, the LOS in this thesis has been observed as frequency fall, where the frequency was dropping towards zero, or frequency rise, where the frequency was increasing towards very high values, due to continuous integration of the sustained estimation error within PLL. However, the integral action in a practical PLL application would have saturation and anti-windup algorithms to avoid unnecessary integration. Taking the PLL structure in figure 5.6 as a reference, saturation limit is applied to two signals within the PLL; at the integral output and at the calculated frequency signal. In addition to saturation at the integral output, an anti-windup algorithm is also implemented. The saturation limit at the output of the integral action can be chosen as the practical value of steady-state deviation from fundamental frequency (50Hz), which would be expected or allowed in the grid, where the wind turbine is connected. Based on generic grid code requirements, which set the allowable steady-state frequency deviations, the integral output in figure 3 can be limited as +/-2Hz, such that the steady-state frequency including the non-faulted conditions would

vary between 48 and 52 Hz. The saturation value at the calculated frequency cannot be set with narrow limits around fundamental frequency since the tracking performance of the PLL would be restricted [44]. In order to allow dynamic changes at the calculated frequency for better dynamic tracking performance, the saturation limits can be set as minimum 45Hz and maximum 55Hz. It is important to note that; instead of PI compensator a PID compensator would be employed, which would be applied with similar saturation algorithms.

However, as discussed above, the LOS is causing sustained PLL error, due to "inconvenient" current references. In figure 5.7, a case, where a frequency rise is observed, is simulated with saturation in PLL applied with maximum frequency limit of 55Hz. Limiting the integral output or the calculated frequency can prevent continuous deviation of frequency but cannot prevent sustained PLL estimation error. Hence, d&q axis estimation is still incorrect during LOS, causing loss of vector control action. As seen, estimated current components are matching with the referenced, while the actual current is differing from the referenced.

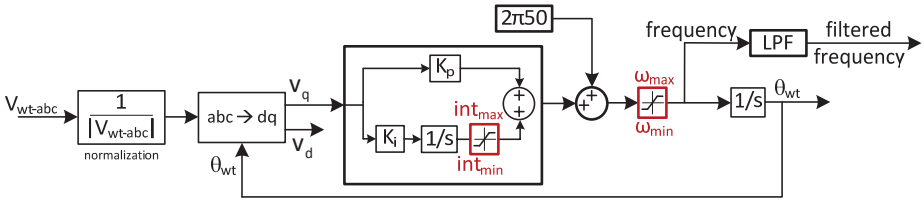

Fig. 5.6 PLL structure with saturation blocks.

Alternatively, adaptive adjustment of PLL parameters, gains or limits during severe faults can help to reduce rate of change of frequency during LOS event, since the rate is highly dependent on PLL dynamics as shown in chapter 4. However, as stated above, these solutions would not prevent incorrect estimation during LOS. Such a frequency, thus a phase difference, during fault, might cause resynchronization problems when the fault is cleared. Hence, adjusting PLL settings cannot be considered as a comprehensive solution to LOS, which is mainly caused by "inconvenient" current references. In the following sections, solution based on modifying the active and reactive current references to avoid "inconvenient" references are given.

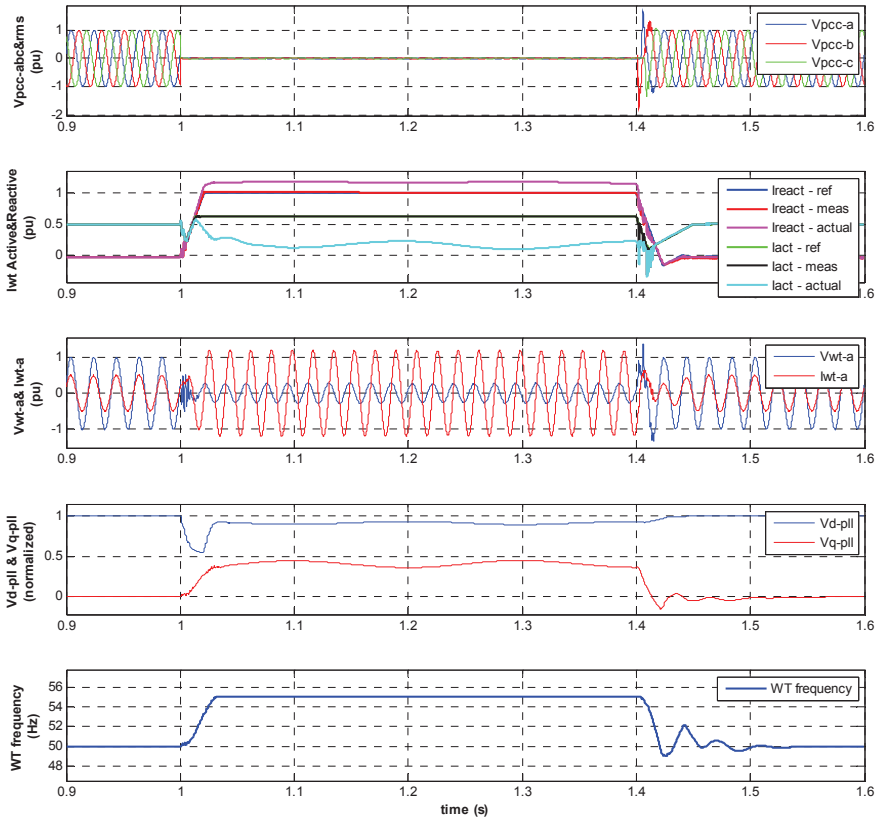

Fig. 5.7 LOS – frequency rise with saturated PLL.

5.3 Limited Current Injection during Severe Faults

As discussed in section 3.4, current references with magnitude smaller than V_f/Z, which are shown as the blue circle in the current transfer limits figure 3.33, do not cause LOS for any injection angle, since that current is always within the transfer limits. The same as (3.17), the current limit for this case is given in (5.3) again;

$$I_{limit} = \frac{V_f}{Z} \qquad (\text{for } 0^\circ < \theta_I < 360^\circ) \tag{5.3}$$

Before the X/R based and PLL frequency based solutions in the following sections, limiting the current injection to stay smaller than V_f/Z is given as reference solution

avoiding LOS. Since for certain grid codes, fault ride-through and reactive current injection is not required below a specific value (e.g. 15%), limited current injection can be considered as acceptable, which guarantees stable operation compromising current injection during fault. However, such a limitation algorithm would also bring practical implementation issues such that the faulted bus voltage or a remote point (e.g. PCC) voltage measurement would be required in order to determine the current injection limit. Therefore, estimation of PCC voltage, or fast communication between the PCC point and the wind turbines would be required, which might be a challenge considering the very short duration of the fault. Additionally, as shown in section 3.4 and figure 3.31, the PCC voltage varies with fault location and the transfer limits are varying with varying fault location. Even though the PCC voltage is known, it is difficult to differentiate between the fault occurring at PCC and a fault occurring at remote points. Hence, it is difficult to set the voltage level for limited current injection. As an example, for the WPP given in figure 2.2, which has impedance of 0.21pu (with X/R of 8) between the wind turbine and the PCC, the safe "injectable" current magnitude versus remaining voltage at the PCC would be as in figure 5.8-(a) below. Based on the linear relation in (5.3), the "injectable" current magnitude increases for higher PCC voltages and 1pu current can be injected when the PCC voltage is larger than the impedance magnitude (0.21pu in this case). A generic FRT curve is shown in figure 5.8-(b), showing the minimum PCC voltage where 1pu current can be injected.

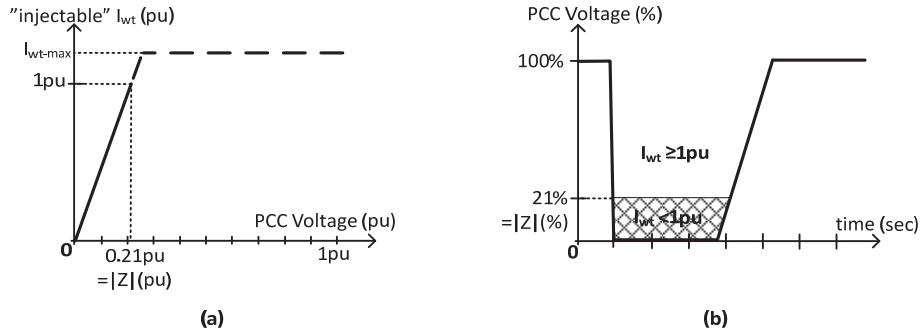

Fig. 5.8. (a) "Injectable" current magnitude versus PCC voltage magnitude, (b) FRT curve for 1pu current injection during fault

As observed in (5.3) and figure 5.8, for WPPs with higher impedance between wind turbines and the PCC (due to distant location of wind turbines and transformer impedances) and also with long radial connection lines (underground cables or overhead lines), the minimum PCC voltage for 1pu "injectable" current would be higher as expected, for instance as high as 40%.

5.4 X/R Based Active Current Injection

As shown in chapter 3 and 4, LOS is occurring when the current reference is out of the current transfer limits. The transfer limits, given in figure 5.9, are shown to be based on remaining voltage at the faulted bus and the impedance between the wind turbine control terminals and the faulted point. Hence, a straightforward solution against LOS would be to give active and reactive current references to the wind turbine such that the referenced current is within the current transfer limits.

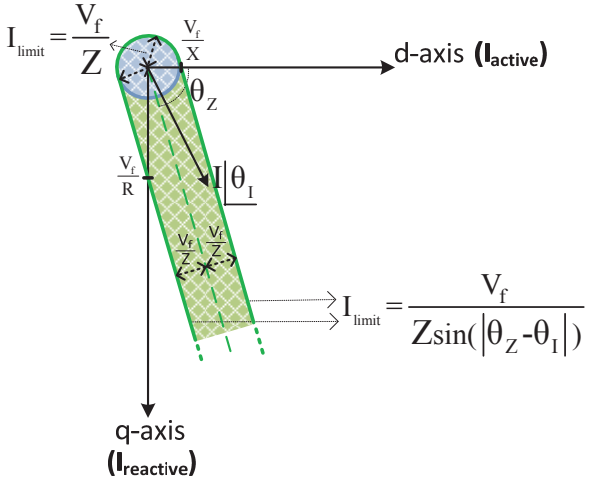

Fig. 5.9 Current transfer limits.

As seen in current transfer limits, when the current has the same angle of the impedance, for any magnitude of the current, the operating point is inside the current transfer limits. The phasor diagram when the current has the same angle of the impedance angle is shown in figure 5.10.

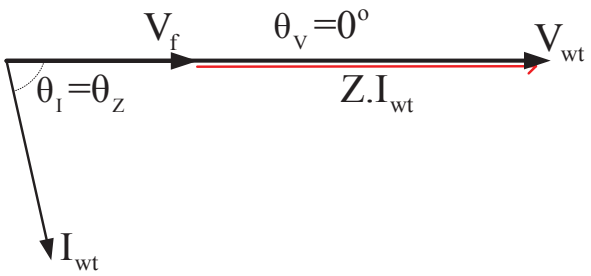

Fig. 5.10 Phasor diagram when current angle equal to impedance angle.

The condition that the angle of the current is equal to angle of the impedance implies that active and reactive currents are related with the X/R ratio of the impedance as below;

$$\theta_I = \theta_Z \quad \Rightarrow \quad \frac{I_{active}}{I_{reactive}} = \frac{R}{X} \tag{5.4}$$

The grid code requirements are giving priority to reactive current injection during fault, and active current is allowed to be freely set, for instance to be decreased in order to stay within the wind turbine current ratings. Hence, for the solutions proposed against LOS, the reactive current is primarily injected and active current is adjusted by the LOS solution algorithms as given in the following parts.

The first proposed control algorithm, which is active current injection based on X/R and the current references are generated based on (5.4), is given in figure 5.11. In figure 5.11, the blocks 1-3 are the same as conventional method, which are employed for non-severe faults. The core of the solution is given in block-5, where the active current reference is generated with the ratio of R/X to the reactive current reference. There is the block-4, decision algorithm, which is enabling either the conventional method block-3 (for non-severe faults) or the solution block-5 (for severe faults), based on the enabling from decision algorithm.

The decision algorithm is playing an important role regarding the DC link voltage regulation for the wind turbine. If the solution is employed for all faults, then the active current would be set to a specific value during any low voltage fault. However, as discussed previously, the instability risk exists for severe faults; and for non-severe

faults active current can be set from the DC link voltage regulator in order to help the active power flow from machine-side converter. Otherwise, use of chopper resistance would increase unnecessarily for non-severe faults. Two cases of active reactive current profiles with and without decision algorithm is shown in figure 5.12 below. It can easily be concluded that it is better to have the response in figure 5.12-(b), with the decision algorithm, rather than having the response in figure 5.12-(a), regarding excess use of chopper resistance. The threshold level to classify a fault whether as severe or non-severe can be determined based on the installation, i.e. the WPP and grid characteristics. The block-6 is important in order to keep the current of the WT within its capacity value. In this block active and reactive current references are down scaled if magnitude exceeds the capability value.

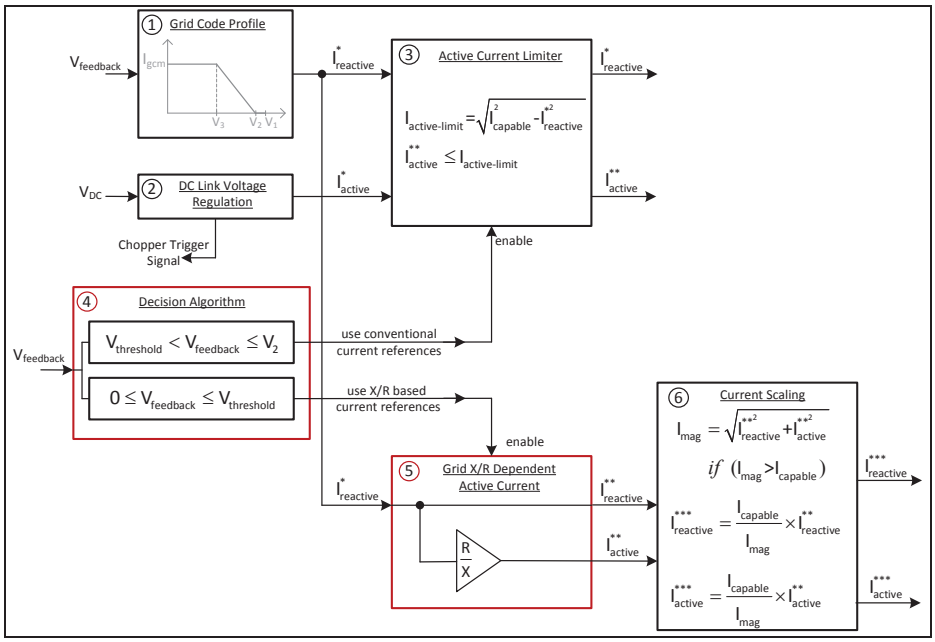

Fig. 5.11. Proposed X/R based current injection algorithm.

As observed in figure 5.12, when the X/R based control method is used, some amount of active current is injected. For the wind turbines having current capacity larger than the maximum reactive current requirement of the grid code (i.e. $I_{capable} > I_{gcm}$), the active

current can be given without compromising the reactive current value, as shown in figure 5.12.

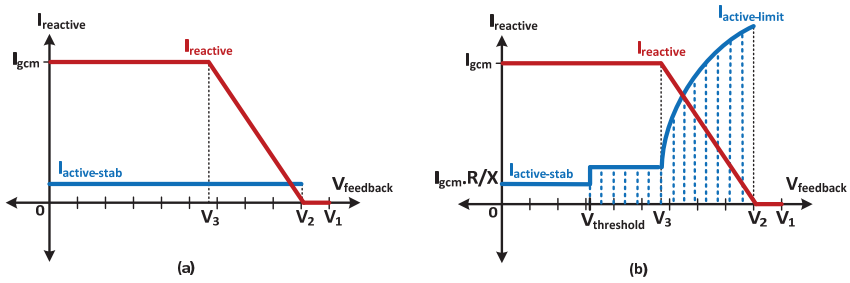

Fig. 5.12. Current references of X/R based solution (a) without, (b) with decision algorithm.

If the X/R based active current reference is high, such that remaining capacity is not enough for that amount of active current; or if the wind turbine capacity is not larger than the grid code reactive current requirement (i.e. $I_{capable} = I_{gcm}$), as shown in figure 5.13, then the reactive current injection would be compromised, such that the injected reactive current magnitude decreases from maximum grid code required amount (I_{gcm}), to a lower value ($I_{gcm'}$).

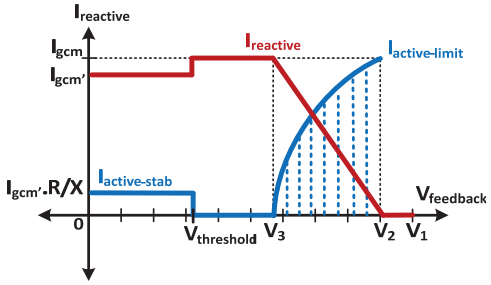

Fig. 5.13 Current references with X/R based solution employing decision algorithm.

The X/R parameter used within the proposed control algorithm is the X/R ratio of the impedance between the wind turbine control point and the faulted point. However, it is practically difficult to obtain value of this parameter. It can be commented that the impedance characteristics of the WPP layout (WT transformers, collector grid, and WPP transformer) and of a connection line (underground cable/overhead line, if exists)

can be known from installation data; and the grid characteristics can be obtained from TSO. Additionally, the X/R parameter can be obtained (or available value's precision can be improved) by offline or online estimation methods based on voltage and current measurements at the wind turbine or WPP level during non-faulty and/or faulted grid conditions. However, it can be concluded that; despite all the available and estimated data, the X/R parameter would be obtained with some uncertainty.

.

5.4.1 X/R parameter uncertainty

Due to the X/R parameter uncertainty, the current references would deviate from the ideal operation of figure 5.10, or even deviate towards out of transfer limits, causing LOS. As the band of the current transfer limits are becoming narrower for lower fault voltages (V_f) and/or with increasing impedance magnitude (Z), the risk of deviation out of transfer limits due to X/R parameter mismatch increases. For very severe faults with very low faulted point voltage (e.g. 1%), the transfer limits band becomes so narrow that almost a line and any X/R parameter mismatch cause LOS. In order to calculate the impedance angle value ($\tan^{-1}(X/R)$) precision requirement, figure 5.14 is utilized. For a given current magnitude, the allowed uncertainty is calculated based on the current transfer limits. The current transfer limit equation is solved when the current magnitude is fixed as in (5.5) to calculate the point where the current reference deviates from impedance angle reaches the limit line. Assuming that the deviation would be small, (5.7) is obtained from (5.6).

$$\left|I_{wt}\right| = \frac{\frac{\left|V_f\right|}{\left|Z\right|}}{\left|\sin(\theta_Z - \theta_I)\right|} = 1pu \quad \Rightarrow \quad \left|\sin(\theta_Z - \theta_I)\right| = \left|I_{wt}\right| \frac{\left|V_f\right|}{\left|Z\right|} \tag{5.5}$$

$$\left|(\theta_Z - \theta_I)\right| \approx \left|I_{wt}\right| \frac{\left|V_f\right|}{\left|Z\right|} \quad (in\ radians) \tag{5.6}$$

$$\theta_I = \theta_Z \mp \left|I_{wt}\right| \frac{\left|V_f\right|}{\left|Z\right|} \quad (in\ radians) \tag{5.7}$$

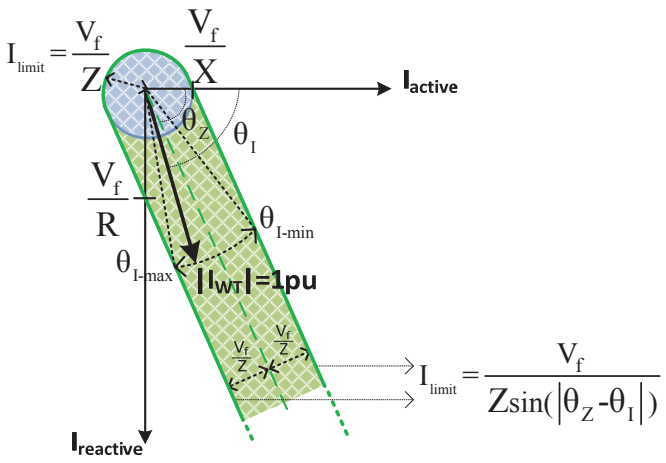

Fig. 5.14 Deviation of current angle from impedance angle.

For instance for a fault with 0.05pu (5%) remaining voltage and impedance magnitude of 0.3pu between wind turbine and faulted point, the current injection angle cannot be injected more than ±10° deviation from the impedance angle, in order to stay within the limits. For a fixed amount of error in the impedance angle estimation, $\theta_{Z\text{-}est\text{-}err}$, a general rule based on minimum fault (PCC) voltage and impedance magnitude can be obtained as in (5.8) such that the current reference with estimation error is still inside the transfer limits;

$$\theta_{Z\text{-}est\text{-}err} \leq |I_{wt}| \frac{|V_f|}{|Z|} \quad (\textit{in radians}) \tag{5.8}$$

When the current reference is given with the $\pm\theta_{Z\text{-}est\text{-}err}$, as in (5.7), the current would still be within transfer limits. For instance allowing an estimation error of 10° (0.175 radians) for 1pu current injection; for impedance magnitude of 0.3pu between wind turbine and faulted point, the minimum remaining voltage has to be above 0.05pu (5%). Below this value, current reference can go out of transfer limits. Hence, due to impedance angle estimation uncertainty, the X/R based method can only work for faults with remaining voltages above a specific value, which is defined by (5.8) based on estimation precision, impedance magnitude and current injection magnitude.

In order to save space and since similar cases have been conducted in the previous parts, simulation or experiment results with X/R dependent active current injection are not shown. As a reference, the experimental results in figure 4.12 and 4.14 can be considered as the cases where the X/R based method is not employed and LOS is observed; and the results in figure 4.13, where the current is injected exactly with the angle of the impedance is an example for employing X/R based algorithm and preventing LOS. However, as discussed above, the X/R based algorithm suffers from the precision requirement for the X/R parameter value.

In summary, the X/R method solves LOS problem for some of problematic cases, but cannot solve most of the problematic cases due to practical difficulties related to obtaining and setting the X/R parameter precisely regarding the impedance characteristics and fault location.

5.5 PLL Frequency Based Current Injection

In the X/R based current injection method in the previous section, active and reactive currents were proposed to be injected based on an estimation of X/R of the impedance between the wind turbines and the faulted point. As mentioned before, such an injection method, which is kind of open loop forward compensation, easily suffers from estimation errors. As given in previous parts, a sustained PLL error arises and frequency deviation occurs when the current reference is out of transfer limits. When a fixed amount of reactive current is injected in accordance with the grid code requirements, it is observed that the frequency is falling when active current is low, i.e. when the current angle is smaller than the impedance angle; and the frequency is rising when active current is high i.e. when the current angle is larger than the impedance angle. The PLL frequency based current injection method in this section is based on this dependency, such that the active current is modified based on the PLL frequency feedback. As seen in figure 5.15, the active current is referenced by a frequency regulator algorithm in order to regulate the wind turbine frequency towards prefault (fundamental) frequency.

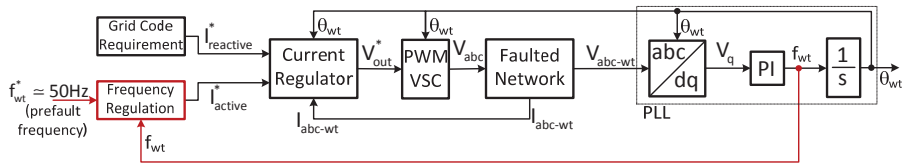

Fig. 5.15 Proposed PLL frequency based active current injection method.

As will be analyzed below, and observed in previous cases, during the LOS event the frequency is decreasing with less (insufficient) active current and increasing with high (excess) active current, which is consistent with the classical inertial frequency behavior in a power system. In fact, as discussed in chapter 3, the current transfer limits are mainly originating from the issue of conduction power losses on the impedance. For a fault occurring at PCC or at the main grid connection point, the system becomes like isolated from the main grid, and power balance between the wind turbine and the

impedance (between wind turbine and the faulted point) defines the frequency behavior. It can be considered that the wind turbine isolated (islanded) from the main grid due to the severe fault and operates as a microgrid. Since the voltage level is very low due to fault, active power balance can easily be supplied by the wind turbines as long as there is a minimum amount of generation. It should be noted that in this case of islanded operation due to fault, there can be no rotational (inertial) element, but only the wind turbine converter and the line impedance. Hence, the frequency is not the conventional inertial frequency, which is determined by the mechanical rotation of the machines; but the electrical frequency which is defined by the PLL.

Dynamic model for the frequency based active current injection method is derived from the PLL model in chapter 4 figure 4.10, which has been originally developed in [79]. In the quasi-stationary PLL model, given in figure 5.16, a feedback from the wind turbine frequency signal is used in the positive feedback path as a corrective term against LOS. As explained above, a frequency deviation is compensated by acting on the current reference and decreasing the positive feedback term, V_{q+}.

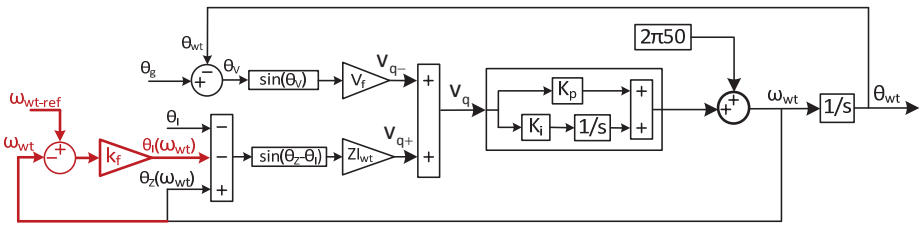

Fig. 5.16 Quasi-stationary model of the PLL with frequency compensator [79].

The frequency compensation term, k_f, comes in the k_θ term of the small-signal model as in (5.9). The frequency compensator is incorporated in the small-signal model and the transfer function is obtained same as in (4.30), except that the positive feedback term includes the frequency compensation. Hence, the stability criteria including the frequency compensation term becomes as in (5.10). Root locus for varying k_f gain from 0 to 1 at an operating point with the faulted point voltage, V_f, as 0.05pu and the system in figure 4.6 is given in figure 5.17 below.

$$k_\theta = \frac{RL}{\left|Z(\omega_{op})\right|^2} - k_f \tag{5.9}$$

$$K_p \cos(\theta_V) V_f > K_i I_{wt} \frac{L}{\left|Z(\omega_{op})\right|} \left(R - k_f \frac{\left|Z(\omega_{op})\right|^2}{L} + \sin\left(\left|\theta_Z(\omega_{op}) - \theta_I\right|\right) L\omega_{op} \right) \tag{5.10}$$

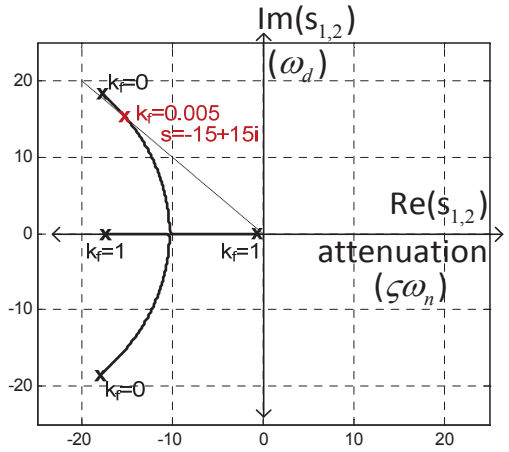

Fig. 5.17 Root locus for varying θ_V, for V_f=0.05pu, for system in figure 4.6.

As seen in figure 5.18, when k_f is chosen to be 0.005, a well damped system is obtained. A root locus for varying θ_V is given in figure 5.18 employing the frequency compensator for the system in figure 4.6, when the faulted point (PCC) voltage is 0.05pu. Referring to figure 4.17 in chapter 4, where system closed-loop poles were driven to right-half plane for θ_V larger than ±85.3°; it is important to note that the system closed-loop poles stay in the left-hand plane for any θ_V value, such that the frequency compensator is providing small-signal stability when θ_V moves towards ±90°. As discussed in chapter 4, for θ_V larger than ±90°, small-signal stability is not provided though with the frequency compensation since the negative feedback term in PLL gets negative gain, causing instability.

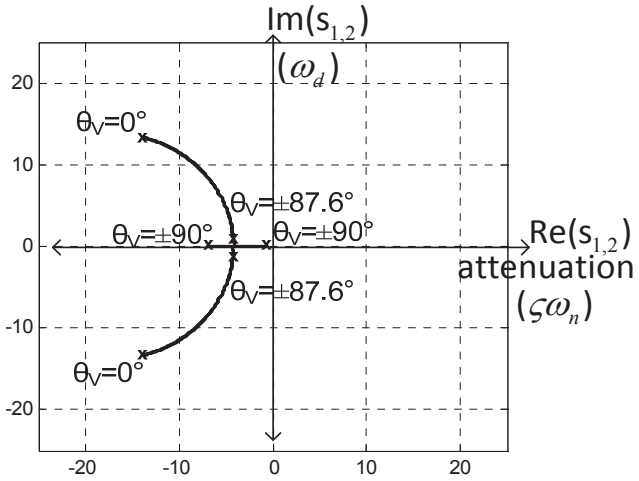

Fig. 5.18 Root locus for varying θ_V, for V_f=0.05pu, with K_f=0.005.

The control diagram for the PLL frequency based active current injection method is shown in Figure 5.19. As discussed above, the reactive current reference is set primarily based on the grid code requirement and the active current, which is flexible, is set by the frequency regulation algorithm. The resultant current reference stays within the transfer limits providing the wind turbine staying synchronized to the grid frequency. The blocks 1-3 and 6 are performing the same functions described in the previous X/R based control algorithm. The core of the PLL frequency based control is given in the block-7. In this block an active current reference, $I^*_{active\text{-}stab}$, is generated by the frequency compensator $K_f(s)$, and this reference is added to the active current reference generated from the active current limiter function. Therefore, the PLL frequency based control is like acting in parallel to the conventional method via modifying the active current reference. The frequency compensator $K_f(s)$ is designed as a PI compensator to include an integral term for steady-state frequency compensation during fault. The frequency feedback is obtained by the PLL from the phase voltages observed at the WT terminals. The calculated frequency is compared with a reference which can be used as the rated (e.g. 50Hz) or prefault frequency. With the use of deadband function, which is applied to frequency error, the controller is acting only to frequency deviations larger than the defined deadband (e.g. +/-100mHz). So, the

controller does not act unnecessarily for small frequency deviations, which occurs for non-severe faults (also due to noise in the frequency measurement). Hence, in contrast to X/R based solution, where a decision algorithm is employed, the PLL frequency based control has its inherent decision algorithm triggering itself only for severe-faults.

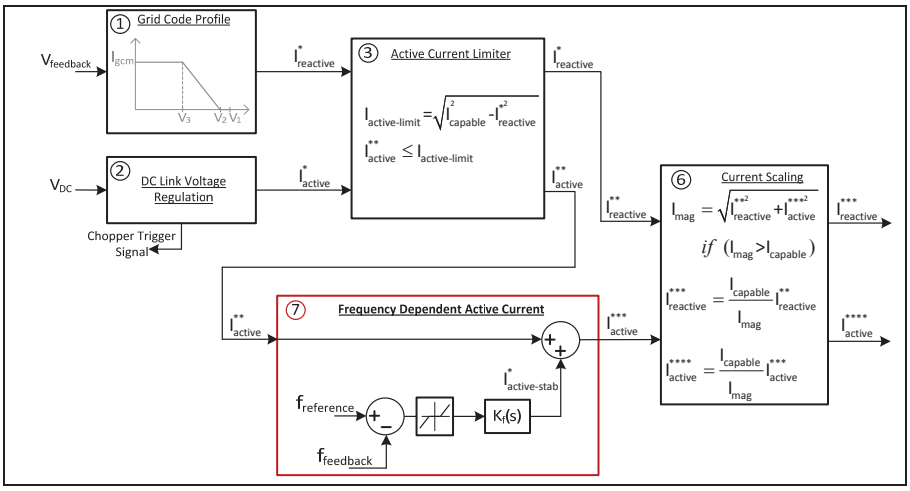

Fig. 5.19 Proposed PLL frequency based control algorithm.

The PLL frequency based control algorithm acts as feedback closed loop system which substantially improves the response during severe faults, such that the LOS is avoided for any severe fault, as shown in the following parts with simulation and experimental results.

5.5.1 Simulation Results of PLL Frequency Based Control Algorithm

In Figure 5.20, simulation result of the PLL frequency based control method is shown for a severe fault (from the case in figure 4.2) where pure reactive (zero active) current is referenced by the conventional method. As seen in second subfigure, the active current reference $I_{act\text{-}FR}$ from the frequency regulator is generated by the algorithm such that the frequency (in fifth subfigure) is kept at 50 Hz. As expected the PLL estimation error (V_q in fourth subfigure) is compensated. In Figure 5.21, the PLL frequency based

control algorithm is employed for the severe fault (from the case in figure 4.3) where highly active current is referenced by the conventional method. As seen in second subfigure, the active current, which is excess and causing frequency rise, is regulated downwards and frequency is kept at 50 Hz.

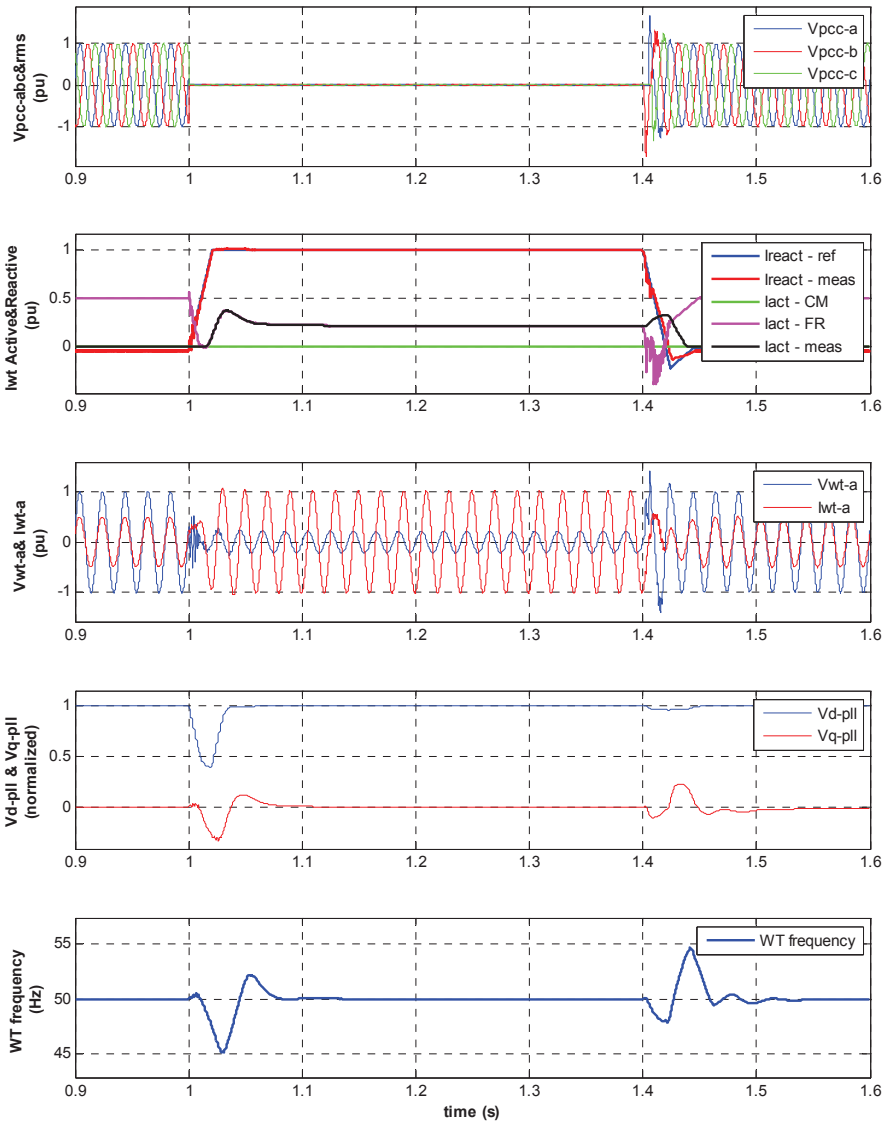

Fig. 5.20 Simulation results with PLL frequency based algorithm – pure reactive case

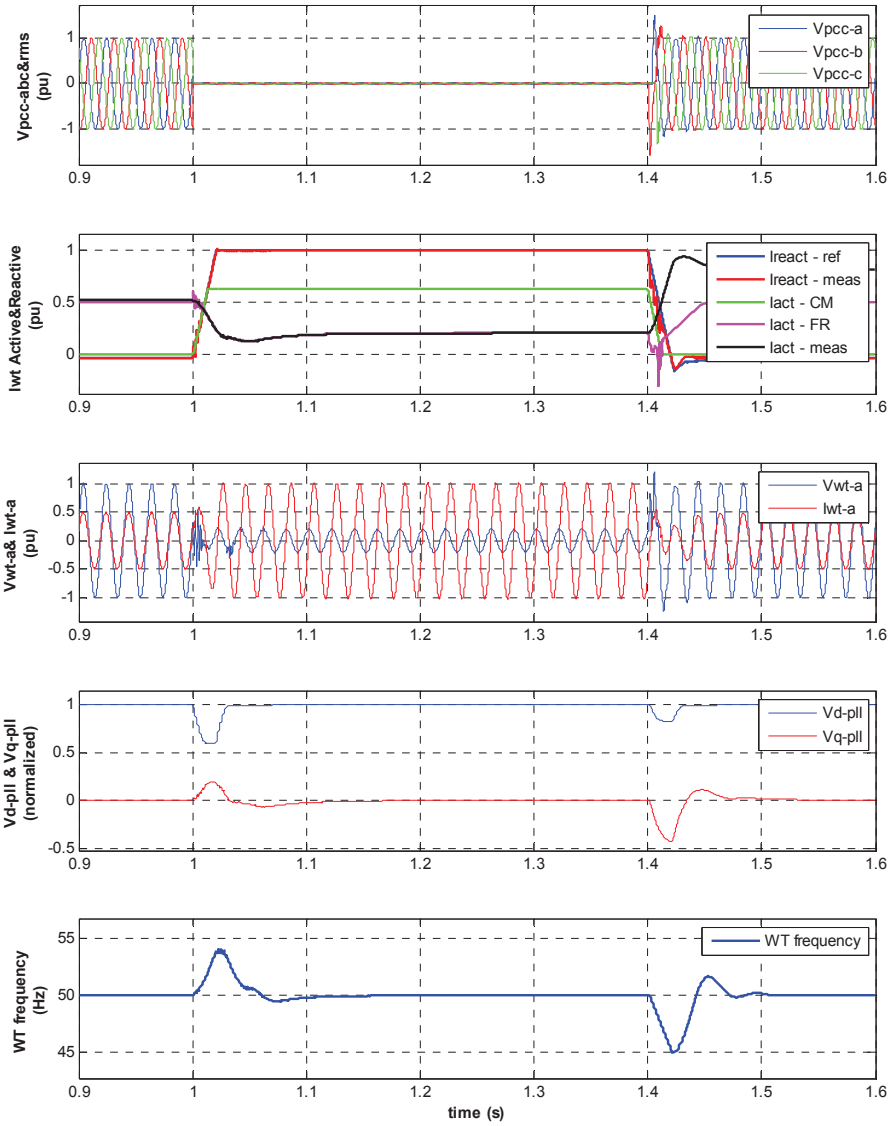

Fig. 5.21 Simulation results with PLL frequency based algorithm – highly active case

5.5.2 Experimental Results of PLL-Frequency Based Algorithm

Experimental verification of the PLL frequency based control method is accomplished with the same setup in figure 4.11. The current reference is given after decreasing the voltage down to very low (1%) of the rated at t equal to 3.1 second in Figure 5.22.

During the voltage sag, 1pu reactive current reference is generated as required by the grid code and the PLL frequency based algorithm generates 0.5pu active current reference as required by the impedance between WT and PCC terminals, which has X/R of 2. As seen in third trace, the PLL error signal is kept at zero, and the frequency is regulated towards 50Hz as seen in fourth trace.

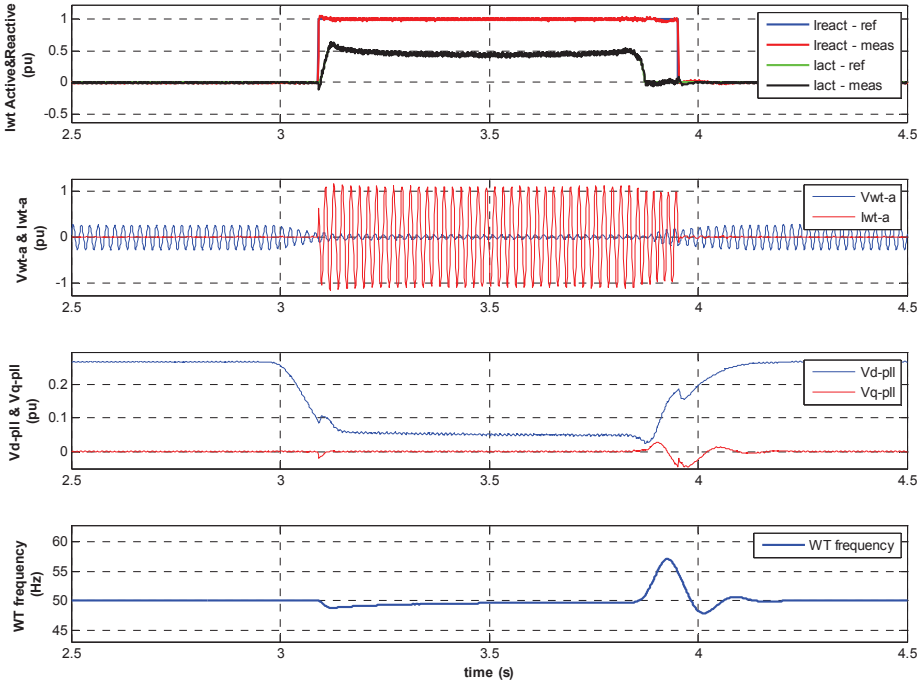

Fig. 5.22 Experimental results with PLL frequency based algorithm.

In summary, PLL frequency based method is acting as fast frequency control for the WPP experiencing LOS problem, such that frequency is deviating from the fundamental frequency of the main grid.

5.6 WPP Level Control

The X/R based and PLL frequency based control algorithms above are implemented at the wind turbine level. However, usually WTs are operating in parallel in a WPP structure, with an additional high level WPP level control architecture. When there is a

WPP controller, which has (voltage and current) feedback from PCC and communication infrastructure with the wind turbines, advanced schemes at WPP level can be implemented. Two WPP level control schemes as current control and X/R based injection at PCC level are discussed below. It should be noted that the PLL frequency based current injection method does not require any implementation or communication at WPP level. The WPP level control is only discussed here; any WPP level control method is not proposed or implemented within this study.

5.6.1 Active and Reactive Current Control at PCC

As seen in chapter 3, during severe faults and/or high WPP internal impedance, the active and reactive currents injected from wind turbines change their characteristics at the PCC point, due to phase change of PCC voltage. Referring to remark 3.8 and figure 3.17, when highly reactive currents are injected by wind turbines, current becomes anti-phase with PCC voltage i.e. active consumption, as seen in figure 5.23 below. As given in chapter 1, active current consumption is not allowed during fault by certain grid codes.

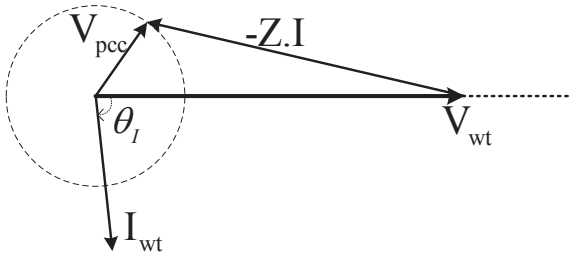

Fig. 5.23 Active and reactive current change from wind turbine to PCC.

Similar case, with highly active current from wind turbine causing reactive power consumption at PCC, has been studied in [84], as discussed in section 5.1.5 above. As accomplished in [84], such a situation of active or reactive power consumption at PCC can be avoided by injecting currents from wind turbines taking this current change into account, as a forward compensation scheme. In case of a WPP controller at PCC level and fast communication with wind turbines, active and reactive current control (vector

control) can be realized at PCC. Implementing such a current control function at PCC, any active or reactive power consumption during faults at PCC can be sensed and corrective current references can be sent to wind turbines, as a closed loop feedback scheme. At the end any active consumption or underexcited reactive current at PCC can be avoided. However, this would require quite fast communication structure to act in short duration of the fault. As discussed in chapter 3, with figure 3.32, injection of controlled current at PCC can help to avoid LOS, especially for faults occurring at PCC. However, for severe faults occurring remote from PCC, can still cause LOS if proper current (with the impedance angle) is not injected from PCC. Hence WPP level current control can help to avoid LOS, but not the ultimate solution.

The X/R based method is based on injection of current from wind turbines with angle of the impedance. However, when there are additional units installed at the WPP, e.g. Statcom, energy storage, the supervisory control of WPP controller is definitely necessary in order to provide parallel operation of WTs and additional units, such that current is injected with the same angle of the impedance to the grid. Hence, a current control function as described above can help to coordinate the wind turbines and the units (e.g. Statcom) at PCC to inject X/R based current at PCC. Moreover, any triggering or decision algorithm based on grid parameters, can be implemented at WPP level and necessary triggering commands can be sent to WTs. For instance, the decision algorithm based on the voltage drop can be employed the WPP controller based on the voltage drop at the PCC, and necessary commands (triggering either the conventional method or the proposed method) can be sent to each wind turbine. Such a grid X/R based current injection at PCC can improve the response regarding avoidance of LOS; however, as discussed above, the X/R based scheme would still suffer from the inaccuracy of X/R parameter, especially when there is a severe fault remote from PCC.

5.7 Minimum Active Power Requirement of Proposed Solutions

Both of the proposed X/R based and PLL frequency based algorithms are based on certain amount of active current injection during severe faults. However, it is well-known that active current depends on the active power production level of the WT (or

WPP). For instance in the cases where PLL frequency based method is employed and results shown in figures 5.20 and 5.21, 0.25pu active current is injected and the WT terminal voltage is 0.24pu, which results in injection of 6% of the rated power.

Hence, for some cases, there is the possibility that the WT experiences a severe fault, but the required active power related to the required active current by the proposed algorithms, is larger than the available active power at that moment. In this case, if the WT tries to inject the active current, it can cause drop of DC link voltage, which should be avoided. The most straightforward way to consider this minimum active power requirement is to add a function to check for the available active power and limit the active current reference from stability algorithms based on this limit. It should be noted that while limiting the active current due to lack of necessary active power, the reactive current injection needs to be limited in order to avoid instability. This implies that when the wind power plants are generating very low or zero active power due to low wind, they should not be expected to inject reactive current during severe faults, since they would not be able inject the necessary accompanying active current.

5.8 Summary of the Current Injection Schemes

In figure 5.24 five current injection schemes given in this thesis avoiding LOS are summarized with their (reactive) current injection and corresponding FRT profiles. The conventional method from chapter 1 is not included here since LOS is not avoided and occurs with conventional method when the current reference is out of the transfer limits. First three schemes in figure 5.24 are based on limiting the current injection during severe faults, considering the current transfer limits. The fourth one is the X/R based injection method and the last one is the PLL frequency based injection method. Z in figure 5.24 is the magnitude of the impedance between wind turbine and PCC, whereas R is the resistance of this impedance.

The first method, keeping the current reference as zero during severe faults is given as a reference. As seen in (a), current is kept as zero when the PCC voltage magnitude is below the magnitude of Z based on (5.3), such that no risk of LOS remains. In this case, the current can be considered as reactive but any current from wind turbine is kept as zero. The corresponding voltage FRT profile is shown in (b). It is important to note

that such a scheme is the safest and simplest one avoiding LOS. However, it has the drawback that no current is injected below a voltage level (e.g. 21% for the system in figure 4.6), which would not be acceptable for certain grid codes' FRT requirements.

The second method in (c) is the limited current injection given in section 5.3. The current magnitude (composed of active and reactive components) is gradually decreased in order to stay inside the safe transfer limits for decreasing magnitude of PCC voltage based on (5.3). In this case, again current magnitude is compromised from maximum value, and the FRT curve in (d) would not comply with certain grid code requirements.

The third method in (e) and (f) is based on pure reactive current injection, without any active current. As analyzed in chapter 3, the minimum PCC voltage magnitude in this case is equal to R of the impedance, as seen in (e) and (f). Remembering the discussion in section 5.6.1 and remark 3.8, active current is absorbed (active power consumed) at the PCC, which would not be accepted by certain grid codes.

In the first three schemes, current injection is being limited based on the voltage at the PCC and impedance between PCC and wind turbine. However, since the current transfer limits vary with varying fault location, there is the difficulty of sensing the faulted point voltage and limiting the current accordingly. As shown in figure 3.31, PCC voltage varies depending on the fault location. Nevertheless, these methods help to avoid LOS, but compromising current injection. Hence, limiting current injection is not a comprehensive solution.

In the fourth scheme, current is injected based on X/R of the impedance. As discussed in section 5.4.1, due to sensitivity to X/R parameter, this method cannot work satisfactorily for very severe faults. Assuming that the impedance will be estimated with ±10° accuracy, the minimum voltage for satisfactory performance of the X/R based method is found as $0.15x|Z|$, based on (5.8). In figure 5.24, the current is kept as zero below this minimum voltage value. The fifth method, PLL frequency based current injection can inject full current even for zero PCC voltage as given in (i). As seen in (j) the FRT curve with the PLL frequency based injection method complies with any grid code requirement. In summary, during severe three-phase grid faults, LOS problem is occurring due to PLL instability with high current injection from wind

turbines. The proposed PLL frequency feedback based current injection method is the strongest candidate to solve the LOS problem during low voltage faults.

The X/R based methods and the proposed PLL frequency based methods are injecting active and reactive currents to the faulted grid in proportion to the characteristic of the grid impedance during fault. Such an injection is similar to the active and reactive power injection of CPPs, which behave as constant voltage sources during faults and inject power in proportion to the grid impedance during fault [1]. Hence, it can be commented that the proposed methods are resulting in WPP behavior in a similar manner to CPPs.

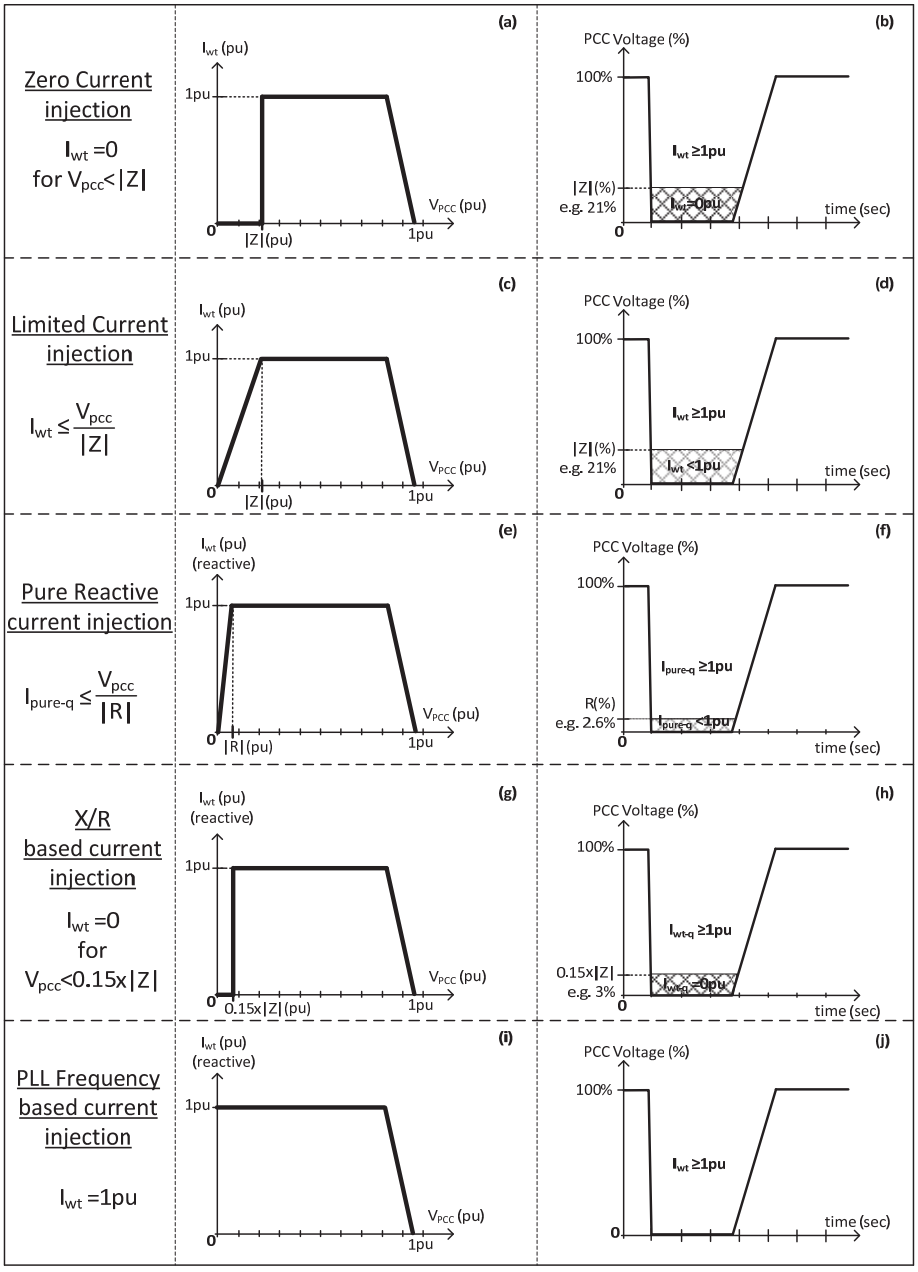

Fig. 5.24 Comparison of current injection schemes during fault.

Chapter 6

Analysis of Asymmetrical Faults

In this chapter, the identified problems during asymmetrical grid faults, which were given in chapter 2, are analyzed in detail. First, effects of unbalanced grid voltages on the power system are summarized as a background for asymmetrical fault solutions. Equivalent circuits of positive negative and zero sequence networks during asymmetrical faults, which are well-known from classical power system theory, are utilized to explain the impact of wind power plant current injection on the grid, and the problem of high phase overvoltages and higher negative sequence voltages.

6.1 Effects of Unbalance

In chapter two, where the identified problems during asymmetrical faults were given, it has been shown that with the use of conventional method of current injection, higher negative sequence voltages and higher phase overvoltages are observed. Before the analysis of these problems and solutions via reducing negative sequence voltage in the following parts, effect of negative sequence voltage, i.e. unbalance in the grid, is reviewed in this section. A survey of literature [88] – [101], which studies long-term (steady-state) and short-term (asymmetrical fault related) effects of unbalance on the power system elements and stability is accomplished in following paragraphs.

Effects of unbalance on electrical equipments differ from equipment to another. Common problems due to unbalance are given below for various components in the power system. Effects of unbalance on rotating machines, induction machines and synchronous generators, are widely analyzed in literature. Induction machines face three kinds of problems due to unbalance [88], [89]. First, the machine cannot produce

its full torque as the negatively rotating magnetic field of the negative-sequence causes a negative braking torque that has to be subtracted from the base torque linked to the normal rotating magnetic field. Secondly, the bearings may suffer mechanical damage because of induced torque components at double system frequency. Thirdly, the stator and, especially, the rotor are heated excessively, possibly leading to faster thermal aging. Synchronous generators exhibit phenomena similar to those described for induction machines, but mainly suffer from excess heating. Special care must be devoted to the design of stabilizing damper windings on the rotor, where the currents are induced by the negative and zero sequence components [88], [89].

Unbalance has also effect on capacity of transformers, cables and lines. The capacity of transformers, cables and lines is reduced due to negative sequence components. Any circulating current in the delta side of a transformer causes heating and the associated zero sequence magnetic flux passes through constructional parts of the transformer causing parasitic losses in parts such as the tank, sometimes requiring an additional derating [88], [89]. Power electronic converters, which are present in many devices such as adjustable speed drives, PC power supplies, efficient lighting, can be faced with additional, uncharacteristic, harmonics. The design of passive filter banks dealing with these harmonics must take this phenomenon into account [88], [89].

For renewable generating units with asynchronous generators; in its normal slip range an asynchronous generator has almost constant negative sequence impedance. High current unbalance can have detrimental effects on the rotor vibration, causing oscillating torque that increases fatigue in the mechanical drive train of the turbine, which may alert the mechanical protection system. So at low wind speeds unbalanced operation can lead to generator disconnection and increased mechanical stresses [92].

From power system transient stability point of view, specifically short-term unbalance during asymmetrical faults is investigated in literature. In [94]-[96], transient stability analysis for synchronous and asynchronous machines is extended to include the unbalanced cases, such as unbalanced load, lines and an asymmetrical fault. An important finding of the investigation in [94] is in networks equipped with single-pole circuit breakers, the SLG fault followed by a line outage represents a worse shock to the system than the traditionally accepted temporary three-phase-to-ground fault. In

[99]–[101], requirements for allowable negative sequence current flow into rotational machines are specified as I^2t values.

In summary, regarding the stability of the synchronous and asynchronous machines during asymmetrical faults, only the series asymmetrical faults can be considered as a risk, not the shunt asymmetrical faults. Any unbalance, which exists for steady-state in the system, can cause long-term detrimental effects on the components. Hence, steady-state unbalance has to be mitigated by means of hardware and software schemes, and has to be taken into account within design of power system. When the unbalance is caused by an asymmetrical fault, the same detrimental effects exist for a very short-term but with high order of severity. Every occurrence of an asymmetrical fault, adds to the fatigue in the mechanical and electrical part of power system elements. Hence, unbalance, i.e. negative sequence voltage, should be mitigated as much as possible during the faults.

6.2 Analysis of the Problems Observed

As given in chapter one, in most of the grid codes of certain countries, WTs are expected to stay connected and to support the positive sequence grid voltage with positive sequence reactive currents during short-circuit grid faults, for both symmetrical and asymmetrical faults [14]. However, grid codes are prepared to target only positive sequence voltage boost, which can be considered as a proportional voltage control in positive sequence.

As known from power system fault analysis [3], during asymmetrical faults, phase-to-ground voltages in non-faulty phases rises over rated values, i.e. phase overvoltages occur. Neutral grounding of the power system is designed to keep zero sequence impedances in accordance with the target of avoiding high phase overvoltages but also avoiding very high fault currents during asymmetrical faults. For instance, a bus is considered to be effectively grounded if the ratio of zero sequence impedance to positive sequence impedance seen from that bus is kept between one and three [3]. This practice in transmission system keeps the earth fault factor, which is per unit value of non-faulty phase voltage value, e.g. less than 1.4, which in turn means avoidance of

phase overvoltages. It should be noted that impedance grounding can be applied in distribution systems.

An interesting phenomenon, which was presented in chapter two, that; in case of asymmetrical faults, if the conventional method (CM) is employed, which is injection of pure positive sequence currents and keeping negative sequence currents as zero, positive sequence voltage is boosted, but also negative and zero sequence voltages are boosted at the fault point (e.g. PCC). In the following section, the reasons of coupling between positive negative and zero sequence voltages during asymmetrical faults, and impact of WPP current injection is analyzed.

6.2.1 Coupling Phenomenon during Asymmetrical Faults

As well-known from power system fault analysis, positive, negative and zero sequences are interconnected at the faulted point through the fault impedance [3], [24]. Hence, sequence voltages are coupled at the faulted bus. Due to this coupling, an action in one of the sequences has effects also on the other sequences. Amount of coupled boost in negative and zero sequences depends primarily on how much the voltage at the faulted point can be altered by the WPP, and also depends on the fault type and fault impedance. Transfer impedance between the WPP and the faulted point defines how much the WPP can alter the voltage at the faulted bus [24]; and the transfer impedance depends on the grid characteristics and fault location. For weak grids (with high grid impedance) and/or for faults occurring near to WPP, coupling is more observed, since WPP can alter the bus voltage more for weak grids, than for a strong grid [32].

Coupling can be better understood when sequence voltages at the faulted point is compared for two cases as; with and without current injection from WPP during the fault. Interconnected equivalent sequence circuits are utilized to show effect of coupling; as for a SLG fault in figure 6.1 [34], [3], [24]. Impact of positive sequence voltage boost obtained by the WPP current injection is superimposed to the positive sequence equivalent voltage, and resulting impact on the negative and zero sequences are simply calculated via voltage division. The equivalent voltage source V^{+}_{th} is the prefault voltage at the faulted point, which depends on the power flow before the fault and usually kept at rated (1pu) value via voltage control action of power plants [34],

[3], [24]. However, positive sequence reactive current injection by WPPs during the fault can be considered as additional reactive power support which was not being given before the fault, and which boosts all phase voltages. Boost obtained by the WPP current injection on the faulted point positive sequence voltage, $V^{+}_{\Delta wpp}$, can be calculated as (6.1) by using the positive sequence transfer impedance Z^{+}_{fw}, from the WPP current injection bus to the faulted point and the WPP current phasor I^{+}_{w}.

$$V^{+}_{\Delta wpp}=Z^{+}_{fw}I^{+}_{w} \tag{6.1}$$

Positive, negative and zero sequence voltages for a SLG fault and effect of WPP support are obtained as in (6.2) to (6.4), from figure 6.1. It is important to note that the voltage boost by WPP, $V^{+}_{\Delta wpp}$, and the impedance Z^{+}_{ff}, Z^{-}_{ff} and Z^{0}_{ff}, are complex quantities. Based on the equations derived below, approximate calculations can be done for sequence voltages, which is used for understanding of coupling action. Detailed and precise analysis requires time-domain simulations, which is given in the following chapter.

$$V^{+}_{f\text{-}SLG}=(V^{+}_{th}+I^{+}_{w}Z^{+}_{fw})\left(\frac{Z^{-}_{ff}+Z^{0}_{ff}+3Z_{f}}{Z^{+}_{ff}+Z^{-}_{ff}+Z^{0}_{ff}+3Z_{f}}\right)=(V^{+}_{th}+V^{+}_{\Delta wpp})\left(\frac{Z^{-}_{ff}+Z^{0}_{ff}+3Z_{f}}{Z^{+}_{ff}+Z^{-}_{ff}+Z^{0}_{ff}+3Z_{f}}\right) \tag{6.2}$$

$$V^{-}_{f\text{-}SLG}=(V^{+}_{th}+I^{+}_{w}Z^{+}_{fw})\left(\frac{Z^{-}_{ff}}{Z^{+}_{ff}+Z^{-}_{ff}+Z^{0}_{ff}+3Z_{f}}\right)=(V^{+}_{th}+V^{+}_{\Delta wpp})\left(\frac{Z^{-}_{ff}}{Z^{+}_{ff}+Z^{-}_{ff}+Z^{0}_{ff}+3Z_{f}}\right) \tag{6.3}$$

$$V^{0}_{f\text{-}SLG}=(V^{+}_{th}+I^{+}_{w}Z^{+}_{fw})\left(\frac{Z^{0}_{ff}}{Z^{+}_{ff}+Z^{-}_{ff}+Z^{0}_{ff}+3Z_{f}}\right)=(V^{+}_{th}+V^{+}_{\Delta wpp})\left(\frac{Z^{0}_{ff}}{Z^{+}_{ff}+Z^{-}_{ff}+Z^{0}_{ff}+3Z_{f}}\right) \tag{6.4}$$

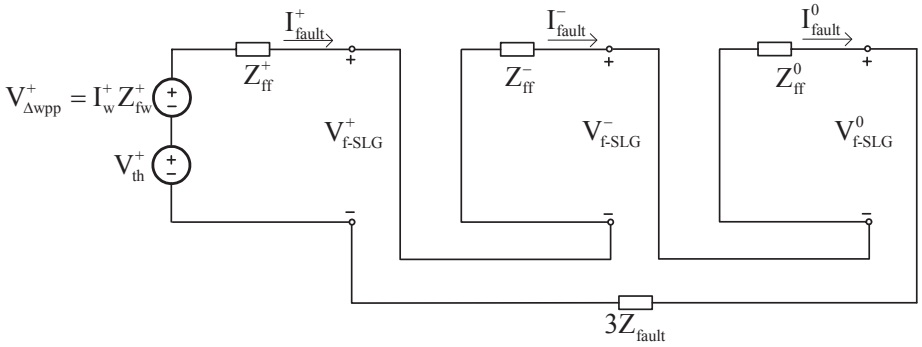

Fig. 6.1. Equivalent circuits during SLG fault.

As observed in figure 6.1 and in (6.2) to (6.4), for a SLG fault, amount of positive sequence voltage boost obtained by WPP current injection, is reflected to negative and zero sequence voltages inevitably, with ratios depending on sequence impedances. For instance, for a system with magnitude of Z_{fw} 0.2pu, injection of 1pu WPP positive sequence reactive current can boost positive sequence voltage approximately by 0.15pu based on (6.2). However, due to the coupling as observed in (6.3) and (6.4), negative and zero sequence voltages are also boosted approximately by 0.05pu and 0.1pu, respectively.

Positive, negative, and zero sequence equivalent circuits seen from the faulted bus during a DLG fault are interconnected as shown in figure 6.2 [34], [3], [24]. From figure 6.2, positive, negative and zero sequence voltages for a DLG fault and effect of WPP support can be obtained as in (6.5) to (6.7).

$$V_{f\text{-}DLG}^{+}=(V_{th}^{+}+I_{w}^{+}Z_{fw}^{+})\left(\frac{Z_{ff}^{-}//(Z_{ff}^{0}+3Z_{f})}{Z_{ff}^{+}+Z_{ff}^{-}//(Z_{ff}^{0}+3Z_{f})}\right)=(V_{th}^{+}+V_{\Delta wpp}^{+})\left(\frac{Z_{ff}^{0}+3Z_{f}}{Z_{ff}^{-}+2Z_{ff}^{0}+6Z_{f}}\right) \quad (6.5)$$

$$V_{f\text{-}DLG}^{-}=(V_{th}^{+}+I_{w}^{+}Z_{fw}^{+})\left(\frac{Z_{ff}^{-}//(Z_{ff}^{0}+3Z_{f})}{Z_{ff}^{+}+Z_{ff}^{-}//(Z_{ff}^{0}+3Z_{f})}\right)=(V_{th}^{+}+V_{\Delta wpp}^{+})\left(\frac{Z_{ff}^{0}+3Z_{f}}{Z_{ff}^{-}+2Z_{ff}^{0}+6Z_{f}}\right)=V_{f\text{-}DLG}^{+} \quad (6.6)$$

$$V_{f\text{-}DLG}^{0}=\left(\frac{Z_{ff}^{0}}{Z_{ff}^{0}+3Z_{f}}\right)V_{f\text{-}DLG}^{+}=(V_{th}^{+}+V_{\Delta wpp}^{+})\left(\frac{Z_{ff}^{0}}{Z_{ff}^{-}+2Z_{ff}^{0}+6Z_{f}}\right)\simeq V_{f\text{-}DLG}^{+} \quad (6.7)$$

As observed in figure 6.2 and in (6.5) to (6.7), for a DLG fault, the positive and negative sequence voltages at the faulted point are equal. When the fault impedance (e.g. 0.02pu), which is small compared to positive sequence impedance (e.g. 0.2pu), is neglected, zero sequence voltage is also equal to the positive sequence voltage, thus the zero sequence voltage is also boosted at the faulted point (e.g. PCC) with almost the same amount. Hence, if the positive sequence voltage is boosted by the WPP at the faulted point (e.g. PCC), the negative sequence voltage is also inevitably boosted to the same value due to coupling. For instance, for a system with magnitude of Z_{fw} 0.2pu,

injection of 1pu WPP positive sequence reactive current would boost positive sequence voltage approximately by 0.1pu based on (6.5), but also the negative and zero sequence voltages with the same amount as seen in (6.6) and (6.7).

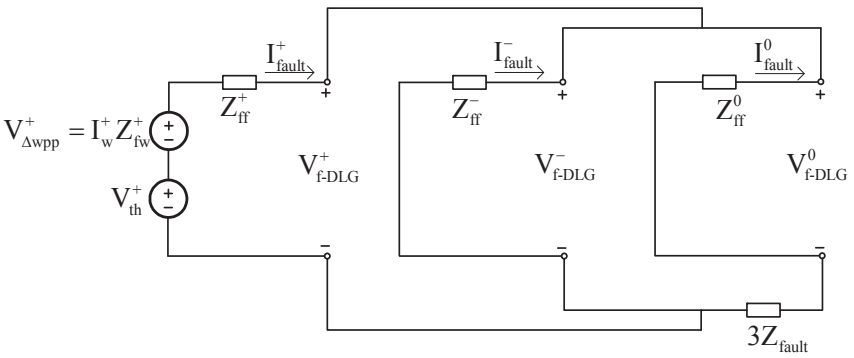

Fig. 6.2 Equivalent circuits during DLG fault.

Positive and negative sequence equivalent circuits seen from the faulted bus during a LL fault are interconnected as shown in figure 6.3 below. As well-known, zero sequence remains unaffected and zero sequence voltage does not arise during LL faults [34], [3], [24]. From figure 6.3, positive, negative and zero sequence voltages for a LL fault and effect of WPP support can be obtained as in (6.8) to (6.10).

$$V^{+}_{f\text{-}LL} = (V^{+}_{th} + I^{+}_{w} Z^{+}_{fw}) \left(\frac{Z^{-}_{ff} + Z_f}{Z^{+}_{ff} + Z^{-}_{ff} + Z_f} \right) = (V^{+}_{th} + V^{+}_{\Delta wpp}) \left(\frac{Z^{-}_{ff} + Z_f}{Z^{+}_{ff} + Z^{-}_{ff} + Z_f} \right) \tag{6.8}$$

$$V^{-}_{f\text{-}LL} = (V^{+}_{th} + I^{+}_{w} Z^{+}_{fw}) \left(\frac{Z^{-}_{ff}}{Z^{+}_{ff} + Z^{-}_{ff} + Z_f} \right) = (V^{+}_{th} + V^{+}_{\Delta wpp}) \left(\frac{Z^{-}_{ff}}{Z^{+}_{ff} + Z^{-}_{ff} + Z_f} \right) \simeq V^{+}_{f\text{-}LL} \tag{6.9}$$

$$V^{0}_{f\text{-}LL} = 0 \tag{6.10}$$

As seen in figure 6.3, and also in (6.8) and (6.9), positive and negative sequence voltages are almost equal at the faulted bus (e.g. PCC) for LL faults, which means that the boost of positive sequence voltage would be observed with same amount in negative sequence voltage. For instance, for a system with magnitude of Z_{fw} 0.2pu, injection of 1pu WPP positive sequence reactive current would boost positive sequence

voltage by 0.1pu, but also the negative sequence voltage approximately with the same amount as 0.1pu based on (6.8) and (6.9). Utilizing (6.2) to (6.9), effect of WPP injection at the faulted bus is obtained approximately. In order to obtain exact voltage values during fault, and to see effect of WPP injection and also prefault operation, time-domain simulations are needed, as given in next chapter.

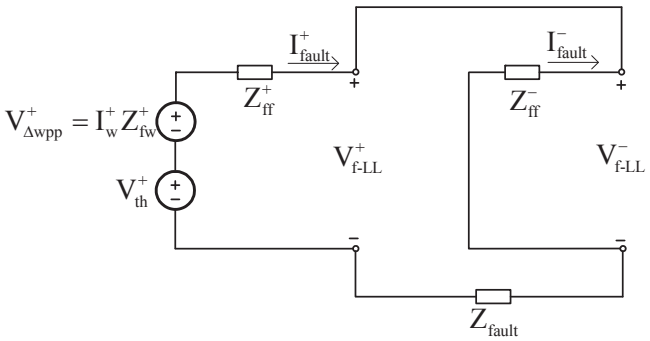

Fig. 6.3 Equivalent circuits during LL fault.

The coupling explored in this section has not been observed in previous wind power asymmetrical fault studies. This is due to the fact that in the previous studies asymmetrical faults was not created as realistic events as short-circuits (solid or with a fault impedance) between phases and/or ground; instead unbalance was being created via modifying voltage sources, which represent grid voltage in the simulation models. Hence, in previous studies, interconnection of positive negative and zero sequences did not exist and it was being observed that when the positive sequence voltage is boosted via injecting pure positive sequence currents, negative sequence voltage remains unaffected. However, as shown here, sequences are coupled and it is important to conduct real faults for asymmetrical fault studies in order to observe interconnection between sequences, especially for high wind power penetration cases.

It is important to note from figures 6.1 to 6.3 that coupling also exists from negative sequence to positive and zero sequences, such that when negative sequence voltage is attenuated by WPPs, positive sequence voltage is also attenuated due to coupling.

Hence at the faulted bus it becomes as a trade-off between boosting positive sequence voltage and balancing the phase voltages.

6.3 Conclusion

In this chapter, the problems observed with the conventional method of injecting pure positive sequence reactive current to asymmetrical faults, are analyzed. The coupling phenomenon, which has not been considered in the previous wind power fault studies, is explored, together with the impact of WPP reactive current injection. As discussed in this chapter, negative sequence voltage has numerous harmful effects on the power system elements, which implies need for attenuation of negative sequence voltage.

In this chapter and chapter two, it is shown that the conventional method of injecting pure positive sequence reactive current has beneficial effects (boosting the positive sequence voltage) but also adverse effects (boosting negative sequence voltage and non-faulty phases). In the next chapter, an alternative to conventional method, dual-sequence (DS) control method is given.

Chapter 7

Control Solutions for Asymmetrical Faults

In this chapter, based on the analysis of the problems during asymmetrical grid fault from previous chapter, a control solution to mitigate the mentioned problems is given as an alternative to the conventional method. A cost function is defined for grid voltage improvements, which helps to quantify and compare conventional and alternative control solutions. It is shown that, behaving in a similar manner to the conventional power plants, response of wind power plants can be improved for better grid support.

7.1 Dual-Sequence Current Injection Method

The response of WPPs during asymmetrical faults have been studied in the literature [58]-[73], and several control methods injecting negative sequence current have been proposed; e.g. to mitigate power and dc link oscillations from the WT, or to balance the grid voltage by reducing the negative sequence voltage. However, these methods mainly targets issues related to WTs themselves or include negative sequence voltage attenuation but not handling the situation considering grid side impact of the WPP current injection during asymmetrical faults. Only in [73], overvoltages at the non-faulty phases are discussed. However, the coupling phenomenon between positive, negative and zero sequences, which causes undesired boost of negative sequence voltage has not been considered in any of the previous studies.

Impact of WPP's pure positive sequence current injection during asymmetrical faults is given in the previous sections. It is shown that, a WPP, employing CM, is causing high negative sequence voltage and high phase overvoltages since WPP is acting as open circuit in negative sequence. Alternative to the CM, which is injecting pure positive sequence reactive (capacitive/overexcited) currents by WPPs, the concept of dual-

sequence (DS) injection is represented here. DS is based on injecting both positive sequence reactive (capacitive/overexcited) currents boosting the positive sequence voltage and negative sequence reactive (inductive/underexcited) currents reducing the negative sequence voltage, as given in figure 7.1.

In contrast to the grid code requirement, where all phases, hence including the non-faulty phases are supported, the DS method distributes the support such that only faulted phases are supported, and non-faulty phases are not supported unnecessarily. Hence, high phase overvoltages in the non-faulty phases are mitigated, and support is shared as between positive sequence voltage boost and negative sequence voltage reduction. The DS method is shown in figure 7.1, where the main contribution of DS method is the negative sequence voltage control in parallel to positive sequence voltage control. Hence in DS method, there is also negative sequence proportional voltage control gain k^-, in addition to the positive sequence proportional voltage control gain, k^+, which was shown in conventional control method in chapter one. These parameters can simply be tuned as having identical values, as is done in this study, whereas alternative tuning methods can be accomplished for setting different priorities between boosting positive and reducing negative sequence voltages.

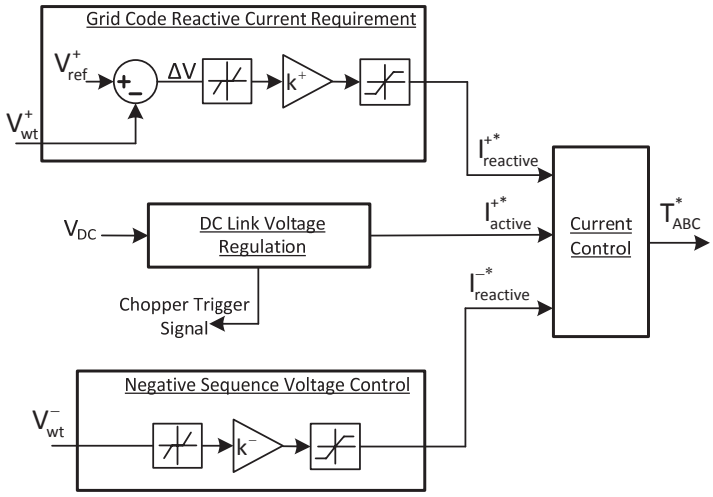

Fig. 7.1 Dual-Sequence (DS) current injection method.

Performance of the DS method is shown in the next section with simulations, where two other methods are also included for comparison.

7.2 Simulation Results

The performance of the proposed DS method, which is injecting both positive and negative sequence currents, is compared against the CM in this section. In order to see the bus voltages during faults without support of the WPP, a third injection case of no support (NS), where WPP is keeping its currents as zero, is also implemented. Three injection methods, namely NS, CM, and DS are simulated. The system used in the simulations, and its equivalent circuits for each sequence are shown in figure 7.2 and figure 7.3, respectively. The negative sequence network is the same as the positive sequence network with zero grid voltage [24]. The grid is modelled with its Thevenin equivalent and the WPP is connected to the grid via 50km long OHL. The OHL and collector network equivalent are modelled as PI models, with details in table 7.1. In the WPP a d5YN and YNd5 type transformers are utilized as WPP main transformer and WT transformer, respectively. The collector network's neutral is grounded via a grounding zigzag transformer.

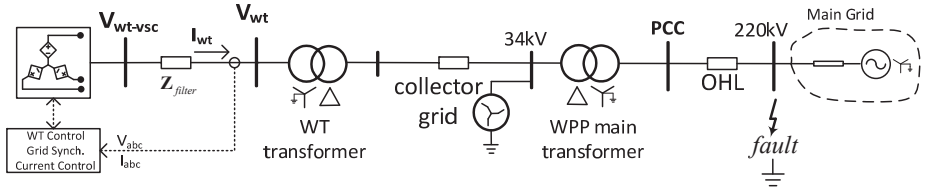

Fig. 7.2. WPP connection, Thevenin equivalent of grid, and fault location.

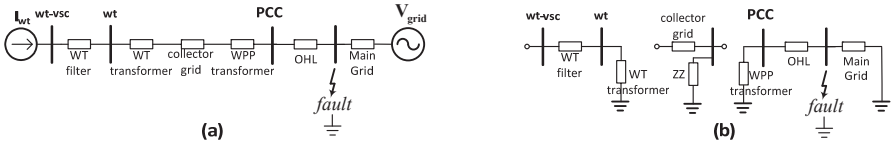

Fig. 7.3. Networks of (a) positive and negative sequences, (b) zero sequence

Table 7.1

Electrical Data of Lines and WPP Components, S_{base}=100MVA, [pu]

		R	X	B
Grid	Pos.	0.01	0.1	-
	Neg.	0.01	0.1	-
	Zero.	0.02	0.2	-
OHL	Pos.	0.022	0.112	0.026
	Neg.	0.022	0.112	0.026
	Zero.	0.088	0.372	0.014
Equivalent Collector Network	Pos.	0.0056	0.0069	0.0175
	Neg.	0.0056	0.0069	0.0175
	Zero.	0.0589	0.0039	0.035
Main Trf		0.01	0.15	-
WT Trf		0.008	0.08	-
ZZ Trf		0.01	0.1	-
WT filter		0.01	0.1	0.05
Fault Impedance		0.02	0	0

In the WT, deadband in the voltage control algorithms are kept as zero, i.e. not applied. Proportional voltage control constant, k+, for the CM case is selected as 5, and the two proportional constants, k+ and k- for DS (control structure given in figure 7.1) case are both kept identical as 2.5. The maximum current that can be injected by the WPP is kept as 1pu. The WPP currents and voltages are measured at the WT terminals. In order to show impact of WPP reactive current injection on grid voltages clearly, only reactive currents are injected during the fault and active current is kept as zero.

Time-domain response for a single line-to-ground fault is shown in figure 7.4, where the fault is created at phase “a”. In order to save space, all three control algorithms are executed during the fault, keeping the fault duration intentionally long as 300ms. Fault is created at t=1.1 second, which is removed at t=1.4. Before and after the fault, the WPP is injecting 20% active power, and 0.2pu balanced phase currents are seen in figure 7.4-(a). For the first 100ms of the fault, WPP currents are kept zero, i.e. NS is applied, in order to observe the case without the WPP support. The rms current values

shown in figure 7.4-(b) are pure reactive components for both positive and negative sequences. At t=1.2, CM is activated and pure positive sequence currents are injected as a positive sequence proportional voltage control. At t=1.3, the DS method is activated and both positive and negative sequence voltage control are realized via injecting both positive and negative sequence currents. In the figure 7.4 V_f represents the voltage at the faulted point.

It is important to note that even though the zero sequence networks of grid and WPP are isolated with the use of dYN transformer, the zero sequence voltage is still increased with use of CM, when compared to NS due to coupling between sequences. It rises inevitably also for DS, but nevertheless negative sequence voltage is attenuated with DS, providing balanced voltages.

It is seen in figure 7.4-(c), at the faulted bus the healthy phase voltages, which are 1.08pu without WPP support, rise up to 1.13pu, when CM is employed. Similarly at PCC in figure 7.4-(e), healthy phases rise up from 0.95pu to 1.04pu value when CM is employed, as shown in figure 7.4-(e). With the use of DS method, at the PCC bus positive sequence voltage is boosted to 0.78pu, negative sequence voltage is attenuated to 0.23pu, and phase overvoltage is mitigated.

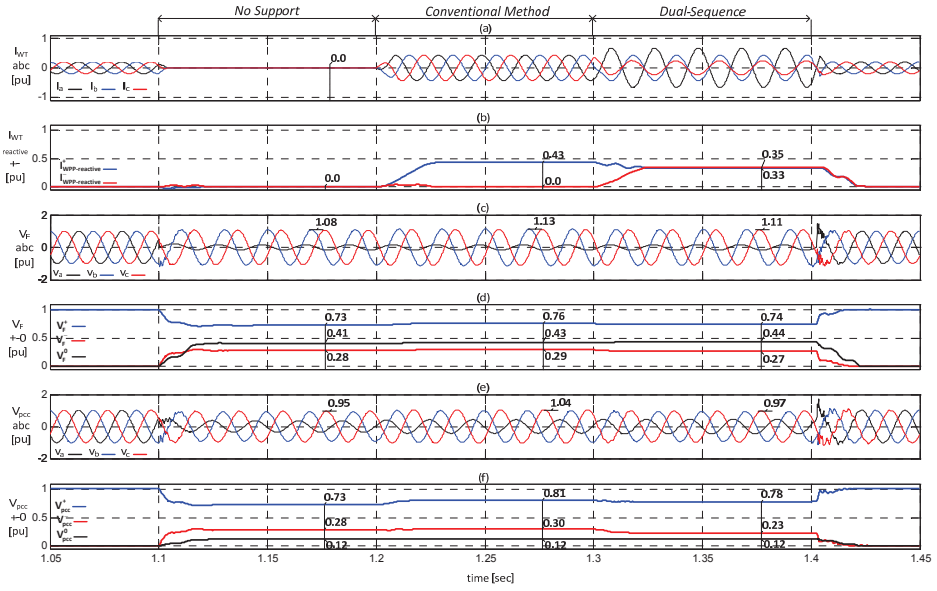

Fig. 7.4. Simulation results for a SLG fault

Since the focus is only on the steady-state period of the faulted duration for DLG and LL faults, time-domain results are given in tables 7.2 and 7.3, showing values for steady-state period of each algorithm. Results of DLG fault is summarized in table 7.2, which shows similar behaviour of SLG fault. As observed in table 7.2, at the faulted bus with CM, all the phase voltages are boosted, which means that the non-faulty phase "a" is boosted unnecessarily from 1.11pu to 1.21pu, where the positive sequence voltage, but also the negative sequence voltage due to the coupling, are both boosted from 0.39pu to 0.43pu. Hence high overvoltages are observed at the faulted bus and the PCC bus. At the PCC bus, DS method is boosting the positive sequence voltage from 0.39pu to 0.47pu while attenuating the negative sequence voltage from 0.39pu to 0.35pu, avoiding unnecessary support to non-faulty phase via boosting only the faulted buses, "b" and "c", whereas non-faulty phase "a" is slightly boosted from 0.87pu to 0.91pu. It should be noted that DS method is boosting and balancing at the PCC compromising high boost obtained by CM, which is from 0.39pu to 0.54pu.

Results for a LL fault are given in table 7.3, where it is seen that with the use of CM both the positive and negative sequence voltages are boosted with the same amount of 0.03pu at the faulted bus due to the coupling, where the non-faulty phase "a" is boosted unnecessarily from 1pu to 1.06pu; and at the PCC bus the non-faulty phase "a" is boosted from 1.01pu to 1.12pu. Due to the coupling between positive and negative sequences at the faulted bus DS method is compromising boost of positive sequence voltage while avoiding the boost of the negative sequence voltage. However, with the balancing effect of the DS method, at the PCC bus positive sequence voltage is boosted and negative sequence voltage is attenuated such that the support is distributed and only faulted phases are boosted.

As seen from figure 7.4 and table 7.2and 7.3, with the use of DS method, peak values of WT phase currents are decreased, which can give chance to additional utilization of the WT for more currents to inject more reactive or active power during the fault.

Table 7.2

Simulation Results for a DLG Fault

		NS	CM	DS
I_{wt}	Pos.	0	1.00	0.60
	Neg.	0	0	-0.40
	a	0	1.00	0.21
	b	0	1.00	0.85
	c	0	1.00	0.89
V_f	Pos.	0.39	0.43	0.40
	Neg.	0.39	0.43	0.40
	Zero	0.35	0.38	0.35
	a	1.11	1.21	1.13
	b	0.14	0.16	0.14
	c	0.14	0.16	0.14
V_{pcc}	Pos.	0.39	0.54	0.47
	Neg.	0.39	0.43	0.35
	Zero	0.10	0.11	0.10
	a	0.87	1.06	0.91
	b	0.31	0.42	0.35
	c	0.31	0.40	0.34

In summary, when only positive sequence reactive current is injected in the case of CM, non-faulty phases are also boosted unnecessarily, which causes severe increase in the phase-to-ground voltages of non-faulty phases. DS method is able to avoid adverse effects of CM such that coupling is mitigated, negative sequence voltage is attenuated towards WPP, and high phase overvoltages are mitigated. As a drawback of DS method the grid voltages are balanced for the expense of less amount of boost positive sequence voltage.

Table 7.3

Simulation Results for a LL Fault

		NS	CM	DS
I_{wt}	Pos.	0	0.53	0.49
	Neg.	0	0.0	-0.51
	a	0	0.53	0.12
	b	0	0.53	0.80
	c	0	0.53	0.92
V_f	Pos.	0.51	0.54	0.51
	Neg.	0.49	0.52	0.49
	Zero	0.00	0.00	0.00
	a	1.00	1.06	1.00
	b	0.59	0.62	0.59
	c	0.42	0.44	0.41
V_{pcc}	Pos.	0.51	0.60	0.57
	Neg.	0.50	0.52	0.44
	Zero	0.00	0.00	0.00
	a	1.01	1.12	0.91
	b	0.59	0.67	0.62
	c	0.42	0.46	0.41

A comparison of the calculated cost for each case is given in figure 7.5 below. Cost is calculated at the grid side as; Cost=$|\Delta V_{pos}|+|V_{neg}|+|\max(Va, Vb, Vc)-1|$ (if any phase exceeds 1pu). As observed, in most of the cases the double sequence method is performing better regarding minimizing cost of asymmetrical fault to the grid, and improving grid support.

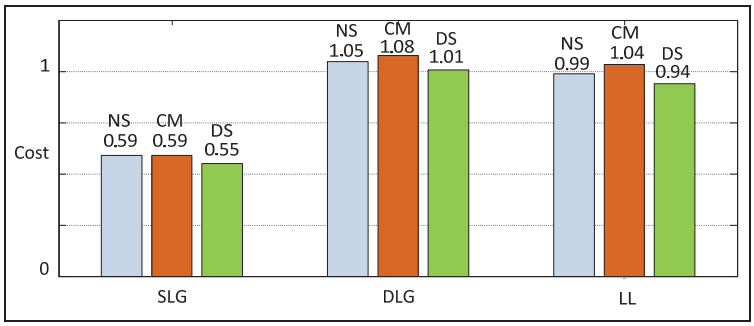

Fig. 7.5 Comparison of cost for each control methods for each fault type.

7.3 Conclusion

In this chapter, alternative to CM, the dual-sequence (DS) method, which is realizing voltage control in both positive and negative sequences, is given and shown to solve adverse effects caused by CM. DS method is boosting only the faulted phases and balancing the grid voltages.

As a general conclusion it can be commented that, with the use of DS method WPP can mimic behaviour of CPP during asymmetrical faults, boosting the positive sequence voltage and attenuating the negative sequence voltage, which results in improved grid support.

Chapter 8

Multi-Turbine Case Studies

In this chapter, the proposed control method given in chapter 5, namely PLL frequency based current injection during severe symmetrical faults is simulated with a WPP model of several wind turbines. The occurrence of the LOS problem and the interaction of parallel connected WTs are investigated.

8.1 LOS Problem for Multi-Turbine Case

The structure of a generic WPP, which is aggregated as a single WT, has been given in figure 1.1 and figure 2.2 and utilized throughout the thesis. In this chapter, the above mentioned WPP, which is composed of 20 WTs of each 5MW ratings, is remodeled as shown in figure 8.1 below. In this case one of the strings is expanded without aggregation as 5 WTs and the rest is still kept as aggregated as 75MW. The PCC of the WPP is again connected to the main grid via a 20km line, which has impedance of 0.1pu with X/R of 4; and the main grid is represented with its Thevenin equivalent with impedance of 0.1pu and X/R of 10 (SCR is 10). The individual WTs in the expanded string are connected with 500m long underground cables.

The purpose of the multi-turbine case is to observe the LOS conditions when the WTs are operating in parallel and injecting active and reactive currents during faults, which is occurring in real WPPs. As discussed in the previous chapters, LOS is occurring when the current injection from the WPP is out of current transfer limits. For a detailed WPP, the current injected into the grid is the combination of the individual currents from each WT. Hence, the LOS can occur when the total current injection is out of the current transfer limits; however each turbine experiences the LOS individually.

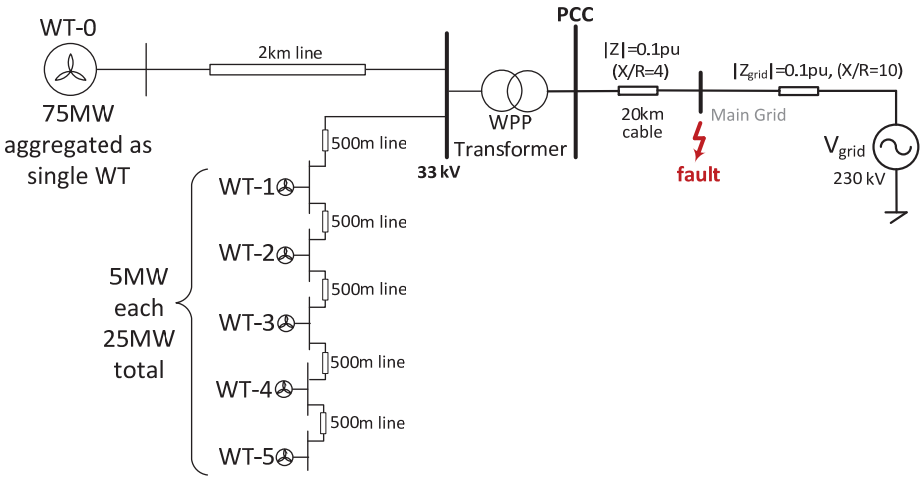

Fig. 8.1 WPP diagram with an expanded string and Thevenin equivalent grid of simulation study.

In order to observe that the parallel connected WTs can respond to the faults without problems, a non-severe fault case is simulated first, where the PCC voltage drops to 25% of the rated. As seen in the second to fifth subfigures in figure 8.2, all the WTs can inject active and reactive currents during fault, and can recover to normal operation after the fault is cleared. In the sixth subfigure, the phase angles of the voltage at the terminals of the aggregated WTs (WT-0), the five individual WTs (WT-1 to WT-5) and the PCC are shown. Due to the resistive fault impedance, a phase jump is observed when the fault is occurring at time is equal to 1 second. The frequency signals of the six WTs (aggregated and individuals) are shown in the last subfigure, where it is observed that all of the turbines stay synchronized at 50 Hz during the fault.

In figure 8.3, a result of a severe symmetrical fault, where the PCC voltage drops down to 2% of the rated is shown. In this case, the WTs are having 1pu pure reactive current references in accordance with the conventional method. As expected, the LOS occurs and all of the WTs experience frequency deviation as fall towards 0 Hz, as observed in the last subfigure. It is important to note that, since the impedance of 500m and 2km long underground cable between the WTs is very small compared to the WPP

transformer impedance and 20km connection line, all the WTs operate almost synchronous to each other having almost the same phase angle characteristics.

If the WPP was consisting of long collector grid between strings, considerable phase differences would occur and LOS would be observed only for some of the WTs in the WPP.

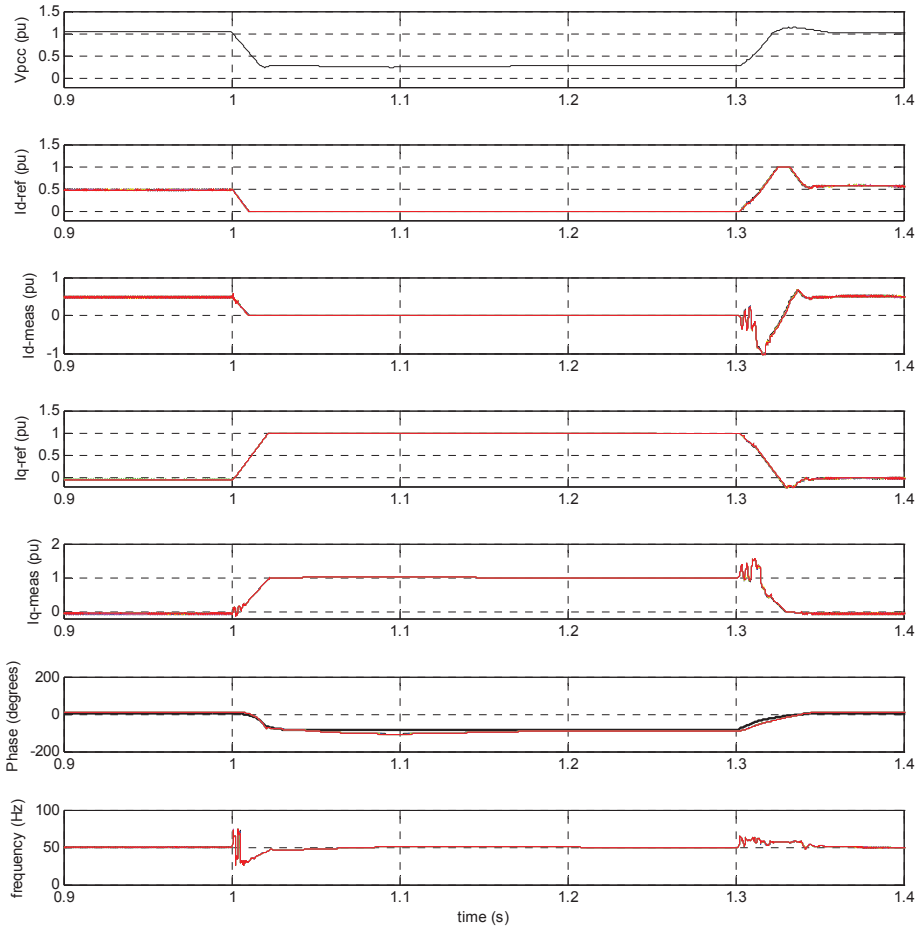

Fig. 8.2 Non-severe fault case and support from the WPP (1) PCC bus voltage magnitude, (2) Active current reference values, (3) Active current measured values (4) Reactive current reference values (5) Reactive current measured values (6) Phase angles (7) PLL frequency signals; WT-0: black, WT-1: blue, WT-2: yellow, WT-3: green, WT-4: magenta, WT-5: red.

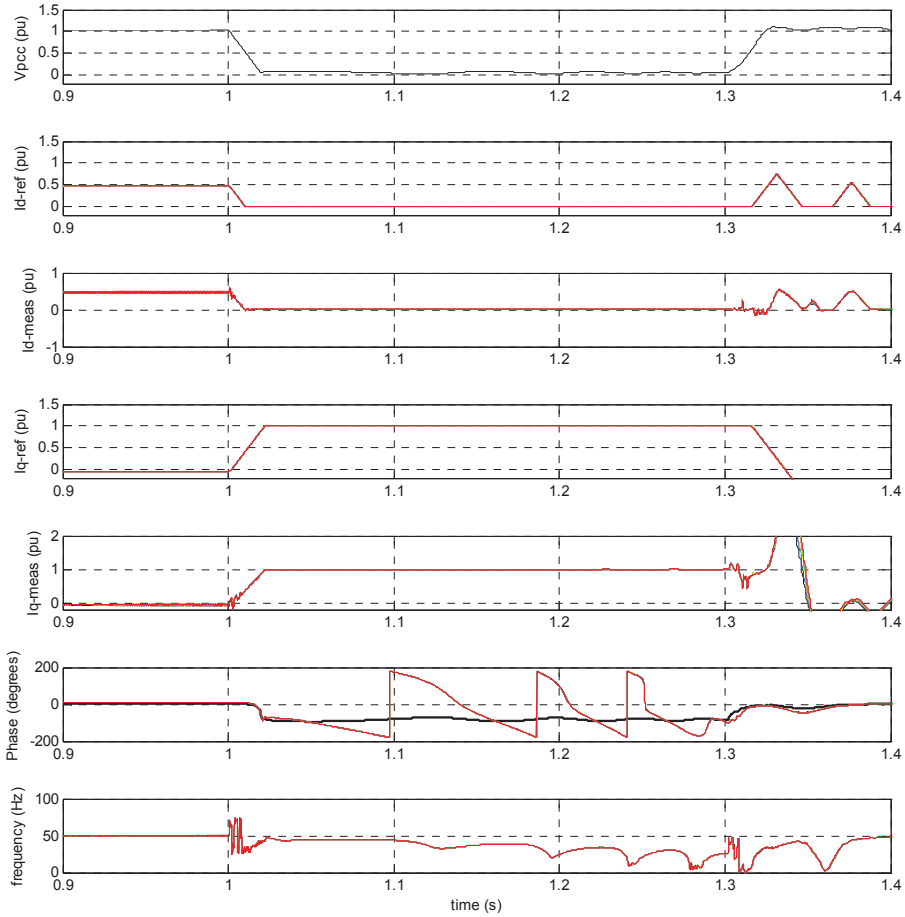

Fig. 8.3 Severe fault case and the LOS problem (1) PCC bus voltage magnitude, (2) Active current reference values, (3) Active current measured values (4) Reactive current reference values (5) Reactive current measured values (6) Phase angles (7) PLL frequency signals; WT-0: black, WT-1: blue, WT-2: yellow, WT-3: green, WT-4: magenta, WT-5: red.

8.2 PLL Frequency Based Solution for Multi-Turbine Case

In figure 8.4, the proposed PLL frequency based active current injection algorithm is employed by all of the WTs in the WPP for the severe symmetrical fault case, which was causing LOS in the previous section. As observed in the second and third

subfigures, all the WPPs generate active current setpoints around 0.4pu by the PLL frequency based method. Since the WT capacity is limited to 1pu, the reactive current references are decreased to less than 1pu in order to be able to inject the necessary active current. As observed in the sixth and seventh subfigures, all of the WTs stay synchronized to the grid fundamental frequency.

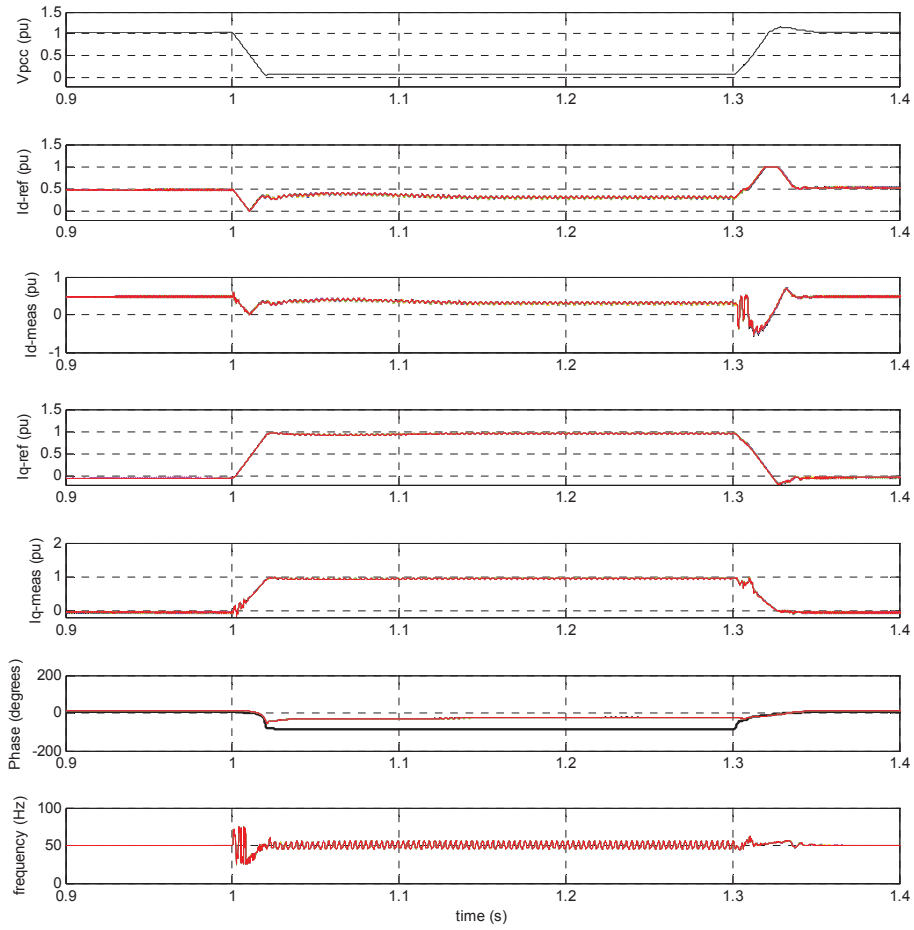

Fig. 8.4 Severe fault case and the PLL frequency based solution (1) PCC bus voltage magnitude, (2) Active current reference values, (3) Active current measured values (4) Reactive current reference values (5) Reactive current measured values (6) Phase angles (7) PLL frequency signals; WT-0: black, WT-1: blue, WT-2: yellow, WT-3: green, WT-4: magenta, WT-5: red.

8.3 Interaction between Wind Turbines

In figure 8.5, the severe symmetrical fault, which was causing LOS and shown to be solved by the PLL frequency based method, is simulated again. However, in this case, the 75MW part (WT-0) of the WPP is employing the conventional method and injecting 1pu pure reactive current and the other 25MW (5 WTs) are employing the PLL frequency based method.

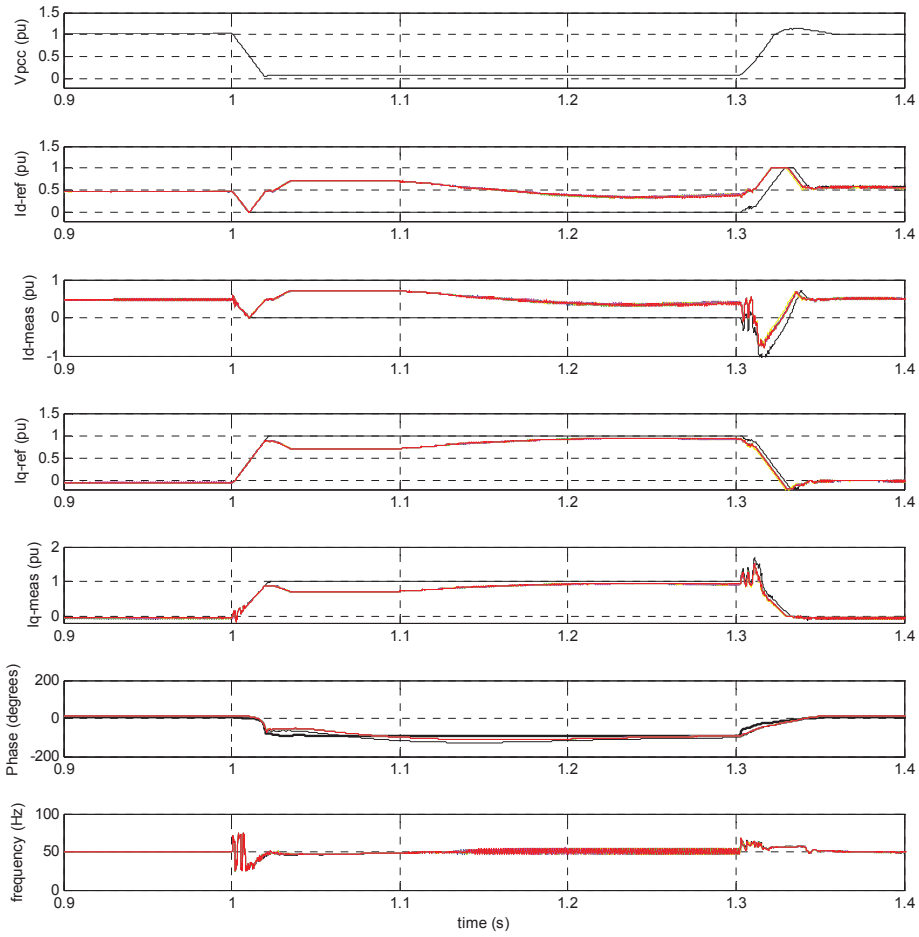

Fig. 8.5 Severe fault and interaction between WTs inside the WPP (1) PCC bus voltage magnitude, (2) Active current reference values, (3) Active current measured values (4) Reactive current reference values (5) Reactive current measured values (6) Phase

angles (7) PLL frequency signals; WT-0: black, WT-1: blue, WT-2: yellow, WT-3: green, WT-4: magenta, WT-5: red.

As observed in the fourth and fifth subfigure, the WT-0 (75MW) is injecting 1pu reactive current; and as observed in the second and third subfigure the 5 individual WTs are injecting 0.7pu active current, which is required to compensate for the active losses on the impedance between WTs and the faulted point. As observed in the fourth and fifth subfigures, the 5 WTs are supplying the necessary amount of active current while compromising their reactive current injection, which decreases to less than 1pu. As observed in the sixth and seventh, with the PLL frequency based method, the WPP can stay synchronized to the grid fundamental frequency, even though the majority of the WPP do not contribute to the stability solution.

In the above case the WTs with PLL frequency based current injection method is avoiding the LOS to occur for the whole WPP, including the other WTs. The above mentioned interaction can also occur between neighboring WPPs; in case two WPPs are connected to the same bus and a fault remote from that bus occurs, each WPP can interact in a manner that the WPP with non-transferrable current references can cause both itself and the other WPP to experience LOS, though the other WPP has current references within current transfer limits. Hence the LOS situation can be triggered by the neighboring power plants, whereas it can also be avoided by the neighboring power plant.

Chapter 9

Conclusions and Future Work

In this chapter, conclusions drawn from the thesis and main contributions are listed, together with the future work.

9.1 Summary

As more renewable energy sources, especially wind power plants, are installed in the power system, concern about stability of the power system increases. In order to provide stable power system operation with high share of wind power, grid codes are enforced by the transmission system operators of countries worldwide. Common to most of the grid codes as a fundamental requirement, wind turbines are expected to stay connected and inject reactive currents during grid faults. In certain grid codes, wind turbines are required to inject positive sequence reactive currents even for severe symmetrical faults with zero grid voltage; and also asymmetrical grid faults.

In this thesis, it is shown that during current injection to severe symmetrical faults with very low (e.g. 5%) grid voltage, wind turbines are experiencing stability problem as Loss of Synchronism (LOS) from grid fundamental frequency. The LOS is proven to be related with active and reactive current transfer limits, which is a basic physical fact not considered in wind power studies before, and derived within this thesis. It is shown that active and reactive current references out of current transfer limits are driving the grid synchronization (PLL) function of the wind turbines to large signal instability, causing LOS. A novel algorithm, namely PLL frequency based current reference generation, is proposed in this thesis as a solution for LOS. Both the LOS problem and

PLL frequency based solution are verified with time-domain simulations and grid-connected experiments.

Regarding the asymmetrical faults, it is shown that when pure positive sequence reactive current is injected in accordance with the grid code requirements, positive sequence grid voltage is boosted as desired, but negative sequence voltage is also boosted, which is not desired considering unbalanced voltages. This coupling between positive, negative and also zero sequence networks is explored for the first time in this thesis. It is also shown that, pure positive sequence reactive current injection is causing higher negative sequence voltages and higher phase overvoltages towards the WPPs. As alternative to conventional method of pure positive sequence reactive current injection, Dual-Sequence current injection method is given, which injects both positive and negative sequence currents such that boosting and balancing the grid.

In summary, response of wind turbines complying with fault ride-through and reactive current injection requirements of grid codes during severe symmetrical faults and asymmetrical faults is investigated. In order to solve the observed problems and to provide stable operation and improved grid support by wind turbines during symmetrical and asymmetrical grid faults, new methods to generate active reactive current references in positive and negative sequences are proposed to make the wind turbines behave in a similar manner to conventional power plants.

Based on the observations, it can be commented that the fault ride-through requirement together with the dynamic step response requirement of reactive current injection is causing problems for wind power plants during severe faults, which can be solved with advanced methods as given in this thesis. These requirements should be re-considered in this manner, and suggestions or modifications should be included within grid codes.

Additionally, it can be commented that the grid code requirements for asymmetrical faults have to be revised considering the impact of wind power plants' current injection on grid voltages and detailed specifications should be provided within grid codes.

Analysis of conventional synchronous generator's response to grid faults is a mature topic in classical power system literature. On the other hand, modern wind turbines employ power electronics based converters, which employ control algorithms to inject active and reactive currents. Hence, grid fault is a critical topic, where the classical power systems and power electronics areas are intersecting. Thus, studies both on the assessment of the grid code requirements and control solutions to satisfy grid code requirements are needed in order to provide stable power system operation.

9.2 Main contributions

Main contributions of this thesis are listed below;

- It is shown that similar to the active and reactive power transfer limits in classical power system theory, active and reactive current transfer limits between two buses exist for wind turbines' current injection. These limits are derived for the first time in this thesis as a fundamental theory to be utilized for specification of current injection limits of wind turbines, and any other current-controlled grid-connected converter.
- Wind turbines' Loss of Synchronism (LOS) problem, which is occurring during current injection to severe (very low voltage) symmetrical grid faults, is explored; such that a physical fact, which has been omitted or not well-understood before, is disclosed with its theory and analysis.
- A novel wind turbine control method, PLL frequency based current reference generation, is proposed for to solve LOS problem during severe symmetrical faults.
- Importance of fault impedance modeling in symmetrical and asymmetrical fault analysis is explained, which gives insight for modeling and simulation studies.
- Impact of coupling between positive, negative and zero sequence networks during current injection of wind turbines to asymmetrical grid faults is explored and analyzed, which has not been considered before.
- Rise of negative sequence and non-faulty phase overvoltages are shown and analyzed in detail when positive sequence reactive current is injected by wind turbines in accordance with the grid code requirement.

- Both for symmetrical and asymmetrical faults, understanding and knowledge is provided, which would influence development of new grid codes for wind power integration.

9.3 Future work

Following up the studies and investigations carried out in this thesis, the future work is summarized in this section as below;

In chapter 2 and 4, it is shown that the wind turbines experience frequency deviation and loss of vector control during an LOS event. In some cases, depending on the duration of the fault and other parameters affecting the LOS event, the wind turbines cannot recover their normal operation even though the fault is cleared. This phenomenon is similar to the "rotor angle stability" of a synchronous generator. Hence, together with a mathematical model and also incorporating the current regulator dynamic bandwidth, a methodology similar to "equal area criteria" of classical power system theory can be developed to analyze whether the wind turbine can recover (re-synchronize) to the grid, based on the duration of the fault. Otherwise, several time-domain simulations can be run to analyze fault response of the wind turbine regarding the fault duration and LOS; as done for synchronous generators to reach critical clearing time.

The current transfer limits in chapter 3 and proposed PLL frequency based control in chapter 5 have been studied for an aggregated wind power plant, and the model for stability analysis is prepared for the same. A methodology can be created to analyze the current transfer limits and LOS response of multi-turbines comprising a WPP. Additionally, any elements like STATCOM, located within the WPP and any (conventional) generators or loads located nearby PCC of the WPP can be included in the methodology.

The frequency compensator of PLL frequency based control is designed as a proportional control based on small-signal model of the PLL. An improved analysis

and design can be accomplished for proportional plus integral plus derivative control, in order to achieve higher dynamic response during severe symmetrical faults.

Current injection by wind turbines during asymmetrical faults should be assessed from protection point of view. Positive and negative sequence current injection and resulting phase currents should be analyzed regarding their interaction with protection units (e.g. relay settings) to observe if any improvement or degradation occurs. Additionally, analysis of power system with high share of renewable energy sources should be accomplished in order to observe effect of current injection on the phase overvoltages and any other consequences during asymmetrical grid faults. WPP level control, incorporating positive and negative sequence voltage management at the PCC point, can be considered as a future asymmetrical fault handling solution.

As discussed in the previous sections, the problems are proposed to be solved by generating active and reactive current references, which resulted in a WPP operation in a similar manner to a synchronous generator. The proposed methods and alternatives can be developed via utilizing advanced techniques and modern infrastructure of the contemporary power system, such as wide area measurement systems and distributed phase measurement units.

9.4 List of publications

P1. Mufit Altin, Ömer Göksu, Remus Teodorescu, Pedro Rodriguez, Birgitte Bak-Jensen, and Lars Helle, "Overview of recent grid codes for wind power integration," International Conference on Optimization of Electrical and Electronic Equipments, Romania, May 2010

P2. Ömer Göksu, Remus Teodorescu, Pedro Rodriguez, and Lars Helle, "A Review of the State of the Art in Control of Variable-Speed Wind Turbines," 9th International Workshop on Large-Scale Integration of Wind Power into Power systems, Quebec, Canada, October 2010

P3. Andrzej Adamczyk, Mufit Altin, Ömer Göksu, Remus Teodorescu, and Florin Iov, “Generic 12-Bus Test System for Wind Power Integration Studies,” EPE Joint Wind Energy and T&D Chapters Seminar, Aalborg, Denmark, June 2012

P4. Ömer Göksu, Remus Teodorescu, Birgitte Bak-Jensen, Florin Iov, and Philip Kjær, "An Iterative Approach for Symmetrical and Asymmetrical Short-Circuit Calculations with Converter-Based Connected Renewable Energy Sources. Application to Wind Power," IEEE Power & Energy Society General Meeting, San Diego, USA, July 2012

P5. Ömer Göksu, Remus Teodorescu, Claus Leth Bak, Florin Iov, and Philip Kjær, "Impact of Wind Power Plant Reactive Current Injection during Asymmetrical Grid Faults,” IET Journal of Renewable Power Generation, accepted.

P6. Ömer Göksu, Remus Teodorescu, Claus Leth Bak, Florin Iov, and Philip Kjær, "Instability of Wind Turbine Converters during Current Injection to Low Voltage Grid Faults and PLL Frequency Based Stability Solution,” IEEE Transactions on Power Systems, under review.

Bibliography

[1] P. Kundur, “Power System Stability and Control”, New York: McGraw-Hill, 1994.

[2] N. D. Tleis, “Power Systems Modeling and Fault Analysis”, Elsevier Publishing Company, 2008.

[3] J. C. Das, “Power system analysis: short-circuit load flow and harmonics”, Marcel Dekker Press, 2002.

[4] BTM Consult ApS, “International wind energy development, world market update”, 2010.

[5] L. Meegahapola, D. Flynn, "Impact on transient and frequency stability for a power system at very high wind penetration," *IEEE Power and Energy Society General Meeting,* pp.1-8, 25-29 July 2010.

[6] F. Shewarega, I. Erlich, J. L. Rueda, "Impact of large offshore wind farms on power system transient stability," *IEEE/PES Power Systems Conference and Exposition,* pp.1-8, 15-18 March 2009.

[7] S. K. Yee, N. Krajisnik, S. Stapleton, J. O'Sullivan, A. Kennedy, "Considerations for the stable operation of a power system with increasing wind penetration," *IET Conference on Renewable Power Generation*, pp.1-6, 6-8 Sept. 2011.

[8] H. Polinder, "Overview of and trends in wind turbine generator systems," *IEEE Power and Energy Society General Meeting,* pp.1-8, 24-29 July 2011.

[9] W. L. Kling and J. G. Slootweg, “Wind turbines as Power Plants,” *in Proceedings of the IEEE/Cigré workshop on Wind Power and the Impacts on Power Systems*, 17 – 18 June 2002.

[10] M. Liserre, R. Cárdenas, M. Molinas, J. Rodriguez, "Overview of Multi-MW Wind Turbines and Wind Parks," *IEEE Transactions on Industrial Electronics*, vol.58, no.4, pp.1081-1095, April 2011.

[11] J. C. Boemer, A. A.van der Meer, B. G.Rawn, R. L.Hendriks, A. R. Ciupuliga, M. Gibescu, W. L. Kling, J. A. Ferreira, "Fault ride-through requirements for onshore wind power plants in Europe: The needs of the power system," *IEEE Power and Energy Society General Meeting,* pp.1-8, 24-29 July 2011.

[12] I. Erlich, U. Bachmann, "Grid code requirements concerning connection and operation of wind turbines in Germany," *IEEE Power Engineering Society General Meeting,* pp. 1253- 1257 Vol. 2, 12-16 June 2005.

[13] Ö. Göksu, R. Teodorescu, P. Rodriguez, and L. Helle, "A Review of the State of the Art in Control of Variable-Speed Wind Turbines," *9th International Workshop on Large-Scale Integration of Wind Power into Power systems as well as on Transmission Networks for Offshore Wind Power Plants*, Quebec, Canada, October 2010.

[14] M. Altin, O. Goksu, R. Teodorescu, P. Rodriguez, B.-B. Jensen, and L. Helle, "Overview of recent grid codes for wind power integration," in *12th Int. Conf. on Optimization of Electrical and Electronic Equipment,* pp. 1152–1160, May 2010.

[15] M. Tsili and S. Papathanassiou, "A review of grid code technical requirements for wind farms," *IET Renew. Power Gener.*, 3, (3), pp. 308–332*,* 2009.

[16] Eon Netz GmbH, "Grid code high and extra high voltage", online: http://www.eon-netz.com/, 2006.

[17] Transmission Code 2007. Networks and System Rules of the German Transmission System operators, VDN-e.v. beim VDEW, www.vdn-berlin.de, August 2007.

[18] Resolution-P.O.12.3-Response requirements against voltage dips in wind installations, by Red Electrica in March 2006, www.ree.es (translated in English by Spanish Wind Association AEE www.aeolica.es), 2006.

[19] Annex of O.P. 12.2 Restricted to the technical requirements of wind power and photovoltaic facilities (Draft), by Red Electrica in October 2008 www.ree.es (translated in English by Spanish Wind Association AEE www.aeolica.es), 2008.

[20] Energinet.dk, "Technical regulation 3.2.5 for wind power plants with a power output greater than 11 kW," online: http://energinet.dk/, 2010.

[21] European network for transmission system operators for electricity: "ENTSO-E network code for requirements for grid connection applicable to all generators", 26 June 2012.

[22] N. R. Ullah and T. Thiringer, "Variable speed wind turbines for power system stability enhancement," *IEEE Trans. Energy Convers.,* vol. 22, pp.52-60, 2007.

[23] F. Sulla, "Fault Behavior of Wind Turbines," Ph.D. Thesis, Lund University, Sweden, 2012.

[24] H. Saadat, "Power system analysis" McGraw-Hill Press, 1999, 2nd edn. 2002.

[25] "IEEE guide for planning DC links terminating at AC locations having low short-circuit capacities," IEEE Std 1204-1997, Tech. Rep., 1997.

[26] M. G. Lauby, J. A. Moura, E. M. Rollison, "Accommodating large amounts of variable generation in North America," *IEEE Power and Energy Society General Meeting,* pp.1-5, 24-29 July 2011.

[27] J. O. G Tande, K. Uhlen, "Wind turbines in weak grids - constraints and solutions," Electricity Distribution, 2001. Part 1: Contributions. CIRED. 16th International Conference and Exhibition on (IEE Conf. Publ No. 482), pp.261, 2001.

[28] G. Ledwich, H. Sharma, "Connection of inverters to a weak grid," *IEEE Power Electronics Specialists Conference,* vol.2, pp.1018-1022, 2000.

[29] R. Reginato, M. G. Zanchettin, M. Tragueta, "Analysis of safe integration criteria for wind power with induction generators based wind turbines," *IEEE Power & Energy Society General Meeting*, pp.1-8, 26-30 July 2009.

[30] M. Rasmussen, H. K. Jorgensen, "Current Technology for Integrating Wind Farms into Weak Power Grids," *Transmission and Distribution Conference and Exhibition: Asia and Pacific, 2005 IEEE/PES*, pp.1-4, 2005.

[31] R. Piwko, N. Miller, J. Sanchez-Gasca, X. Yuan, R. Dai, J. Lyons, "Integrating Large Wind Farms into Weak Power Grids with Long Transmission Lines," *Power Electronics and Motion Control Conference, CES/IEEE*, vol.2, pp.1-7, 14-16 Aug. 2006.

[32] T. Neumann, C. Feltes, I. Erlich, "Response of DFG-based wind farms operating on weak grids to voltage sags," *IEEE Power and Energy Society General Meeting,* pp.1-6, 24-29 July 2011.

[33] V. O. Zambrano, E. B. Makram, and R. G. Harley, "Transient response of synchronous and asynchronous machines to asymmetrical faults in an unbalanced network," *Electric Power Systems Research*, vol. 14, no. 2, pp. 155-166, 1988.

[34] P. M. Anderson, "Analysis of Faulted Power Systems", IEEE Press, 1995.

[35] F. Blaabjerg, R. Teodorescu, M. Liserre, and A. V. Timbus, "Overview of Control and Grid Synchronization for Distributed Power Generation Systems," *IEEE Trans. on Ind. Electronics,* Vol. 53, pp1398 – 1409, Oct. 2006.

[36] A. Timbus, M. Liserre, R. Teodorescu, P. Rodriguez, F. Blaabjerg, "Evaluation of Current Controllers for Distributed Power Generation Systems," *IEEE Transactions on Power Electronics,* vol.24, no.3, pp.654,664, March 2009.

[37] R. Teodorescu, F. Blaabjerg, M. Liserre, P. C. Loh, "Proportional-resonant controllers and filters for grid-connected voltage-source converters," *IEE Proceedings Electric Power Applications*, vol.153, no.5, pp.750-762, September 2006.

[38] R. Teodorescu, M. Liserre, and P. Rodriguez: "Grid converters for photovoltaic and wind power systems", Wiley Press, 2011.

[39] S. Yongsug, V. Tijeras, T. A. Lipo, "Control scheme in hybrid synchronous-stationary frame for PWM AC/DC converter under generalized unbalanced operating conditions," *IEEE Transactions on Industry Applications*, vol 42, no. 3, pp.825-835, June 2006.

[40] I. Etxeberria-Otadui, U. Viscarret, M. Caballero, A. Rufer, S. Bacha, "New Optimized PWM VSC Control Structures and Strategies Under Unbalanced Voltage Transients," *IEEE Transactions on Industrial Electronics*, vol.54, no.5, pp.2902-2914, Oct. 2007.

[41] B. Yin, R. Oruganti, S. K. Panda, A. K. S. Bhat, "An Output-Power-Control Strategy for a Three-Phase PWM Rectifier Under Unbalanced Supply Conditions," *IEEE Transactions on Industrial Electronics*, vol.55, no.5, pp.2140-2151, May 2008.

[42] L. Xu, B. R. Andersen, P. Cartwright, "VSC transmission operating under unbalanced AC conditions - analysis and control design," *IEEE Transactions on Power Delivery*, vol.20, no.1, pp. 427- 434, Jan 2005.

[43] A. V. Stankovic, T. A. Lipo, "A novel control method for input output harmonic elimination of the PWM boost type rectifier under unbalanced operating conditions," *IEEE Transactions on Power Electronics*, vol.16, no.5, pp.603-611, Sep 2001.

[44] A. Yazdani and R. Iravani, "Voltage-Sourced Converters in Power Systems: Modeling, Control, and Applications", John Wiley & Sons, Inc., Hoboken, NJ, USA, 2010.

[45] A. D. Hansen, G. Michalke, "Multi-pole permanent magnet synchronous generator wind turbines' grid support capability in uninterrupted operation during grid faults," *IET Renewable Power Generation*, vol.3, no.3, pp.333-348, Sept. 2009.

[46] J. F. Conroy, R. Watson, "Low-voltage ride-through of a full converter wind turbine with permanent magnet generator," *IET Renewable Power Generation*, vol.1, no.3, pp.182-189, September 2007.

[47] V. Akhmatov, "Full-load Converter Connected Asynchronous Generators for MW Class Wind Turbines," *Wind Engineering*, vol.29, no. 4, pp. 341-351, June 2005.

[48] M. Molinas, B. Nass, W. Gullvik, T. Undeland, "Control of Wind Turbines with Induction Generators Interfaced to the Grid with Power Electronics Converters," *Proc. of the International Power Electronics Conference*, Niigata, Japan, 2005.

[49] C. Abbey, G. Joos, "Effect of low voltage ride through (LVRT) characteristic on voltage stability," *IEEE Power Engineering Society General Meeting,* pp. 1901-1907 Vol. 2, 12-16 June 2005.

[50] N. R. Ullah , T. Thiringer and D. Karlsson "Voltage and transient stability support by wind farms complying with the E.ON Netz grid code", *IEEE Trans. Power Syst.*, vol. 22, pp.1647-1656, 2007.

[51] C. Jauch "Transient and dynamic control of a variable speed wind turbine with synchronous generator", *Wind Energy*, 10, (3), pp. 247–269, 2007.

[52] C. Jauch, P. Sørensen, I. Norhem, and C. Rasmussen, “Simulation of the impact of wind power on the transient fault behaviour of the Nordic power system,” *Electric Power Syst. Res.,* no. 77, pp. 135–144, 2007.

[53] A. Mullane, G. Lightbody, R. Yacamini, "Wind-turbine fault ride-through enhancement," *IEEE Transactions on Power Systems*, vol.20, no.4, pp. 1929-1937, Nov. 2005.

[54] N. A. Cutululis, A. D. Hansen, T. J. Larsen, P. E. Sørensen, F. Iov, “Wind turbines structural loads during fault ride-through operation,” *in 2008 European Wind Energy Conference and Exhibition* (pp. 77-80), 2008.

[55] P. Brogan, "The stability of multiple, high power, active front end voltage sourced converters when connected to wind farm collector systems." in *Proc. 2010 European Power Electronics Conf.* 2010.

[56] I. Erlich, F. Shewarega, S. Engelhardt, J. Kretschmann, J. Fortmann, and F. Koch, “Effect of Wind Turbine Output Current during Faults on Grid Voltage and the Transient Stability of Wind Parks,” *IEEE Power & Energy Society General Meeting,* pp.1-8, 26-30 July 2009.

[57] J. N. Nielsen, V. Akhmatov, J. Thisted, E. Grøndahl, P. Egedal, M. N. Frydensbjerg and K. H. Jensen, “Modelling and Fault-Ride-Trough Tests of Siemens Wind Power 3.6 MW Variable-speed Wind Turbines”, *Wind Engineering*, vol.31, no.6, pp.441-452, 2007.

[58] P. Rodriguez, A.V. Timbus, R. Teodorescu, M. Liserre, F. Blaabjerg, "Flexible Active Power Control of Distributed Power Generation Systems During Grid Faults," *IEEE Transactions on Industrial Electronics*, vol.54, no.5, pp.2583-2592, Oct. 2007.

[59] P. Rodriguez, A.V. Timbus, R. Teodorescu, M. Liserre, F. Blaabjerg, "Reactive Power Control for Improving Wind Turbine System Behavior Under Grid Faults," *IEEE Transactions on Power Electronics*, vol.24, no.7, pp.1798-1801, July 2009.

[60] F. Wang; J.L. Duarte, M. A. M. Hendrix, "Active power control strategies for inverter-based distributed power generation adapted to grid-fault ride-through requirements," *European Conference on Power Electronics and Applications*, pp.1-10, 8-10 Sept. 2009.

[61] F. Wang; J. L. Duarte, M. Hendrix, "Active and reactive power control schemes for distributed generation systems under voltage dips," *IEEE Energy Conversion Congress and Exposition,* pp.3564-3571, 20-24 Sept. 2009.

[62] G. Saccomando and J. Svensson, "Transient operation of grid-connected voltage source converter under unbalanced voltage conditions," *in Conference Record of the IEEE Industry Applications Conference*, vol. 4, pp. 2419-2424, 2001.

[63] C. Ng, L. Ran, J. Bumby, "Unbalanced Grid Fault Ride-Through Control for a Wind Turbine Inverter," *IEEE Industry Applications Conference*, pp.154-164, 23-27 Sept. 2007.

[64] D. Roiu, R. I. Bojoi, L. R. Limongi, A. Tenconi, "New Stationary Frame Control Scheme for Three-Phase PWM Rectifiers Under Unbalanced Voltage Dips Conditions," *IEEE Transactions on Industry Applications,* vol.46, no.1, pp.268-277, Jan.-Feb. 2010.

[65] S. Alepuz, S. Busquets-Monge, J. Bordonau, J. A. Martinez-Velasco, C. A. Silva, J. Pontt, J. Rodriguez, "Control Strategies Based on Symmetrical Components for Grid-Connected Converters Under Voltage Dips," *IEEE Transactions on Industrial Electronics,* vol.56, no.6, pp.2162-2173, June 2009.

[66] A. Junyent-Ferre, O. Gomis-Bellmunt, T. C. Green, D. E. Soto-Sanchez, "Current Control Reference Calculation Issues for the Operation of Renewable Source Grid Interface VSCs Under Unbalanced Voltage Sags," *IEEE Transactions on Power Electronics,* vol.26, no.12, pp.3744-3753, Dec. 2011.

[67] A. Sannino, M. H. J. Bollen, J. Svensson, "Voltage tolerance testing of three-phase voltage source converters," *IEEE Transactions on Power Delivery*, vol.20, no.2, pp. 1633- 1639, April 2005.

[68] M. H. J. Bollen, O. Gabriel and M. Martins, "Voltage dips at the terminals of wind power installations," *Wind Energy*, no. 3, pp.307-318, 2005.

[69] F. Wang, J. L. Duarte, and M. A. M. Hendrix, "Design and analysis of active power control strategies for distributed generation inverters under unbalanced grid faults," *IET Generation, Transmission & Distribution*, no. 8 pp. 905-916, 2010.

[70] F. Wang; J. L. Duarte, M. A. M. Hendrix, "Pliant Active and Reactive Power Control for Grid-Interactive Converters Under Unbalanced Voltage Dips," *IEEE Transactions on Power Electronics*, vol.26, no.5, pp.1511-1521, May 2011.

[71] C. T. Lee, C. W. Hsu, P. T. Cheng, "A Low-Voltage Ride-Through Technique for Grid-Connected Converters of Distributed Energy Resources," *IEEE Transactions on Industry Applications*, vol.47, no.4, pp.1821-1832, July-Aug. 2011.

[72] M. Castilla, J. Miret, A. Camacho, J. Matas, E. Alarcon-Gallo, L. G. de Vicuna, "Coordinated reactive power control for static synchronous compensators under unbalanced voltage sags," *IEEE International Symposium on Industrial Electronics,* pp.987-992, 28-31 May 2012.

[73] A. Camacho, M. Castilla, J. Miret, J. Vasquez, E. Alarcon-Gallo, "Flexible Voltage Support Control for Three Phase Distributed Generation Inverters Under Grid Fault," *IEEE Transactions on Industrial Electronics*, vol.60, no.4, pp.1429,1441, April 2013.

[74] E. Muljadi, C. P. Butterfield, A. Ellis, J. Mechenbier, J. Hocheimer, R. Young, N. Miller, R. Delmerico, R. Zavadil, J. C. Smith, ”Equivalencing the Collector System of a Large Wind Power Plant”, *IEEE Power Engineering Society, Annual Conference,* Montreal, Quebec, June 12-16, 2006.

[75] Y. Cheng, M. Sahni, J. Conto, S-H. Huang, J. Schmall, "Voltage-profile-based approach for developing collection system aggregated models for wind generation resources for grid voltage ride-through studies," *IET Renewable Power Generation*, no. 5 pp.332-346, 2011.

[76] J. Brochu, C. Larose, R. Gagnon, "Generic Equivalent Collector System Parameters for Large Wind Power Plants," *IEEE Transactions on Energy Conversion*, vol.26, no.2, pp.542-549, June 2011.

[77] J. F. Conroy and R. Watson, “Low-voltage ride-through of a full converter wind turbine with permanent magnet generator,” *IET Renew. Power Gener.*, 1, (3), pp. 182–189, 2007.

[78] J. F. Conroy and R. Watson, “Aggregate modelling of wind farms containing full-converter wind turbine generators with permanent magnet synchronous machines: transient stability studies,” *IET Renew. Power Gener.*, 3, (1), pp. 39–52, 2009.

[79] D. Dong, J. Li, D. Boroyevich, P. Mattavelli, I. Cvetkovic, X. Yaosuo, "Frequency behavior and its stability of grid-interface converter in distributed generation systems," *IEEE Applied Power Electronics Conference and Exposition* (APEC), pp.1887-1893, 5-9 Feb. 2012.

[80] S. Engelhardt and A. Geniusz, "Method for Operating a Wind Turbine," US2011/0006528 A1, Jan. 13, 2011.

[81] E. V. Larsen, A. M. Klodowski, and S. A. Barker, "Method and Systems for Operating a Wind Turbine," US 8,046,109 B2, Oct. 25, 2011.

[82] V. Diedrichs, A. Beekmann, and S. Adloff, "Loss of (Angle) Stability of Wind Power Plants – The Underestimated Phenomenon in Case of Very Low Short Circuit Ratio," *Wind Integration Workshop, 2011* Aarhus, 24 October 2011.

[83] W. Kuhn, "Method and Apparatus for Automatic Network Stabilization in Electric Power Supply Systems Using At Least One Converter," WO 2012/119136 A1, Oct. 21, 2010.

[84] J. M. Garcia, P. C. Kjaer, P. Rodriguez, and R. Teodorescu, "Active Current Control in Wind Power Plants during Grid Faults," *Wind Energy,* Vol. 13, No. 8, 2010.

[85] V. Diedrichs, A. Beekmann, K. Busker, S. Nikolai, and S. Adloff, "Control of wind power plants utilizing voltage source converter in high impedance grids," *IEEE Power and Energy Society General Meeting*, pp. 1-9, 2012.

[86] M. Kayikci, J. V. Milanovic, "Reactive Power Control Strategies for DFIG-Based Plants," *IEEE Transactions on Energy Conversion*, vol.22, no.2, pp.389-396, June 2007.

[87] N. R. Ullah and T. Thiringer; " Effect of operational modes of a wind farm on the transient stability of nearby generators and on power oscillations: a Nordic grid study," *Wind Energy,* Vol. 11, No. 1, 2008.

[88] J. Driesen and T. Van Craenenbroeck, "Voltage disturbances, introduction to unbalance," Power Quality Application Guide, Copper Develop. Assoc., pp. 1–11, May 2002.

[89] R. Targosz, "Evaluating cost of inadequate quality of supply," *IEEE Power and Energy Society General Meeting,* pp. 1–8, 25-29 July 2010.

[90] P. Pillay, P. Hoftmann, M. Manyage, “Derating of induction motors operating with a combination of unbalanced voltages and over or under voltages,” *IEEE Trans. Energy Conversion,* vol. 17, pp. 485–491, Dec. 2002.

[91] Technical Rules for the Assessment of Network Disturbances, set up by four Electricity Associations, VDN, VEÖ, VSEAES, CSRES, 2nd Edition, 2007.

[92] J.F. Conroy and R. Watson, ”Investigation of the Effects of Transmission Faults upon a Renewable Energy Generating Plant,” *IEEE Power Tech Conference*, pp. 1–7, 27-30 June 2005.

[93] C. Saniter et al., “Modelling the effects of ac system impedance unbalance on pwm converters using frequency coupling matrices,” in *IEEE Power Tech Conference*, Bologna, Italy, June 2003.

[94] V.O. Zambrano, E.B. Makram and R.G. Harley, “Stability of a synchronous machine due to an unsymmetrical fault in unbalanced power systems,” *In 20th Southeastern Symp. on System Theory,* pp. 231–235, March 1988.

[95] V. O. Zambrano, E. B. Makram, and R. G. Harley, "Transient response of synchronous and asynchronous machines to asymmetrical faults in an unbalanced network," *Electric Power Systems Research,* vol. 14, no. 2, pp. 155-166, 1988.

[96] R. G. Harley, E. B. Makram, and E. G. Duran, "The effects of unbalanced networks on synchronous and asynchronous machine transient stability," *Electric Power Systems Research,* vol. 13, no. 2, pp. 119-127, 1987.

[97] P. Gnacinski, "Windings Temperature and Loss of Life of an Induction Machine Under Voltage Unbalance Combined With Over- or Undervoltages," *IEEE Transactions on Energy Conversion,* vol.23, no.2, pp.363-371, June 2008.

[98] E. Muljadi, T. Batan, D. Yildirim, and C. P. Butterfield, “Understanding the unbalanced-voltage problem in wind turbine generation”. *Proc. 34th IAS Annual Meeting*, vol. 2, pp. 1359–1365, October 1999.

[99] P. Gnacinski, “Windings temperature and loss of life of an induction machine under voltage unbalance combined with over- or undervoltages” *IEEE Trans. on Energy Convers.,* 23, (2), pp. 363–37, 2008.

[100] "IEEE Standard for Cylindrical-Rotor 50 Hz and 60 Hz Synchronous Generators Rated 10 Mva and Above," IEEE Std C50.13-2005 , vol., no., pp.0_1-48, 2006.

[101] K. Chen, L.W. Montgomery, G. Klempner, J. Yagielski, J. Amos, M. Brimsek, M. Sedlak, "Comparing IEEE 50.13 and IEC 60034 standards for large cylindrical rotor synchronous machines," *Proc. IEEE Power and Energy Society General Meeting*, pp.1-9, July 2010.

[102] J. Niiranen, "Experiences on voltage dip ride through factory testing of synchronous and doubly fed generator drives," *European Conf. Power Electronics and Applications,* Dresden, 2005.

[103] G. Ziegler, "Numerical Distance Protection Principles and Application", Siemens-Erlangen Pulicis, pp.142 -1451999.